IAEA TECDOC SERIES

IAEA-TECDOC-1897

Radiotracer Technologies for Wear, Erosion and Corrosion Measurement

IAEA
International Atomic Energy Agency

RADIOTRACER TECHNOLOGIES FOR WEAR, EROSION AND CORROSION MEASUREMENT

The following States are Members of the International Atomic Energy Agency:

AFGHANISTAN
ALBANIA
ALGERIA
ANGOLA
ANTIGUA AND BARBUDA
ARGENTINA
ARMENIA
AUSTRALIA
AUSTRIA
AZERBAIJAN
BAHAMAS
BAHRAIN
BANGLADESH
BARBADOS
BELARUS
BELGIUM
BELIZE
BENIN
BOLIVIA, PLURINATIONAL STATE OF
BOSNIA AND HERZEGOVINA
BOTSWANA
BRAZIL
BRUNEI DARUSSALAM
BULGARIA
BURKINA FASO
BURUNDI
CAMBODIA
CAMEROON
CANADA
CENTRAL AFRICAN REPUBLIC
CHAD
CHILE
CHINA
COLOMBIA
CONGO
COSTA RICA
CÔTE D'IVOIRE
CROATIA
CUBA
CYPRUS
CZECH REPUBLIC
DEMOCRATIC REPUBLIC OF THE CONGO
DENMARK
DJIBOUTI
DOMINICA
DOMINICAN REPUBLIC
ECUADOR
EGYPT
EL SALVADOR
ERITREA
ESTONIA
ESWATINI
ETHIOPIA
FIJI
FINLAND
FRANCE
GABON
GEORGIA
GERMANY
GHANA
GREECE
GRENADA
GUATEMALA
GUYANA
HAITI
HOLY SEE
HONDURAS
HUNGARY
ICELAND
INDIA
INDONESIA
IRAN, ISLAMIC REPUBLIC OF
IRAQ
IRELAND
ISRAEL
ITALY
JAMAICA
JAPAN
JORDAN
KAZAKHSTAN
KENYA
KOREA, REPUBLIC OF
KUWAIT
KYRGYZSTAN
LAO PEOPLE'S DEMOCRATIC REPUBLIC
LATVIA
LEBANON
LESOTHO
LIBERIA
LIBYA
LIECHTENSTEIN
LITHUANIA
LUXEMBOURG
MADAGASCAR
MALAWI
MALAYSIA
MALI
MALTA
MARSHALL ISLANDS
MAURITANIA
MAURITIUS
MEXICO
MONACO
MONGOLIA
MONTENEGRO
MOROCCO
MOZAMBIQUE
MYANMAR
NAMIBIA
NEPAL
NETHERLANDS
NEW ZEALAND
NICARAGUA
NIGER
NIGERIA
NORTH MACEDONIA
NORWAY
OMAN
PAKISTAN
PALAU
PANAMA
PAPUA NEW GUINEA
PARAGUAY
PERU
PHILIPPINES
POLAND
PORTUGAL
QATAR
REPUBLIC OF MOLDOVA
ROMANIA
RUSSIAN FEDERATION
RWANDA
SAINT LUCIA
SAINT VINCENT AND THE GRENADINES
SAN MARINO
SAUDI ARABIA
SENEGAL
SERBIA
SEYCHELLES
SIERRA LEONE
SINGAPORE
SLOVAKIA
SLOVENIA
SOUTH AFRICA
SPAIN
SRI LANKA
SUDAN
SWEDEN
SWITZERLAND
SYRIAN ARAB REPUBLIC
TAJIKISTAN
THAILAND
TOGO
TRINIDAD AND TOBAGO
TUNISIA
TURKEY
TURKMENISTAN
UGANDA
UKRAINE
UNITED ARAB EMIRATES
UNITED KINGDOM OF GREAT BRITAIN AND NORTHERN IRELAND
UNITED REPUBLIC OF TANZANIA
UNITED STATES OF AMERICA
URUGUAY
UZBEKISTAN
VANUATU
VENEZUELA, BOLIVARIAN REPUBLIC OF
VIET NAM
YEMEN
ZAMBIA
ZIMBABWE

The Agency's Statute was approved on 23 October 1956 by the Conference on the Statute of the IAEA held at United Nations Headquarters, New York; it entered into force on 29 July 1957. The Headquarters of the Agency are situated in Vienna. Its principal objective is "to accelerate and enlarge the contribution of atomic energy to peace, health and prosperity throughout the world''.

IAEA-TECDOC-1897

RADIOTRACER TECHNOLOGIES FOR WEAR, EROSION AND CORROSION MEASUREMENT

INTERNATIONAL ATOMIC ENERGY AGENCY
VIENNA, 2020

COPYRIGHT NOTICE

For further information on this publication, please contact:

Radioisotope Products and Radiation Technology Section
International Atomic Energy Agency
Vienna International Centre
PO Box 100
1400 Vienna, Austria
Email: Official.Mail@iaea.org

Printed by the IAEA in Austria
February 2020

IAEA Library Cataloguing in Publication Data

Names: International Atomic Energy Agency.
Title: Radiotracer technologies for wear, erosion and corrosion management / International Atomic Energy Agency.
Description: Vienna : International Atomic Energy Agency, 2020. | Series: IAEA TECDOC series, ISSN 1011–4289 ; no. 1897 | Includes bibliographical references.
Identifiers: IAEAL 20-01295 | ISBN 978–92–0–101520–4 (paperback : alk. paper) | ISBN 978–92–0–101620–1 (pdf)
Subjects: LCSH: Nuclear activation analysis. | Radioactive tracers in metallurgy. | Mechanical wear.

FOREWORD

Over the years, the IAEA has contributed substantially to the promotion of industrial applications of radiation and radioisotope technologies. It has enabled developing Member States to introduce these technologies into well defined industrial processes, and in many places radiation and radiotracer techniques are now in routine use.

The thin layer activation (TLA) method is one of the most effective and precise methods of corrosion and wear measurement and monitoring in industry, used for on-line remote measurement of the wear and corrosion rate of critical parts in machines or processing vessels under real operating conditions. The TLA technique was developed in the early 1970s in a number of industrialized countries. While most of the development and commercial applications took place in developed countries, some laboratories in developing countries have introduced this technique for tribological investigations.

A coordinated research project (CRP) on the TLA method and its application in industry was carried out in 1991–1995. The CRP contributed to a better understanding of the TLA method and the development of new measuring and application techniques. In 1997, the IAEA issued IAEA-TECDOC-924, The Thin Layer Activation Method and Its Applications in Industry, based on the CRP results and describing its main achievements.

Since that time, radiotracer techniques for measuring wear and corrosion have developed, the range of potential applications has expanded, and techniques have become more accurate and technically and economically competitive. Developing Member States with appropriate and relatively simple radiation facilities and detection capabilities are starting to use the TLA method, which has already proved to be a safe, efficient, precise and cost effective technique in industrialized countries. It is important to make the technique better known to industry and to make end users aware of its benefits.

This publication is an update of IAEA-TECDOC-924. It is intended to assist radiation and radioisotope technologists in promoting these competitive technologies to end users. It is also intended to provide managers and decision makers in Member States with a better understanding of the role of radiation and radioisotope technologies in everyday life. The publication presents different aspects of the methods and techniques, as well as typical case studies; highlights important achievements of the technology in research and development; and demonstrates the present and potential value of the industrial applications of the technology.

The IAEA officer responsible for this publication was P. Brisset of the Division of Physical and Chemical Sciences.

EDITORIAL NOTE

This publication has been prepared from the original material as submitted by the contributors and has not been edited by the editorial staff of the IAEA. The views expressed remain the responsibility of the contributors and do not necessarily represent the views of the IAEA or its Member States.

Neither the IAEA nor its Member States assume any responsibility for consequences which may arise from the use of this publication. This publication does not address questions of responsibility, legal or otherwise, for acts or omissions on the part of any person.

The use of particular designations of countries or territories does not imply any judgement by the publisher, the IAEA, as to the legal status of such countries or territories, of their authorities and institutions or of the delimitation of their boundaries.

The mention of names of specific companies or products (whether or not indicated as registered) does not imply any intention to infringe proprietary rights, nor should it be construed as an endorsement or recommendation on the part of the IAEA.

The authors are responsible for having obtained the necessary permission for the IAEA to reproduce, translate or use material from sources already protected by copyrights.

The IAEA has no responsibility for the persistence or accuracy of URLs for external or third party Internet web sites referred to in this publication and does not guarantee that any content on such web sites is, or will remain, accurate or appropriate.

CONTENTS

1. INTRODUCTION

1.1. BACKGROUND

Wear and corrosion substantially limit the endurance and reliability performance of nearly all machines, industrial equipment, transportation systems, power plants, pipes etc. Consequently, the development of effective methods of detection, measurement and monitoring of such processes is of great importance. Appropriate methods of monitoring can prevent dangerous accidents during operation of industrial installation and provide production losses due to unforeseen breakdown of machinery.

When the surfaces are not accessible or are concealed by overlaying structures, nuclear methods such as Charged Particle and Neutron Activations, become the most powerful tool for measurement and monitoring of wear and corrosion [1]. Gamma-radiation passes through the materials and even low activities can be detected with high sensitivity and precision.

The neutron activation method by using nuclear reactors produces homogeneous activity distribution in the whole sample (bulk activation). The advantage of this bulk activation is that one can measure the average wear of every part of the irradiated sample that wears. However, the removed activity portion is so small compared to the total activity of the part, that it can only be measured in the cooling or lubricating liquid to reach a reasonable sensitivity. Thus, a large surplus activity is produced in the bulk, which allows the use of the method only in laboratories with suitable radiation protection [1].

To reduce the radiation dose to the user of this nuclear method and to increase its sensitivity concerning measurement precision and selectivity of the areas to be activated, the activation with charged particles was developed.

For the charged particles activation, different names are commonly used, like Thin Layer Activation (TLA) or Surface Layer Activation (SLA). A list of acronyms used for this activation, the measurement technology and equipment, is given at the end of this publication.

In the case of thin layer activations with charged particles only the surface layers in the micrometer (μm) range are activated and only that area on the total part being subject of the wear or corrosion. The sensitivity is high because the specific activities can be very high, compared to the now lower total activities. Often activities below the free handling limits are possible.

Radiotracer techniques of machine part wear and corrosion control being applied in different fields of modern industry are in constant progress. The modifications of the technique differ in method of radioactive label creation in the material of components under investigation.

When the above-mentioned procedures of radioactivation by neutrons or charged particles cannot be used because of the structure of the material (e.g. polymers), alternative methods to produce activity in the surface layers are used [1].

Some alternative methods are (this list does not claim to be exhaustive):

- Isotope diffusion; activity in the sample is produced by allowing controlled diffusion of radioactive tracers from special solutions into the surface of the sample;
- Recoil activation; heavy radioactive products from nuclear reactions with several MeV energy are implanted into a very thin layer (UTLA = Ultra Thin Layer Activation) with relative low activity in the sample;
- Irradiation with radioactive beams; implantation of radioactive nuclei;
- Radionuclide absorption;
- Thermal-spraying;
- Galvanic deposition;
- Surface treatment with radioactive electrode.

1.2. OBJECTIVE

The main objective of this publication is to evaluate issues related to the radiotracer methodologies and technologies as applied for monitoring and measuring the wear and corrosion in industrial processing and manufacturing.

1.3. SCOPE

The general scope of this publication is:

- To discuss different aspects of the methods and techniques;
- To present typical case studies recorded mostly from developed countries;
- To highlight important achievements of the technology in research and development, as well in commercial services;
- To demonstrate the present and potential values of industrial applications of the technology;
- To assist radiation and radioisotope technologists in promoting radiation methods for monitoring the wear and corrosion in processing plants and vessels.

1.4. STRUCTURE

This publication is organized into eight sections and 2 annexes.

Section 1 is the introduction, which contains the background, objective, structure, acronyms and a short history of radioisotopes applied for wear and corrosion measurements. The activation method is presented in the Section 2, where the bulk neutron activation and its experimental design are presented.

The Thyn Layer Activation (TLA) methodology is covered in Section 3, which describes the principles of the TLA method, the TLA theory, the advantages of the TLA compare to conventional techniques, and scope of applications.

The Section 4 is dedicated to radiation measuring methods, especially to the direct and indirect measurement, as well as detection systems such as detector selection and data acquisition system. Section 5 deals with application of radiotracer techniques for wear and corrosion measurements, illustrating with case studies.

Section 6 presents conclusions, while Section 7 gives the references.

Annex I provide the theory of the charged particle activation. Annex II gives the tables of nuclear reactions, cross sections and activation parameters needed for applying the technology.

2. THE ACTIVATION METHODS

2.1. BULK NEUTRON ACTIVATION

One of the first methods employed to create radioactive isotopes in wear components is still commonly used today. Thermal neutron activation is also referred to as bulk neutron activation since the entire (bulk) of the part is made homogeneously radioactive using a neutron flux within a nuclear reactor. This method is often cost effective as research reactor time is typically less costly per hour than accelerator beam time and multiple parts can be made radioactive simultaneously. The method is also highly sensitive. Depending upon the specific activities of the components and total fluid volume of the test system, wear rates of less than 1 nm/h can be accurately measured.

Use of this process to activate engine components for wear testing began in the early 1950s as research reactors began to come online. In this process, engine components of interest are sealed into a watertight vessel and lowered into or near the core of a nuclear research reactor. In the reactor the components are exposed to a strong thermal neutron flux typically on the order of 10^{12} to 10^{13} neutrons/cm^2/sec. Since neutrons are inherently neutrally charged, they are not affected by the atomic electron clouds and easily penetrate through the component material. A small percentage of thermal neutrons directly interact with the atomic nuclei within the structure through nuclear collisions. If there is sufficient collision energy for the neutron to penetrate the nucleus it can cause a nuclear reaction. The specific reaction and resulting isotope from the collision is dependent upon the parent nucleus. For example, the nuclear reaction for Iron 58 (^{58}Fe), a naturally abundant isotope in steel, when bombarded with thermal neutrons is:

$$^{58}\mathrm{Fe}(n,\gamma)^{59}\mathrm{Fe} \tag{1}$$

The resulting unstable isotope is Iron 59 (^{59}Fe), which has a half-life of 44.5 days and emits two useful high energy gamma rays (1099 keV, 1291 keV) when it decays.

For a given nuclear reaction, the combined probability of interactions resulting in a particular isotopic nucleus is known as the cross section. Nuclear cross sections are empirically derived and summarized in nuclear data tables. Sources for these values can be found in literature and on the internet and a limited set has been included in annexes. By combining the neutron flux of the reactor at the core position of the component undergoing irradiation, the time of exposure, the composition of the material and the reaction cross section, the total and specific activities can be determined through the equation:

$$A = \frac{m}{w} * \theta * 6.023 * 10^{23} * \sigma * \phi * \left[1 - e^{-\lambda * t_{irr}}\right] \tag{2}$$

Where,

A = activity (dps)
m = total element mass in irradiated sample (g)
w = atomic weight
θ = isotope abundance
σ = cross-section (barns)
ϕ = neutron flux (n/cm^2/sec)
λ = decay constant ($0.693/t_{1/2}$)
$t_{1/2}$ = isotope half-life (hours)
t_{irr} = irradiation time (hours)

As an example, for a typical activation for a radioactive tracer wear test using the concentration method for a light duty gasoline engine, an 80 hours exposure to a thermal neutron flux of 6.8 $.10^{12}$ n/cm^2/sec would produce 96.2 MBq of ^{59}Fe in a single piston ring.

2.1.1. Experimental design

Further description of the various measurement methods for radioactive tracer wear measurement will be covered later in this document. With neutron activation, the entire component becomes radioactive, and thus the signal-to-noise ratio becomes too high for direct measurement of loss-of-activity to be feasible. Bulk activated parts therefore require use of the indirect oil accumulation method.

The first step in designing a radiotracer experiment is to determine the base metallurgy at the wear surface of the component(s) of interest. The metallurgy must contain a uniform distribution of elements in sufficient quantity that when exposed to a thermal neutron flux can be transmuted into radioactive isotope(s) of sufficient half-life and sufficient activity to be able to make the measurement. The created isotopes must also emit gamma radiation when they decay.

Elemental analysis of wear surfaces is typically performed by cross-sectioning the wear component and using scanning electron microscopy (SEM) combined with energy dispersive X ray spectroscopy (EDS). Figure 1 shows an example SEM for a top piston ring from a diesel engine.

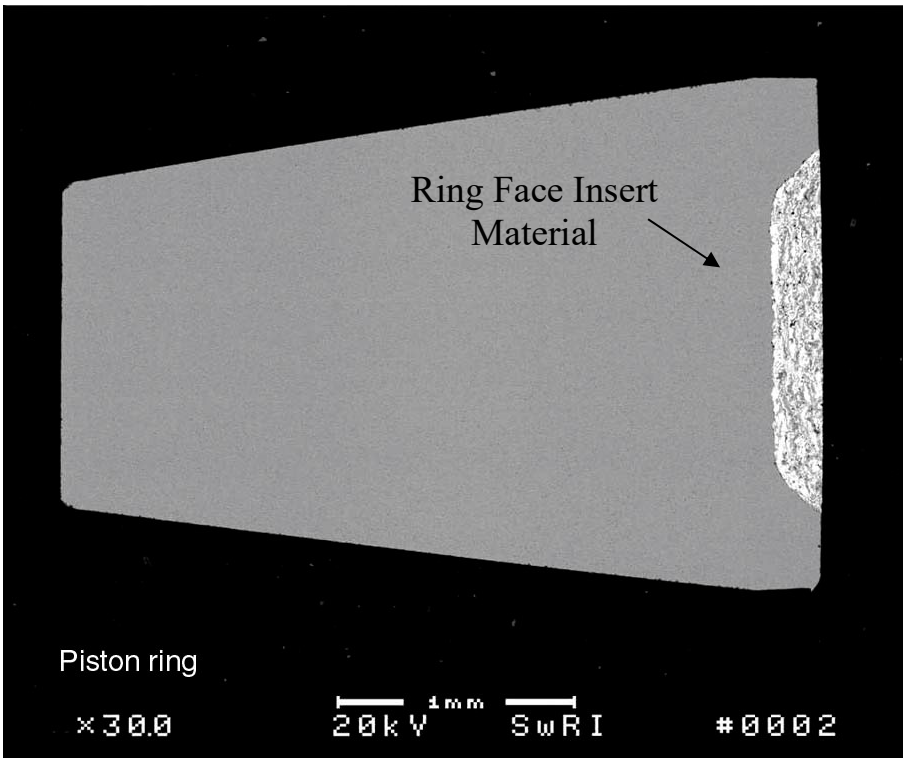

FIG. 1. SEM of diesel piston ring cross-section [2].

Figure 2 shows results of EDS analysis of the ring face insert [2].

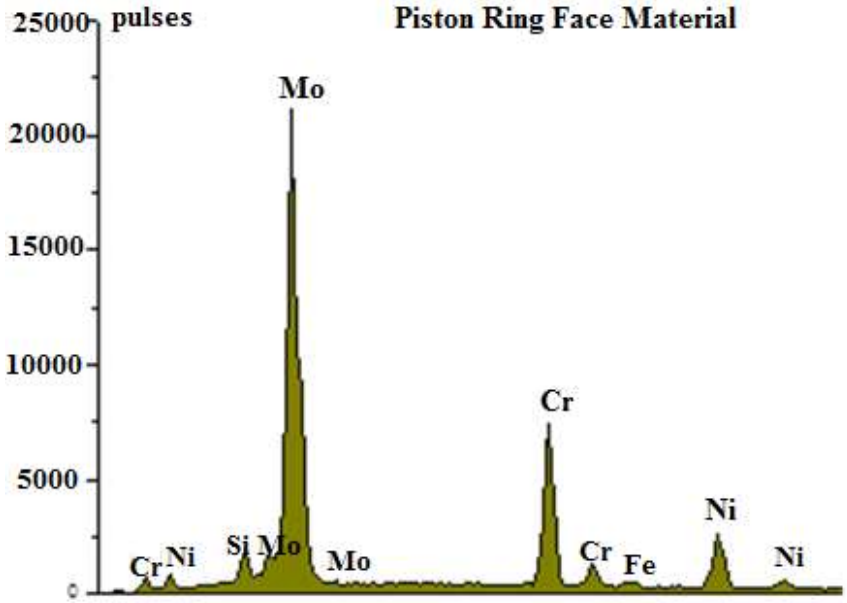

FIG. 2. EDS analysis of piston ring insert [2].

When designing an experiment, there are several considerations that must be taken into account to determine how much activity is needed in a given wear component. These include:

- Safety;
- Regulatory restrictions;
- Cost;
- Amount of wear expected;
- Wear resolution desired;
- Length of testing expected;
- Volume of fluid in system;
- Measurement system efficiency.

2.1.2. Neutron activation calibration

In order to convert measurements from a gamma spectroscopy system to absolute engineering units useful for wear measurements a calibration can be performed. Note that calibration is not strictly necessary if the interest is only to make relative measurements based upon the same experimental setup. In this case counts per unit time can be directly compared after making appropriate time decay corrections.

In order to perform a calibration, calibration samples of the same metallurgy as the part to be measured are prepared. As an example, for engine rod bearings, scrapings of the inner wear surface of identical bearings from the same manufacturing lot are made. These scrapings are carefully weighed and placed in the activation canister along with the rod bearings to be activated. In the reactor, these calibration samples are exposed to the same neutron flux for the same amount of time as the measurement components.

Once activated, the calibration samples are removed from the activation canister, dissolved in an acidic solution and diluted to a series of known liquid concentrations. The calibration liquids are placed in the

detector measurement well using the same geometric setup as in the wear experiment. Counts are collected over a fixed period of time and gamma spectroscopy is performed. The measurement is repeated over the series of concentrations to develop a calibration curve for the component of interest. A linear regression is performed on the curve to determine the calibration factor.

2.2. THIN LAYER ACTIVATION METHOD

The physical basis of the TLA is explained in Fig. 3. If, for example, iron material is bombarded with high energy protons or deuterons of an accelerator, the particles penetrate into the material, slow down and come to rest after some millimetres way in the iron. Some of the protons or deuterons react with the iron nuclei according to the following nuclear reactions:

$$^{56}Fe(p,n)^{56}Co \qquad ^{56}Fe(d,n)^{57}Co \tag{3}$$

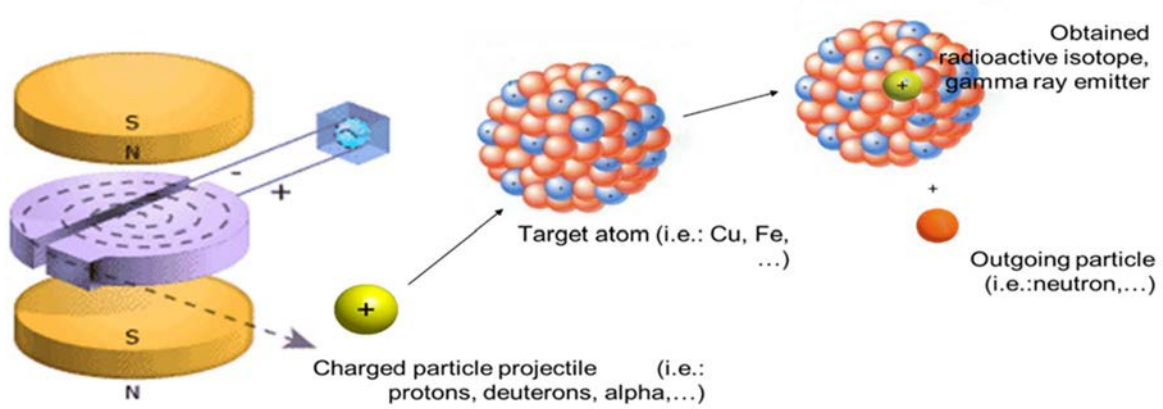

FIG. 3. Working principle of charged particle activation [3].

The stable ^{56}Fe atoms are converted to the radioisotopes ^{56}Co or ^{57}Co. The probabilities (cross sections, Fig. 4) of such nuclear reactions very much depend on the energy of the incident particles. The energy of the incident protons or deuterons can be chosen in such a way that a region of nearly constant, homogeneous activity is produced directly on the surface of the material or machine part.

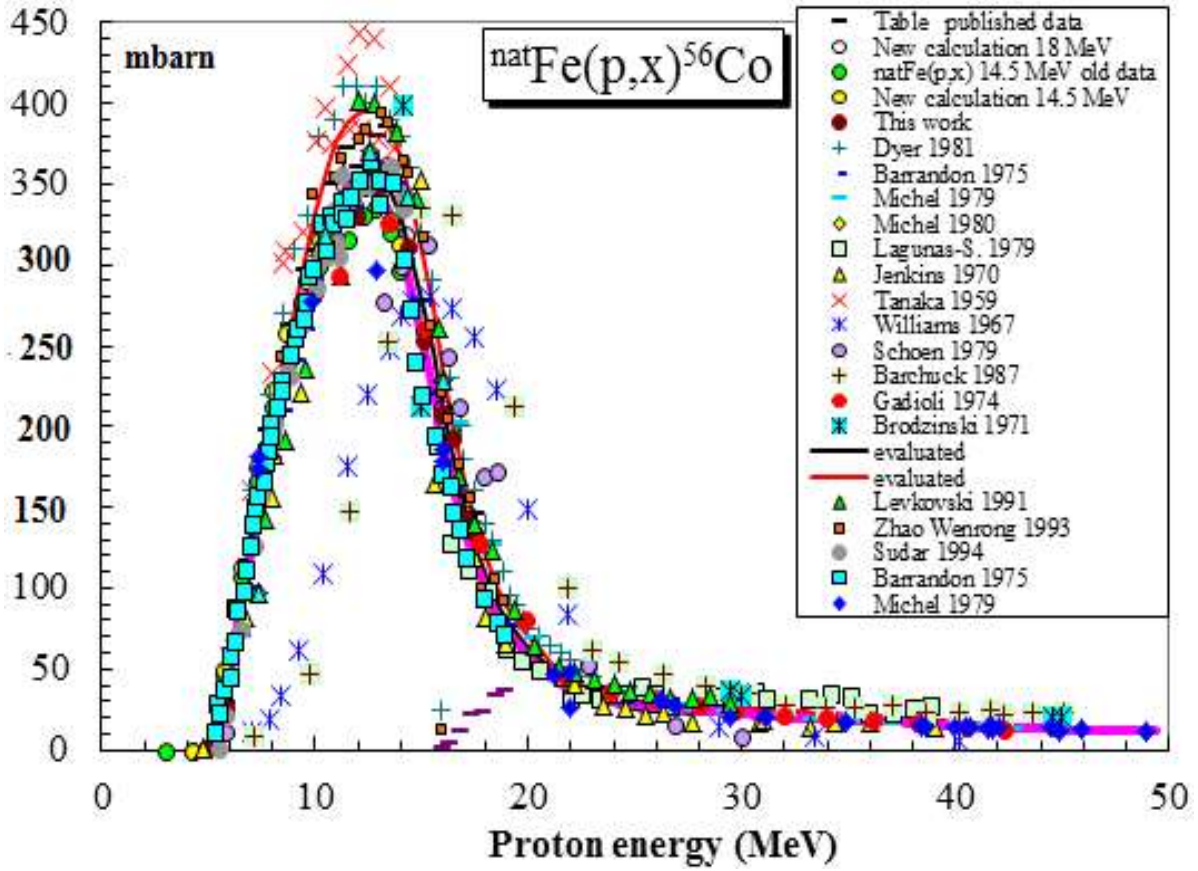

FIG. 4. Experimental measurements for the $^{nat}Fe(p,n)^{56}Co$ cross section up to 50 MeV bombarding energy[4].

The length of the linear region for measurement SM mainly depends on the activated material and can be varied by technical measures in the range between 20 µm and 1 mm or even more, according to the measurement problem. Figure 5 presents an example for a measured activity-versus-depth distribution of ^{56}Co in an iron alloy [5].

As shown in the above example all steel alloys used in mechanical engineering, stellite, sintered metal, non-iron metals and their alloys of Al, Co, Cr, Cu, Mo, Ni, Pb, Sn, Ti, V, W, Zn can be activated in that way with a linear region for measurement in the surface.

Important for this technology is the linear region for measurement, which means a homogeneous activity concentration at the surface of the material. The measured amount of wear is a mean value averaged over the radioactive labelled area. Inside this area the local wear depth can vary like, for example, on a piston ring surface. Only if the labelled area is very small, like a spot of 2 or 3 mm in diameter, an inhomogeneous activity distribution could be acceptable.

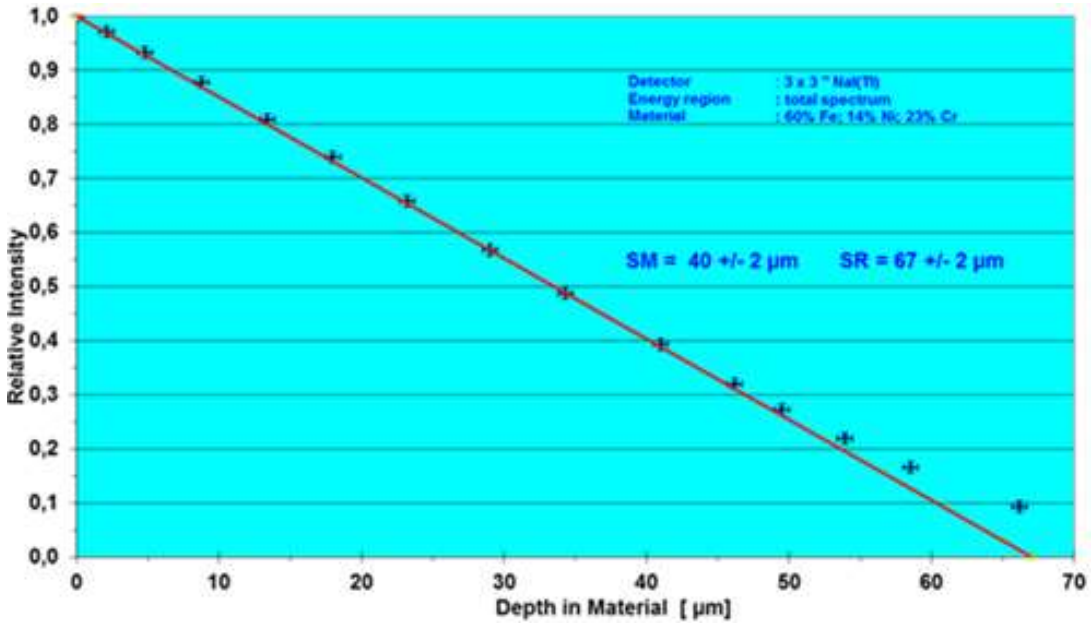

FIG. 5. Example for a measured activity-versus-depth distribution of ^{56}Co in an iron alloy [5].

In special cases, where the excitation function curve (cross section) has a local maximum in the energy range in question, one can also produce constant activity distribution within a thin surface layer section. In this case a depth profile curve is not necessary, only a number (kBq/µm) and its validity range must be given, which makes the life of the user much easier. For example, the ^{nat}Cu (p,x) ^{65}Zn nuclear reaction, where a copper containing material is irradiated by proton beam producing constant activity down to a depth of 10.9 µm.

The necessary amount of activity for a given task of wear measurement can be estimated by knowing the main parameters of the measurements (detector type, detector-source distance, machine wall thickness and material, expected wear rate, expected wear depth, etc.). To produce this activity in a given material (metal, alloy, etc.) a deep physical knowledge is necessary. To simplify this calculation IAEA provides an on-line or downloadable tool based on a TLA database and Excel calculation sheets, which makes possible to calculate the necessary irradiation parameters as well as the resulted isotopes and activities. The software is available at https://www-nds.iaea.org/tla/ [6].

2.3. RECOIL NUCLEI IMPLANTATION (UTLA)

In technologically advanced sectors like metallurgy, car industry, industry of energy, the race to better competitiveness brings continuously to improve on the one hand quality of the products and on the other hand the productivity of the production lines. In both cases, the use of materials presenting the best wear and corrosion resistance is a guarantee of success. The endurance and the durability of the components can be evaluated starting from small matter losses. In order to effectively test innovative materials in reasonably short times, the research laboratories and industries need very sensitive techniques to measure significant and precise matter loss on a nanometric scale.

The UTLA (Ultra Thin Layer Activation) technique allows to access to nanometer sensitivity and to radiolabel all materials, including materials that cannot be directly activated by charged particles beam, such as plastics or some ceramics [7-9]. It consists in the implantation of heavy radioactive nuclei of a small area of the piece which will be subjected to wear or corrosion. Heavy radioactive nuclei are produced by irradiation of a sacrificial thin foil with ^{1}H, ^{2}H, or ^{4}He beam.

The thin foil (thickness of few micrometers) of elementary composition A bombarded by the primary beam a is activated following the nuclear reaction A (a,b) B*. Some generated radioactive heavy nuclei B*acquire sufficient kinetic energy (maximum energies of a few hundred keV to a few MeV) to recoil out of the target and be implanted in the exposed material. The implantation may be realized with the sample of interest in frontal or in tubular geometry. A mask is placed on the piece of interest to define an area to be implanted. This mask limits the B* implantation to an acceptance cone [Φmin,Φmax], where Φ is the angle between the velocity vector of the radioactive nucleus and the primary beam. After being transmitted through the thin target, the incident beam a. is stopped by a Faraday cup [7, 10].

Figure 6 shows tubular implantation geometry [7].

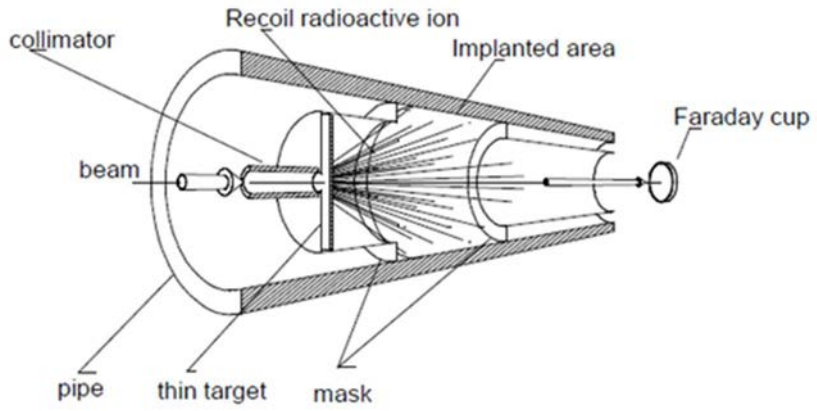

FIG. 6. Tubular implantation geometry [7].

After activation, the piece is placed in the real conditions of its operation, where it is subjected to wear. The direct measurement technique is implemented to follow the residual activity of the part as a function of test time. The reduction in the residual activity corrected to the natural radioactive decays is directly transformed by using the calibration curve to wear rate.

The calibration curve reports the residual activity in relative value A/A_0 (where A_0 indicates the initial activity of the studied part) according to X (depth of material loss). The activated depth being submicrometric, its measurement is performed by implanting several thin films with increased thicknesses of the studied material. Films of composition similar to the sample of interest are deposited on substrates by physical vapor deposition (PVD) technique.

The thickness of films is measured by RBS technique [11]. The pair film-substrate is positioned in same irradiation geometry than the investigated piece to preserve the acceptance cone [Φ_{min},Φ_{max}]. After irradiation, the total activity A_0 implanted in the pair film-substrate is measured with a HPGe detector. A chemical attack specific to the thin film enables us to dissolve the film avoiding any transfer of radioactive ions from the substrate to the chemical solution.

The radioactivity A of the substrate is then measured. The ratio A/A_0 expresses the residual radioactivity after a surface loss equal to the film thickness. The irradiation of various thickness films enables to establish the correlation between the residual activity and the surface loss or the calibration curve (Figure 7).

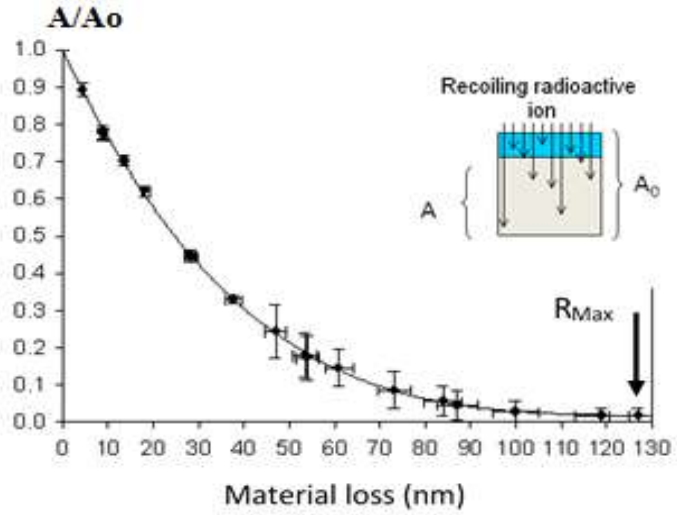

FIG. 7. Calibration curve A/A0=f (x) with ^{56}Co nuclei implantation into nickel (16 MeV protons, tubular geometry and acceptance cone [30°-38°])[7].

The procedure is as follows:

- Thin layer of material deposited on substrate;
- Thickness (< 1µm) of film is measured by RBS;
- Irradiation of samples;
- Measurements of the total activity Ao of the film-substrate pair;
- Chemical dissolution of film to measure A.

The long step of measurement of the calibration curve could be considered as a brake of the extension of UTLA applications. An appropriate computer simulation code (IRIS: Ion Recoil Implantation Simulation) is related in literature to calculate $A/A_0 = f(X)$ [12-13].

2.3.1. Implantation depth

In case of a two body ***A(a,b)B**** nuclear reaction, the E_4 kinetic energy of ***B**** recoil nucleus as a function of Φ emission angle is calculated from the rules of energy and momentum conservation. The value of R_{max} maximum implantation depth can be calculated by SRIM software by the following formula in frontal irradiation geometry [14]. The recoil nuclei ***B**** are supposed to be in their ground state.

$$R_{max} = R\left(E_4(\phi_{min})\right) \cdot \cos\phi_{min} \quad (4)$$

Where: R is the projected range of ***B**** in the studied matrix (nm)

As the angle and energy spectrum of the B* recoils depends on the implantation angle, the irradiation conditions of the calibration curve must be rigorously similar to the ones defined for the studied piece. The UTLA technique allows to radiolabel a depth from 0,1 to 1µm.

2.3.2. Implantation yield of recoil nuclei

For ***A(a,b)B**** nuclear reaction, the ***B**** implantation rate is linked to the cross section at the incident beam energy, the recoiling energy spectrum and the angular acceptance. The number of ***B**** heavy nuclei recoiling out of the target is about 10^{10} to $2 \cdot 10^{11}$ for $2 \cdot 10^{17}$ incident particles.

Only a fraction of these nuclei is emitted in the [Φ_{min},Φ_{max}] acceptance cone and then implanted in the sample. In experiments performed with the $^{56}Fe(p,n)^{56}Co$ nuclear reaction, the implanted ^{56}Co radioactivity is about 1 kBq for a charge of 40 mC (few hours of irradiation) received by the iron foil and for an [30°- 40°] acceptance cone.

2.4. RADIOACTIVE ION IMPLANTATION

Polymer materials like PTFE, PEEK, PE, PA, PAI and so on, as well as their composites are by orders of magnitude more radiation-sensitive as metallic materials. Therefore, it is not possible to label such materials by bombardment with Protons or Deuterons. One possibility to label such materials is the implantation of radioactive ions. So most suitable isotope for this implantation is ^{7}Be with a half-life of 53.3 days and a single γ-line at 478 keV.

The implantation of radioactive ions like ^{7}Be has by 8 orders of magnitude less affect to the radiation sensitive materials in comparison to the classic labelling procedure. The wear characteristics of the materials are not affected by the labelling. The concentration of the radioactive atoms in the material is less than one per hundred billion unmodified atoms (<10-11). The radioactive layer thickness is only in the range of some µm. Therefore, one speaks of Ultra-Thin-Layer-Activation UTLA.

The ^{7}Be activity is produced by bombarding Lithium with Protons of a cyclotron. With chemical and mechanical processes a cathode for a sputter-ion-source is produced. The ^{7}Be ions are then accelerated up to 8 MeV in a linear accelerator. The part to be implanted must be inside the vacuum of the accelerator and beam line. Figure 8 gives the principle of the ^{7}Be implantation, while Figure 9 presents the ^{7}Be distribution into a PTFE target.

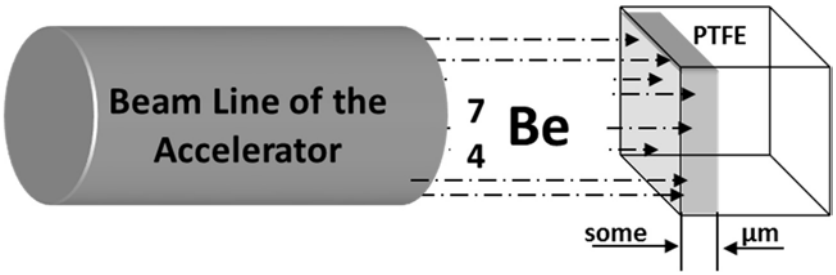

FIG. 8. Principle of the ^{7}Be implantation [8].

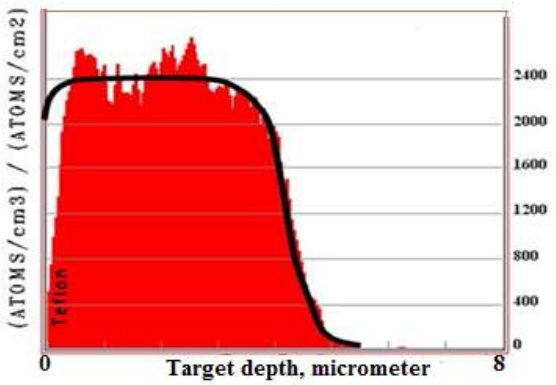

FIG. 9. ^{7}Be distribution in a PTFE target [8].

The activity levels of radioactive ion implantation are far below the free-handling limit. The handling of such parts is very easy and no license is required for such handling. There are no other radioisotopes in the sample than the implanted one. Typical total activities of ^{7}Be implanted into e.g. a bearing are 200 to 400 kBq.

2.5. QUALITY CONTROL - INFLUENCE OF IRRADIATION ON PHYSICAL CHARACTERISTICS OF THE MATERIAL

When using radioactive isotopes for wear measurement, the concentration or depth distribution of these isotopes in the sample or component has to be known precisely, as the measured activities need to be converted into a wear height or wear volume.

The terms “activity depth profile” or “depth profile” are used to describe the isotope concentration or depth distribution. The depth profile is strongly dependent on which irradiation process is used: neutron (bulk) activation, thin layer activation or recoil implantation.

With neutron activation, a homogenous concentration of isotopes is generated throughout the whole irradiated sample. In contrast, thin layer activation and recoil implantation do not result in a homogenous concentration through the whole sample, but rather an accumulation of activity close to the irradiated surface.

There are two ways to determine the depth profile - either by measurement, or calculation based on irradiation beam parameters and published cross sections for nuclear reactions. Knowledge of the activity depth profile and the corresponding cross section for a certain material can be seen as equivalent – they can be used to calculate each other.

In practice, the usual approach is to calculate the cross sections for chemically pure materials by measuring the depth profile for these elements. The cross sections are subsequently used to calculate the depth profile for more complex materials, such as alloys. This is done by superimposing the cross sections for the alloy elements according to their concentration in the alloy. This approach can be assumed to be valid for materials if their structure is homogeneous, the chemical elements are distributed uniformly and the irradiation is perpendicular.

The two main approaches for the calculation of cross sections found in literature are based on activity measurement (as other methods generally lack the necessary sensitivity):

- Step-by-step removal of thin layers from a solid body via cutting, grinding or etching with subsequent activity measurement [15,16]: These methods are valid as long as the influence due to the removal process itself is negligible compared to the thickness of the removed layer. Squeezing or inaccurate thickness and parallelism of the removed slices affect the accuracy of the depth profile. The accuracy of grinding or etching methods suffers from intermixing of different layers and subsequent smearing of the activity distribution.

- Irradiation of a stack of foils and activity measurement of each foil [17, 18]: The foils are usually separated by a thin layer, which is used as a checkpoint for the energy of the irradiating particles between the foils [19]. In order to avoid possible reflection and scattering effects, the stack-of-foils method is mainly applied to perpendicular irradiation. This approach is the benchmark for cross section measurements for the pure elements with depth profiles of several hundreds of micrometres depth. The sensitivity of this approach for depth profile measurements is determined by the limitations of foil manufacturing processes regarding minimum foil thickness (iron foils: typically, ~10 μm; 7.6 μm used by Kiraly [20]) and variations in thickness (e.g. roughness).

Both methods are subject to a further problem, which is the accurate measurement of the thickness of each layer. For cutting, grinding or etching, the measurement of the removed layer is mostly done via a

micrometre screw or similar techniques. Taking roughness and alignment into account, this limits the sensitivity of the profile measurement to some micrometres. Similar considerations can be made for the thickness measurement of the foils.

In summary, both approaches suffice for measurement of depth profiles of several 100 µm, deriving stopping powers [20] and consequently nuclear cross sections. In literature, the uncertainty of these cross sections is given in the range of a few percent. For the measurement of shallower depth profiles, an advanced profiling method was developed [21-24]. A powerful tool for deriving activity depth profiles [25] is publicly available for customers of wear measurement with radioactive isotopes at: https://www-nds.iaea.org/tla/abouttla.html.

The TLA2 tool takes into account the beam parameters, material concentration and state of the art nuclear reaction cross sections. As a result of the calculation, the concentration of isotopes is obtained. By adjusting the beam parameters, a constant isotope concentration can be obtained for a certain total depth. A constant depth profile is the appropriate choice for most applications, in order to provide a direct correlation between measured activity and wear.

3. THIN LAYER ACTIVATION METHODOLOGY

3.1. PRINCIPLES

The working principles of the Thin Layer Activation (TLA) method is illustrated by the example of a combustion engine, very schematically delineated in Figure 10 by the piston ring and the cylinder wall. Subject to wear measurement is the cylinder wall, which has been labelled in its critical zone around the upper dead point of the piston ring (TDC Top Dead Centre) by thin layer activation at a cyclotron with protons on iron. A detector outside the engine monitors the activity of the cylinder wall in TDC.

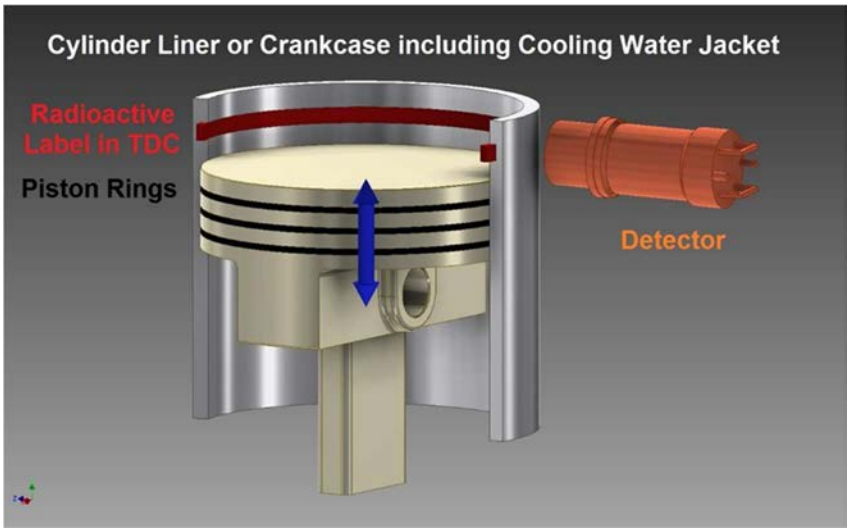

FIG. 10. Principle of TLA method (Courtesy A. Kleinrahm).

Figure 11 shows a simplified calibration curve of total activity versus material depth [25].

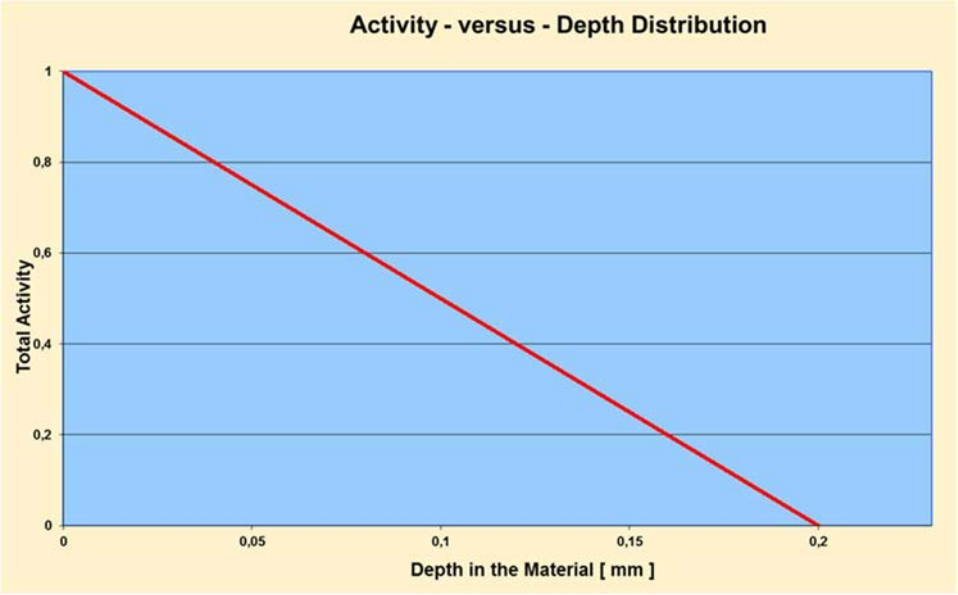

FIG. 11. Simplified calibration curve of total activity versus material depth [25].

The thickness of the radioactive surface layer is adjustable by beam energy and angle alteration to within 20 micrometres (μm) up to around 0.2 mm, according to the expected total wear measurement depth at the end of the measurement period.

The characteristic gamma radiation emitted from the labelled zone of the component penetrates the cylinder wall, water jacket and housing wall without major attenuation and is recorded by a radiation measuring equipment (detector) appropriately located outside the machine, as indicated in Fig. 1 (upper part). The lower part of the figure shows the linear relation between measured activity and wear depth, the calibration curve. Via the variation of activity caused by loss of material the wear of the component can be observed easily and exactly. It is essential that the radioactive wear particles must be removed from the area where they were produced.

3.2. THEORY OF THE TLA

When a beam of accelerated ions enters a material, the particles rapidly lose energy and come to rest at a well-defined depth (Figure 12). A small number of charged particles interact with atomic nuclei of the material, induct a nuclear reaction and produce radioactive isotopes. The concentration of radioactive atoms produced within the under-surface layer is very low (1 to 10^6 up to1 to 10^{12}). The activation produces only a minute level of radioactivity, typically 100 kBq up to some MBq, depending on the isotope and the desired test length. Once the radioactive label is created under the surface, it decays with the emission of gamma rays.

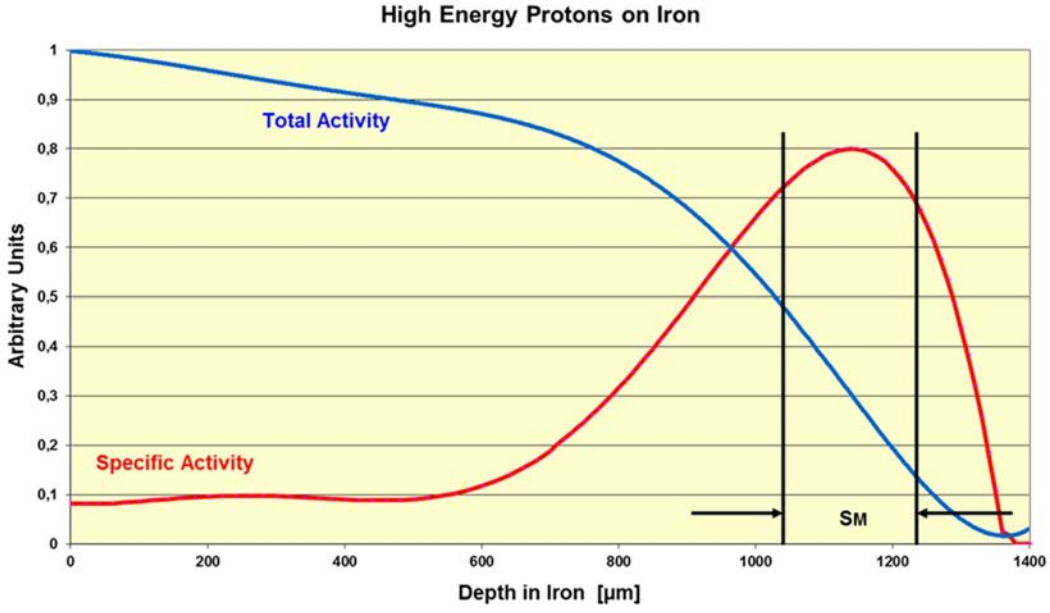

FIG. 12. The scheme of TLA: Dependence of specific and total activity concentration on depth for irradiation of iron by 25 MeV protons. The area between black vertical lines indicates the depth range SM of approximately constant activity concentration [26]. SM is the linear range that can be used for wear measurements.

The parameters of a label must correspond to the problem under consideration in the best way. Its radionuclide composition must be utmost simple to have reliable measurement results in industrial conditions. The depth of radioactive layer must be comparable with the expected loss.

The activity versus depth distribution must be constant or linear in depth and precisely known as it is used to convert the decrease of counting intensity in linear or mass destruction parameters.

Creation of a label adequate to the problem needs a certain information base including range-energy data in matter, values of nuclear reaction thresholds, thick target yields and their energy dependence. Ranges of charged particles in different elements are well-known and available information [27] permit to select the appropriate particles energy for a specific problem. Ranges in compounds and alloys maybe calculated according to Bragg's formula and the depth d of the radioactive layer is determined from range values. Q-reaction values and threshold energies are tabulated [28] in handbooks, but one must bear in mind that real effective thresholds include the values of Coulomb barrier.

The TLA technique allows adjusting the thickness d of the label and thereby the sensitivity of the control.

The activation of chemical elements and the main construction materials in the majority of cases is well studied [29-31]; some recommendations are given in Table 1. These recommendations may serve only as a rough guide since a large variety of problems, materials and irradiation means may lead to another choice of radionuclides and solutions. For example, for lack of high-energy alpha particles the Al-alloys can be studied by any admixture. 2% to 4% Copper content allows to investigate the wear of this material by ^{65}Zn.

The main characteristic of material activation is the thick target yield [32]. The thick target yield is a physical constant, which depends on bombarding particle energy and describes the numerical ratio of radionuclides produced in nuclear reactions at certain irradiation conditions in a given matrix. It is an indicator of the usefulness of a nuclear reaction for TLA applications and is determined as the radionuclide activity per irradiation unit, usually μAh.

$$Y = \frac{A_o}{I}\frac{\lambda}{1 - e^{-\lambda t_i}} \tag{5}$$

Where:

- A_0 - the radionuclide activity at the end of irradiation.
- I - beam intensity (μA)
- λ - decay constant (s^{-1})
- t_i - irradiation time (s)

The yield from the alloy can be calculated from the formula:

$$Y_\Sigma = Y_i \times \eta_i \frac{R_\Sigma}{R_i} \tag{6}$$

Here Y_Σ - is the yield from the alloy, Y_i- the radionuclide yield from pure element *i* and η_ii - the weight proportion of the element *i* in the alloy.

3.3. MAIN ADVANTAGES OF TLA COMPARED TO CONVENTIONAL TECHNIQUES

The main conventional method to measure the wear of e.g. a combustion engine of a car or truck is to measure the dimensions of all parts before and after a long-time test run. In the best case, one knows afterwards the total wear of each interesting part but one does not know *when* this wear had occurred.

The best measurement systems are limited to an accuracy of 1 µm, maybe a tenth of a µm. If such an engine is reassembled after these dimensional measurements, again there will be a new running in of all parts, increasing the wear in total.

Another conventional method is the analysis of the metallic contents in the lubricating oil or in the oil filter. This method gives information about the actual status of the wear in the engine, but it cannot determine which part added to the iron or copper found in the oil.

The thin layer activation technology now allows the measurement of the wear or corrosion of only one, two or more selected parts of the complete engine. Even on these parts only the interesting areas of highest wear can be labelled. This method allows a non-destructive remote monitoring of surface degradation, including wear, corrosion and erosion.

The engine with the radioactive labelled part(s) runs on a test bench as before. While the engine is running, the wear behaviour of the labelled part(s) can be studied now. Dynamic measurements and transient wear or corrosion conditions can be examined. The quasi on-line measurements show every some minutes a new value of the wear status on the computer screen. Simultaneous measurements of surface degradation of two or more parts can be studied. The sensitivity of such measurements is very high. Wear rates in the scale of nanometres per hour (nm/h) can be detected, impossible with conventional methods. Parameter fields of the engine can be measured as well as fast changing operating conditions. All the measurements have no influence to the engine itself and, of course, the labelling does not change the materials behaviour.

That leads to a much shorter developing time of new engines, engine components, material formulations or surface coatings. More precise results in reduced time compared to conventional methods truncates the necessary time on test benches and of men power. The developing costs are reduced significant. With this activation and measurement methods it is even possible to optimize the running in procedures of components and complete engines. This is impossible with conventional methods.

3.4. SCOPE OF APPLICATIONS

Thin Layer Activation (TLA) method is prevalent in the following applications (Table 1):

TABLE 1. Typical applications of TLA

Industry	Applications
Automobile and engine industry	Piston rings (running surface and flanks) (Figure 4) Piston ring groves, piston skirt, all kinds of bearings: crankshafts, Camshafts (Figure 5) and tappets, connecting rods, etc. Cylinder liner, crankcase (Figure 6) Valves, valve seats and valve guides in cylinder heads Fuel injection nozzle, injection pump, fuel tubes All kind of gear wheels
Pumps	Pistons [33], all kinds of sealing surfaces of the housing, blades, roller, wheelers, etc.
Turbines	Blades, distance-pins, shaft bearings
Refrigeration systems	Compressor parts, Piston skirts, Cylinder wall, Shaft bearings, rod bearings Blades, roller wheels and valves
Printing machines	Needles, guidance, bearings
Textile industry	Knitting machines: guidance, needles, connecting rod and bearings mills: bearings, shafts, guidance
Railway	Wheel surface, brake discs (Figure 7), brake shoes, part of rails
Chemical industry	reactor vessels, tubes and pipes (Figure 8)), valve systems, nozzle
Oil industry	Oil qualification for automotive industry, Test of anti-wear and anti-corrosion properties of lubricants
Machinery	Fabricating tools, indexable inserts
Medical	Prosthetic joints [34]

Figures 13-17 show experimental setup of some characteristic TLA applications.

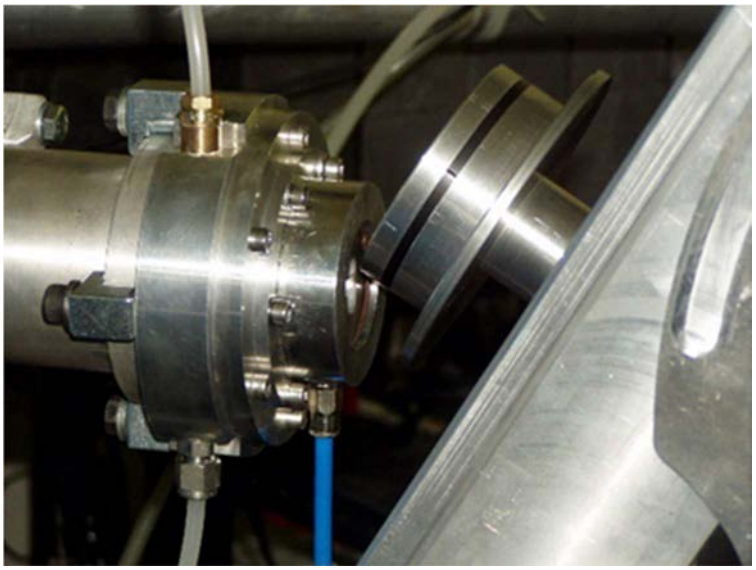

FIG. 13. Piston rings with DLC surface in activation position [35].

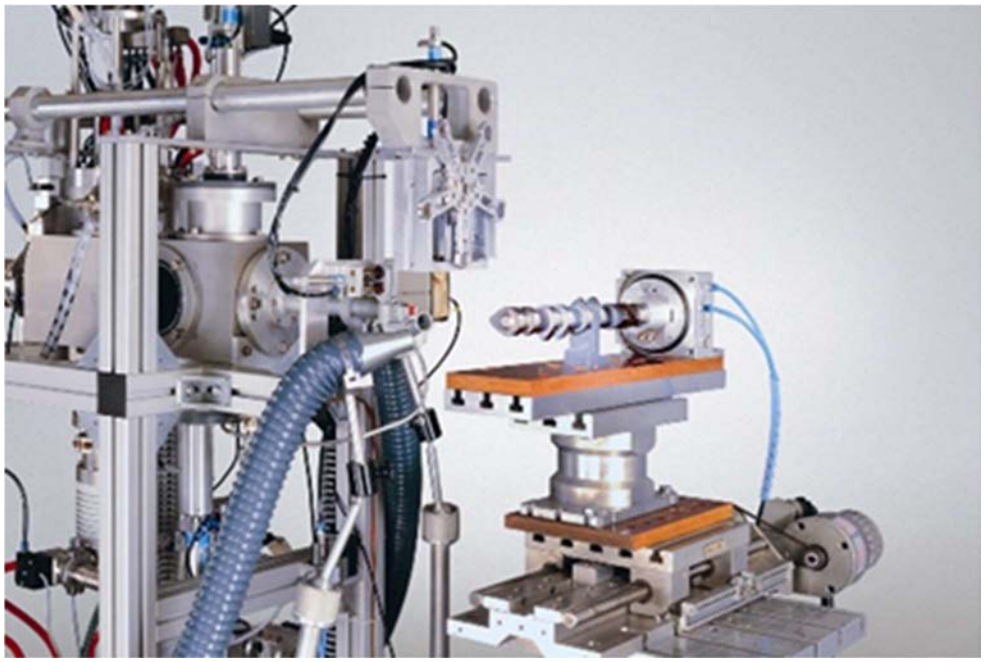

FIG. 14. Camshaft in activation position [36].

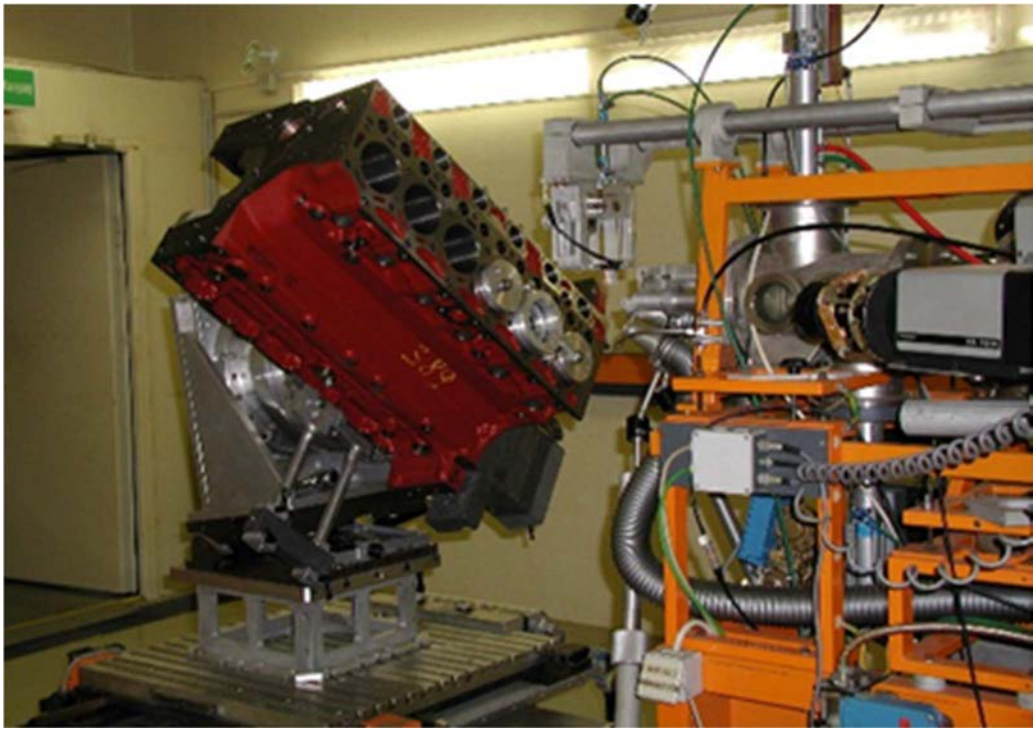

FIG. 15. Crankcase of truck engine to be activated in TDC of cylinder 2 [37].

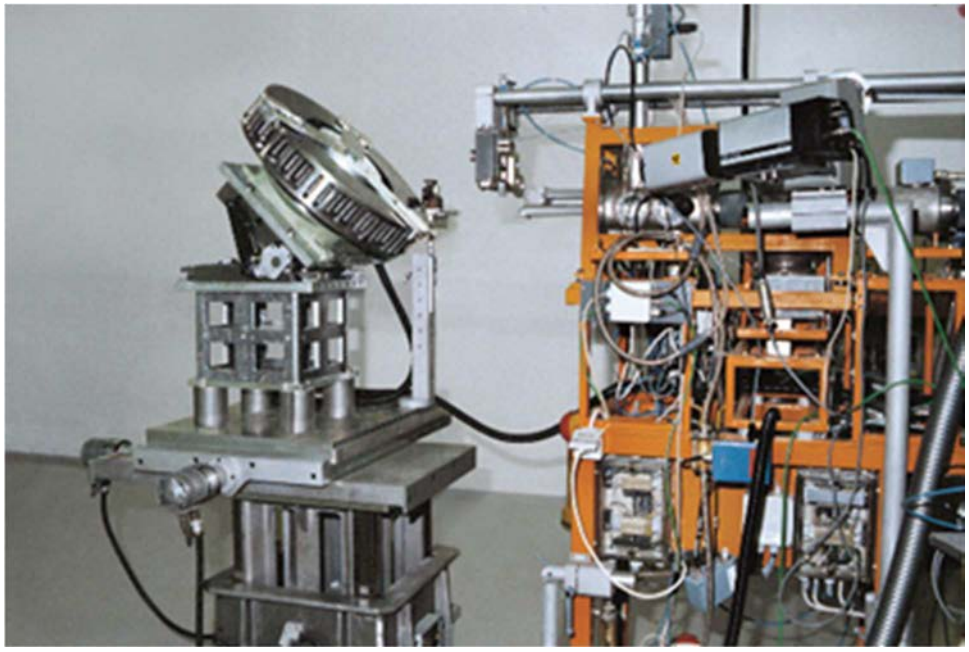

FIG. 16. Brake disc of a train in activation position [38].

FIG. 17. Elbow of an Ethylene pipe in activation position [39].

4. MEASURING METHODS

The measurement of the activity and activity change of the irradiated parts can be performed in two different geometries, called direct method and indirect method (concentration measurement) (Figure 18). In the first case of the direct method, the remaining activity on the wear part is measured. In the case of indirect method (concentration measurement), the active wear particles removed from the labelled area are measured. Both methods require that the produced wear particles are removed from their points of origin.

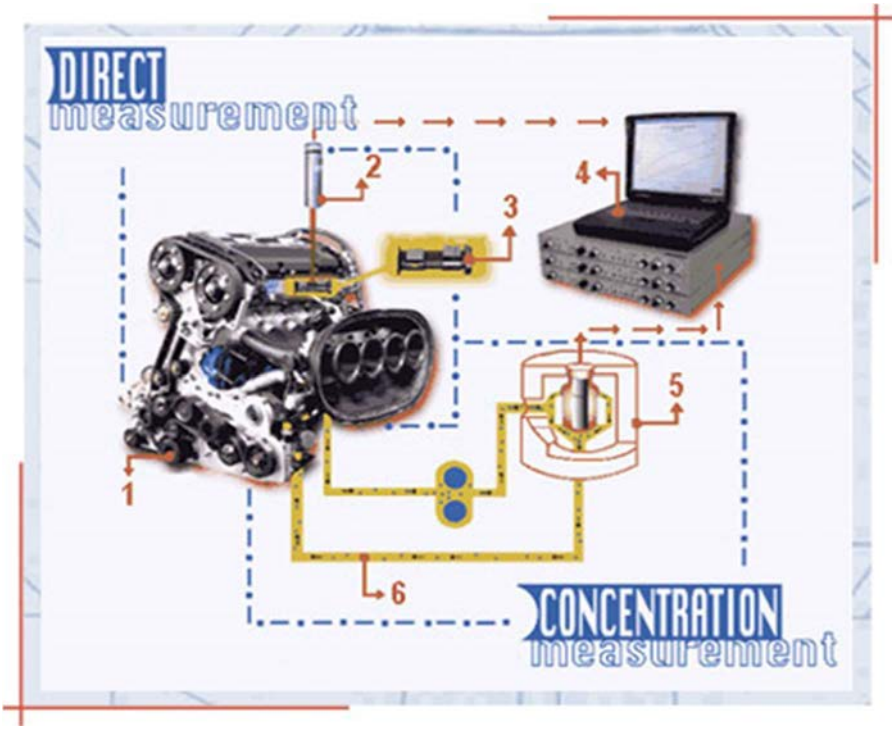

FIG. 18. Two measuring set-up for wear measurement with TLA. 1. Assembled engine in working condition; 2. Radiation detector for direct measurement; 3. Irradiated part built in into the engine; 4. Electronics and computer for data processing and evaluation; 5. Oil filter for catching worn radioactive part with radiation detector; 6. Cooling/lubricating oil circuit.) (Courtesy: www.ipnas.org).

During the direct measurement, the activity of the irradiated and assembled part is measured directly through the machine wall and the wear (material loss) is calculated from the change of the activity during the wear process, including a correction for the decay of the measured isotope. During the indirect measurement, the worn particles are removed by the cooling/lubricating liquid from the place of wear and collected e.g. by an appropriate filter. In this case the increase of the activity in the filter is measured.

For both geometries (direct and indirect measurement), the irradiation/activation of the part is usually performed in the same way. The only difference that could possibly arise is that different activities are required due to the different measuring geometries that are used in the two cases (different detector to sample distance). The wear resolution capacity of the indirect measurement method is lower than a few nanometers or micrograms at measuring times of some minutes, while the direct method has a higher resolution limit.

4.1. DIRECT MEASUREMENT

In the direct measurement, the radioactive area is monitored directly with a gamma spectrometer for loss in activity as wear particles are removed from the surface and transported away by lubricating oil or any medium. This mechanism results in a decrease in the total activity of the components. The direct technique is limited to either SLA or radioactive particle implantation methods, as the measured loss in activity from bulk activation would be too low to measure compared to the total activity of the sample.

Figure 19 shows the schematics of the direct measurement setup:
1. Activated part
2. Detector
3. Calibration curve (activity versus depth in the material).

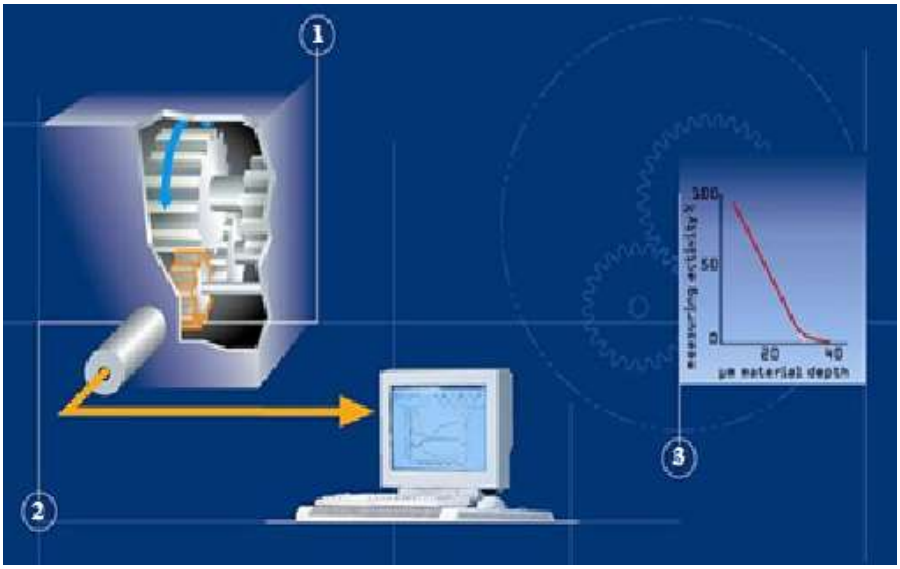

FIG. 19. Schematics of the direct measurement setup; 1. Activated part 2. Detector 3. Calibration curve (activity versus depth in the material) [38].

The typical setup for the direct measurement geometry shown in Fig 19 was used when the activated part was a cogwheel (or only a wear sensitive region of it) and the gamma detector is mounted near the housing. The typical calibration curve [39] (activity versus depth in the material) and possible wear curve (wear versus runtime) are stylized on the PC screen. Measurement sensitivity for this technique under well-controlled conditions is in the order of 1-2% of the total depth of activation.

In the case of direct measurement, the activated part is assembled back to its original place (e.g. on the piston in the case of activated piston ring) after irradiation and the whole appliance (e.g. the internal combustion engine) runs normally on a test bench (or, if it is possible, in real life conditions). The gamma detector (Figure 19) used for the measurement is mounted on the test bench as close to the activated part as possible. Because of the engine wall and the possibly larger distance in the case of direct measurement, the required activities are usually larger than in the indirect case. The evaluation is even more difficult, because a relatively large activity is measured and the real wear, which corresponds to the change in activity, might easily be covered by the statistical errors. (The wear is proportional to the difference of two large numbers, counting rates).

The advantage of the direct method is that the radioactive worn particles in the cooling/lubricating circuit need not be collected or filtered. The disadvantage of this method is that the mounting of the detector is

not very easy. The detectors are sensitive to, for example, rapid temperature changes and mechanical shocks. The measured counting rates e.g. are influenced by the temperature of the machine part housing. With changing temperature of the engine/housing the distance between detector and radioactive part is changed slightly. This change in geometry (distance) influences the measured counting rate.

The direct method can be useful in cases where the wear particles cannot be collected, and the indirect method would therefore not be possible, e.g. where there is no lubricating or cooling liquid. For example, valves, valve seats or valve guides in a cylinder head must be measured using the direct method. Corrosion monitoring can also be achieved by irradiating the component in a manner that results in the radioactive nuclei being produced at a specified depth. A change in activity then indicates that this critical depth has been reached. Monitoring of essential components that limit the life time of a whole facility, for example due to corrosion, is therefore a possible application for the direct method – e.g. corrosion of an elbow in a nuclear power plant water pipe.

4.2. INDIRECT MEASUREMENT

The second, more common, technique is the indirect method or concentration method. For this method, radioactive wear particles are transported away from the activated surface by the lubricating medium (e.g. engine oil) and the accumulated radioactivity in this medium is measured. This method has much better sensitivity over the direct method as the signal-to-noise ratio is much higher. Appropriate shielding substantially reduces the number of gamma rays from the activated components in the test rig reaching the detector. This means that the wear particles can be detected with a very high sensitivity; wear rates on the order of nm/h or µg/h can easily be detected.

Figure 20 shows an engine test example for indirect measuring method.

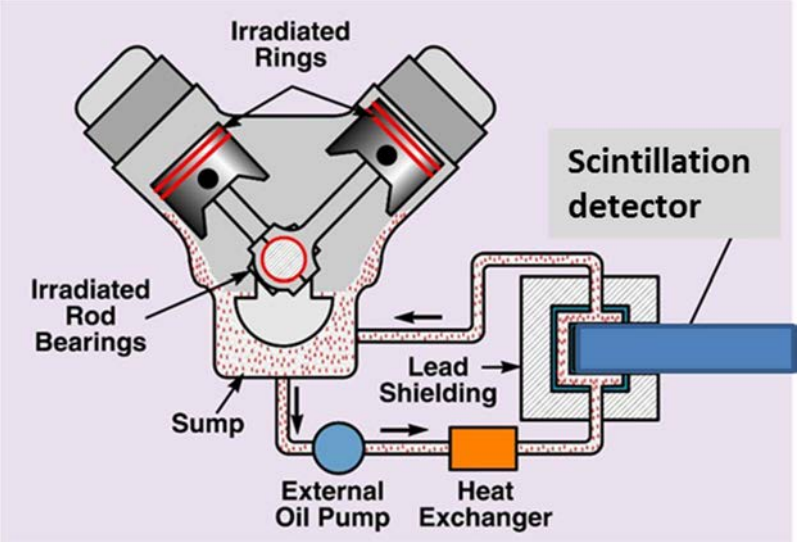

FIG. 20. Engine test example for indirect measuring method.

The indirect measurement or concentration measurement (Figure 20) is a sophisticated method to test the wear of different parts by radioactive tracers. In this case, the irradiated machine part can be assembled anywhere deeply in the machine - it does not matter how far it is from the machine wall or how thick the wall is. However, it has to be ensured that the worn particles (including the radioactive ones) are removed from the place of wear to an easily accessible measuring point. This task is usually performed by an extension of the existing cooling/lubricating circuit of the investigated machine, or adding a cooling/lubrication/washing circuit if it does not already exist. There are still two ways the

measurement can be performed: 1. measuring the increase of radioactivity of the continuously flowing liquid at any accessible point, or 2. installing an appropriate filter in the circuit on which the gamma radiation detector is mounted.

The second method seems to be more promising, because the concentration of the activity in the filter is more significant than in the whole liquid circuit, which makes a more precise measurement possible. This filter accumulation method, however has been seldom used as it is difficult in many situations to find a practical filter that will capture the wear particles with close to 100% efficiency. In addition, calibration of the accumulated wear particles within the filter geometry with respect to the gamma efficiency of the detector must be considered.

Sensitivity of this method is dependent upon the specific activity of the wear surface, the efficiency of the transporting fluid to remove particles from the worn surface and homogeneously mix the particles without dropout, the total volume of the transport fluid and the efficiency of the gamma detection system.

4.3. DETECTION OF RADIOACTIVITY

For both the direct and the indirect measurement methods, the main principle is based on a detector measuring the signal from ionizing particles, which are emitted from the activated area of the component (direct measurement) or by the worn particles (indirect measurement). Considering that both alpha and beta particles penetrate matter poorly, gamma rays are the appropriate choice for wear measurement.

When detecting gamma-rays, the following issues need to be taken into account [40]:

1) Natural background: There is always natural background radiation, namely cosmic, terrestrial and radon background radiation. Most of the cosmic radiation is deflected by the magnetic field of the earth and the atmosphere, but some remnants are still detectable at earth level. Further, some elements in the composition of the earth are radioactive as well, contributing to the environmental radiation. Background correction can either be done by analysing the spectrum or by comparison measurements (measurements without source and with source).

2) Calibration for wear measurement: The process of a radioactive decay is a statistical process. Which atom decays, and in which direction the resulting radiation is emitted, is unknown. Consequently, the wear measurement set-up (including position of the activated component, fluid circuit, arrangement between measurement volume and detector, etc.) needs to be calibrated. This can be done by a standard radiation source (for direct measurement) or dissolving the standard into the fluid (for indirect measurement). Generally, two effects are contributing here:

    a. Ratio of total activity to activity in the measured volume that can be measured by the detector: For direct measurement, this ratio can be regarded as 100% for the measured volume minus shielding of the elements between the activated area and the detector. For indirect measurement, the worn particles are distributed in the complete fluid circuit and only a part of the fluid volume is accessible to the detector (measured volume), except the case when the worn particles are captured with a filter (with known efficiency) and the detector measures the activity in the filter

    b. Geometrical factor: This factor represents the relation between total number of decays in the measured volume and the probability of the emitted gamma rays crossing the detector.

3) Energy efficiency: The penetration depth of a gamma ray depends on its energy. Low energy rays have a high attenuation in matter and consequently do not reach very far. So, even small amounts of matter, such as the lubricant or the reservoir wall, may absorb most low-energy rays (< 50 keV) before they can reach the detector. Conversely, high energy rays (>MeV) may also remain undetected, as they can travel through the detector without interacting with the detector material.

4) Detector intrinsic efficiency: The probability of a gamma ray interacting with a detector also depends on the material of the detector, and subsequently on the design and working principle of the detector. The absolute efficiency is the ratio of the number of events produced by the detector to the number of gamma rays emitted by the source over 4 π steradians. The relative efficiency is defined at 1.33 MeV as the efficiency of a point ^{60}Co source at 25 cm from the end-cap of a standard 3" x 3" circular cylinder NaI(Tl) detector.

5) Variable/inducted background: When using multiple radioactive nuclei (e.g. measuring multiple sources of wear simultaneously or using a reference isotope for wear calibration), the background can increase due to the increase of the Compton background and/or photo peaks occurring at similar energies and interfering with each other's detection. If multiple sources of wear are measured simultaneously, this background increases during the test and a simple comparison measurement (as described above) is no longer an option. Activities can still be quantified, but the uncertainties increase due to the inferior signal-to-noise ratio.

For most commercially available gamma-rays detectors, an efficiency data sheet is available considering geometrical factor (standard position), energy and material efficiency, summarized as intrinsic detector efficiency (Fig. 21).

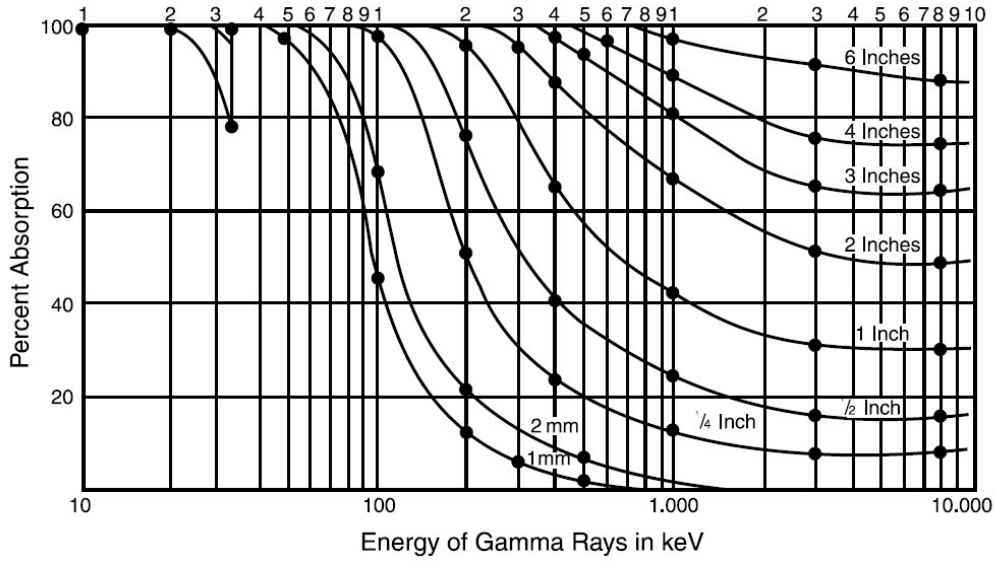

FIG. 21. Absorption in percent of gamma rays with certain energy for various penetration path lengths in NaI, which are determined by detector size and sample positioning (1 inch = 25.4 mm) [41].

For NaI crystal, the absorption with respect to energy of the gamma photon and the length of penetration path is well known (Figure 21). The detector efficiency is consequently a result of the attenuation and the geometric factor. Especially for a non-trivial shape of the detector crystal, the possible pathways through the scintillation material must be calculated and weighted accordingly.

4.3.1. Guidelines in detectors selection for TLA measurements

Gamma rays are used as signature of the behaviour against wear or corrosion of a component in industrial system (car engine, gas pipe line, etc.). Detection of gamma rays requires both spectroscopy capability and knowledge of absolute specific detector response. The detector choice relies on its ability to distinguish radioisotopes (energy resolution) and its sensitivity (detection efficiency). The detection

system is often installed within a processing line or other active facility and is submitted to extreme conditions of running, in term of vibration, microphony, temperature and temperature variability, etc. The approach has to be completed by the cost, ruggedness, reliability and stability of the detector and of its electronics, particularly in the pre-amplifying stage of the signal emitted from the absorption of the gamma rays in the crystal.

The two main detector technologies are inorganic scintillation detectors and semiconductor detectors, with significant new advances in both technologies.

4.3.1.1.Scintillation detectors

Inorganic scintillators, such as alkali halides (NaI and CsI) or bismuth germanate ($Bi_4Ge_3O_{12}$ or BGO) are mounted with photomultiplier tubes for converting scintillation light to electronic pulses. BGO competes favorably with NaI for its high density but its energy resolution (12% at 662 keV) is close to two times lower than NaI (7% at 662 keV). NaI(Tl) scintillation detectors are the standard detectors used for wear measurements at test benches. It is robust enough to be used in industrial environment and must only be cooled to room temperature. Ruggedized assemblies allow good scintillator/ PMT performance under high mechanical stress. Such a detector system remains low in cost in comparison to semiconductor technology, but its low energy resolution is a drawback when several radioisotopes have to be measured simultaneously.

Families of new scintillators with improved energy resolution are now available in large sizes. The lanthanum halides $LaCl_3$(Ce) offers an energy resolution of 3-4% at 662 keV that means two times higher than NaI(Tl) for a comparable density, a fast emission and an excellent linearity. The lanthanum halides detectors are the near future trend in low-resolution scintillation spectroscopy. The disadvantage (at least for the time being) is much higher price compared to NaI(Tl) crystals. Figure 22 presents the spectrometric characteristics of 1.5”x1.5” $LaCl_3$(Ce), 3”x3” NaI(Tl) and standard HpGe detectors.

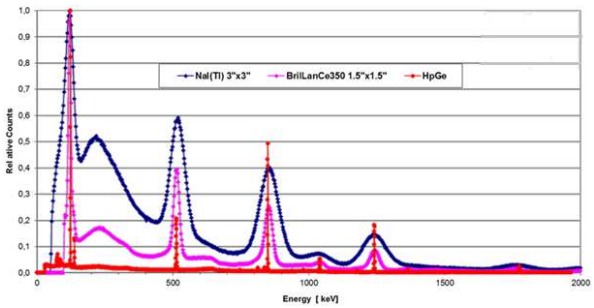

FIG. 22. Three spectra of a radioactive source containing a mixture of ^{57}Co and ^{56}Co measured with NaI, LaCl3(Ce) and HPGe detectors (source ZAG Zyklotron AG).

4.3.1.2.Semiconductor detectors

High purity Germanium detectors (HpGe) represent the state-of-the-art in energy resolution (0,2% at 662 keV), but offer a low intrinsic efficiency. For experiments requiring high resolution with sensitivity in wide energy range, large HPGe crystals are now commercially available and become more and more affordable. But, conventional HPGe detectors are cooled with liquid nitrogen complicating the installation of such a measurement setup in industry. Commercial electrically-cooled HPGe detectors are produced with an energy resolution comparable to that with liquid nitrogen cooling. This portable system is reliable, compact and vibration-free from the thermoelectric cooling and opens the door to applications with measurements that cannot be supported by liquid nitrogen. The remnant disadvantage of HPGe detectors is the sensitivity against noise (microphonic effect) in test benches that reduces the

energy resolution dramatically. The HPGe cost is high comparatively to NaI, but some applications with radiotracers, such as UTLA technique, require absolutely a high-resolution detector.

When large crystals are not required, compound semiconductor materials can be an alternative to HPGe if compromise in energy resolution is acceptable and to scintillators when better resolution is required. Cadmium zinc telluride (CdZnTe) detectors operate at room temperature with an energy resolution of 3% at 662 keV, which is comparable to LaCl3(Ce), but the largest crystal being limited to a cube with 15 mm on a side, its detection efficiency at 662 keV is moderate. In comparison with $LaCl_3$(Ce) performances, the use of CdZnTe detectors does not offer an added value for TLA application. Cadmium telluride (CdTe) detector can run at room temperature but a gain in energy resolution is achieved by cooling to just below 0°C. The crystal thickness being limited to 3 mm, CdTe detector is dedicated to spectroscopy for gamma-ray energies lower than 200 keV. Peltier-cooled CdTe detectors allow to reach an energy resolution only two times lower than HpGe. CdTe detectors can be useful to solve interferences between the radiotracer of reference and parasite signals in the low energy range.

4.3.2. Nuclear electronics

For TLA applications, typical analogical nuclear electronics consists of a NaI detector, high voltage power supply, amplifier, Analogue to Digital Converter (ADC) and Multi-Channel Analyser (MCA) (Figure 23). Most of the times, a spectrum analysis software is utilized to visualize the spectrum and perform analysis, mainly the measurement of the counting time, the selection of gamma rays and peak area calculation.

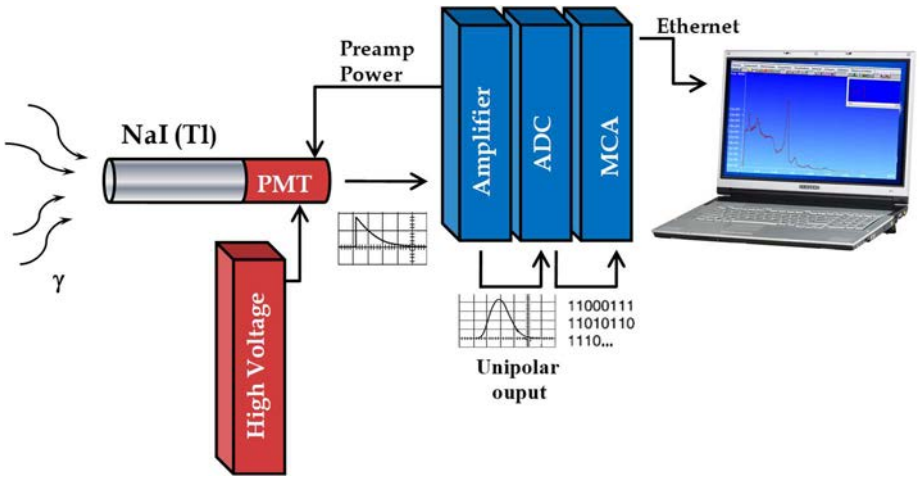

FIG. 23. Analogous nuclear electronics system [2].

Different types of components are available allowing the system to be tailored to the precise needs of the application and the budget. The components are chosen for their performances in term of stability and linearity. User can implement low-end amplifiers, but experiments with high count rate and/or needing high energy-resolution require amplifiers with Pileup Rejection/Live Time Correction (PUR/LTC) feature and both Gaussian /Triangular shaping. For ADC, a more economical Wilkinson ADC or a faster Fixed Dead Time (FDT) can be used. The scientist can substitute the MCA by a single channel analyser (SCA) connected to a Counter/Timer. The SCA and Counter/Timer system is more convenient when you want to track only one specific region of interest and is less expensive than MCA.

Digital signal processing (DSP) configurations replace the amplifier and ADC with digital signal processing electronics with a substantial impact on energy resolution.

The major inconvenience of spectroscopy with NaI(Tl) detector is the influence of temperature on the scintillation response. The consequence is the change in gain with temperature. Many commercial spectrometer systems propose a stabilizer feature with analogue adjustments of the gain. Semiconductor photodiodes can be an alternative to PMT for converting scintillation light to electronic signal, because they are more rugged than PMT, more compact and insensitive to external electric fields.

4.4. WEAR PARAMETERS AND THEIR INFLUENCES

The measuring principle can be seen as a black box: on one side radioactive decays are counted and on the other side a wear parameter is documented. A close look inside this black box uncovers two main non-trivial calculations that need to be done with expertise. Firstly, the number of detected counts needs to be transformed into an activity that is representative for the worn volume (e.g. wear particles), e.g. by detector calibration.

Secondly, a wear parameter (wear height, wear volume or wear mass) has to be calculated from the measured activity and the known activated volume of the machine part or component. The relationship between the measured activity and resulting wear depends on the total number of radioactive isotopes in the material produced during the irradiation process and their distribution in the material.

Wear is defined as the loss of material, which can be associated with a loss of activity for the direct measurement, or an increase of activity in the lubricant circuit for the indirect measurement. When the activity per volume of the wearing part is known, the change of activity can be directly correlated to a wear volume. Consequently, the easiest method is based on a constant activity concentration throughout the whole component, such as achieved by bulk irradiation. When TLA is applied, in most cases the irradiation is done in such way that a constant activity concentration (=constant part of the depth profile) is achieved for the assumed total depth of wear measurement. For example, when a total wear depth is expected in the range of 20 µm, then the activity concentration will be constant at least for this range. With this approach, the activity is concentrated in the expected wear zone and a high sensitivity is achieved by simultaneous reduction of the total activity of the component in comparison to bulk activation.

4.4.1. Wear volume

The activity per volume in the irradiated part is the key factor for the quantification of wear volume. There are two main working principles: a comparison measurement with a reference foil or a calculation on the basis of a depth profile.

In most cases, the reference foil is made of the same material as the wearing component or even taken from the component. To calibrate the wear measurement, the size or mass of the reference foil is quantified independently, usually by weighing with a microscale or, rarely, using a thickness measurement. Due to the prevalence of weighing as a reference method, wear measured using reference foils is often given in units of g (gram) or µg. To ensure similarity of reference foil and irradiated component, the irradiation is performed in parallel on both and irradiation parameters are chosen so that the activity concentration is constant at least for the thickness of the reference foil. For wear measurement, the reference foil can either be applied as comparison in a parallel measurement set-up or for calibration purposes before and after wear measurement. The calibration can be done with the foil in solid form or dissolved into the fluid.

The second working principle utilizes the calculated depth profile, which in turn depends on the reference methods described for depth profile or cross section measurements. The calculation of wear on the basis of the depth profile is more sophisticated and may result in higher uncertainties compared to the reference foil method, but the constant part of the depth profile can be made much smaller than is reasonably achievable for the reference foil working principle.

4.4.2. Wear height

For most practical engineering purposes, wear height is regarded as the critical parameter of a machine component. To calculate wear height from wear volume, the worn area with respect to the activated area must be known exactly. Two situations illustrate the challenges involved:

- The activated area fully covers the worn area: The quantification of the wear volume can be made precisely, but a constant activity concentration is essential. Subsequently, the average wear height can be calculated by dividing the wear volume by the worn area. The maximum wear height can only be calculated if the 3D-shape of the wear mark is known.
- The activated area is a (small) spot in the central (representative) part of the wear zone: In this case, the wear height of this spot is precisely known, even when applying a non-constant activity concentration. The total wear volume (i.e. including the non-activated worn volume), however, can only be extrapolated.

5. APPLICATIONS

5.1. ADVANTAGES OF USING RADIOACTIVE ISOTOPES FOR WEAR MEASUREMENT

Modern engines or engine components are designed and constructed for optimum performance. Small changes of this design, such as the ones due to wear during operation, may reduce the efficient performance or even limit functionality. Consequently, the wear behaviour of these parts during operation needs to be understood in order to construct a machine with optimum performance over the envisaged lifetime.

To understand these small changes of wear and their influencing factors, adequate measurement methods must be applied. Generally speaking, two different methodologies can be differentiated: on-line or post-test methods. For post-test methods, the machine has to be stopped, the component dissembled and cleaned, and subsequently measured.

Typical methods for post-test measurement are weighing or topography measurement. Topography measurement (or profilometry) is used for characterising the wear mark and using this to calculate the wear volume, but such measurements are limited by the initial roughness of the surface. Changes of the surface, which are smaller than the roughness, cannot reasonably be detected. For example, if the average roughness is one micrometer, wear smaller than one micrometer cannot be detected by optical means.

Online methods are very often limited by the accessibility of the wear zone and consequently use an indirect approach. Distance sensors, such as capacity or eddy-current sensors, usually use a reference area for measurement and thus elongations, vibrations or presence of wear particles or fluid may interfere with the sensor signal. Although a resolution of nm is given for many of these sensors, for wear applications a resolution in the range of 0,1 μm is reasonable.

Special information about the phenomena in the wear zone can be gained when a lubricant/fluid circuit is available which transports the wear particles. Most particle sensing methods are limited by the characteristics of used lubricants and thus the sensitivity is limited to the microscopic range. Samples of oil can be used for elemental analysis, such as with optical emission spectroscopy (OES), and the concentration of metal in the oil can be recalculated into a wear volume. Unfortunately, this method does not provide any information about the origin of these wear particles.

This is different when radioactive isotopes are used for tracing wear. Due to irradiation, the isotopes are located in a specific component or even at a certain surface area. Thus, when an increase of activity is detected in the lubricant circuit (indirect method), the origin of these wear particles is defined. Furthermore, the wear particles send out a high-energy photon (gamma ray) that can be detected easily, even after penetration through matter. Every single gamma photon can be counted and so a very high sensitivity with respect to wear can be achieved. Applying radioactive isotopes is the only reasonable method to measure wear in the range of nm/h or μg/h.

5.2. GUIDELINES AND GENERIC EXAMPLES

5.2.1. Guidelines

For the layout of a wear measurement using the radionuclide technique the user must answer the following questions:

1. What accelerator-particle and particle energy is available for the production of the radioactive label isotope?

2. What is the material of the wear part to be measured? The material (Fe, Cu, Sn, …) and the available bombarding particle/energy defines the radioisotope that can be produced (^{56}Co or ^{57}Co, ^{65}Zn, ^{120m}Sb, …). The radioisotope and activation energy/particle define the maximum possible linear region for measurement. Depending on the half-life of the radioisotope the maximum possible length of the measurement is given. (See Annex 2)

3. What is the maximum expected wear at the end of the test procedure? This defines the linear region for this measurement. If the expected total wear is only in the region of 20 µm it would be of no sense to activate the part to 50 µm or more. The less linear region is chosen the higher specific activity can be produced at the same total activity level. The higher the specific activity is, the better counting statistics will be, the wear rates can be measured with higher precision.

4. What area of the part must be labelled? Only that area of the part should be activated, that really is affected by wear. If the measurement is done by the concentration measurement method in an oil circuit, only the worn particles are measured. If areas on the part are labelled that are not affected by wear processes it has no effect on the measurement itself, but the unnecessary activity complicates the handling by higher doses for the engineer.

5. How much oil is in the oil circuit of the engine and measurement system? The higher the oil volume the higher the specific activity has to be to give good statistics for the measurement.

5.2.2. Examples

5.2.2.1.The TDC-region in cylinder 3 of a 4-cylinder crankcase shall be measured.

1. The crankcase is made of cast iron. The radioisotope for the measurement is ^{56}Co with a half-life of 77.3 days. The measurement can be done for at least half a year.

2. At the end of the measurement a wear depth of only 20 µm is expected.

3. The TDC region of cylinder 3 shall be activated, a 360° band with a width of 10 mm. The labelled area must begin 5 mm below the sealing surface to the cylinder head. The bore diameter of the cylinders is 80 mm. The total area to be activated therefore is 2513 mm^2.

4. The total oil volume including measurement system is 8 liters.

The linear region for this measurement should be chosen to be 30 µm, to be on the safe side. The radioisotope will be ^{56}Co. With 8 liters of oil a specific activity of 2 kBq/mg is sufficient. 2 kBq/mg correspond in this example to 37 kBq/µm. The total activity of such an activated crankcase would be in the range of 5 MBq ^{56}Co.

5.2.2.2. The first piston ring of cylinder 3 of a 4 cylinders engine shall be measured in a two component-measurement together with the TDC area of this cylinder.

1. The contact surface of the piston to the cylinder wall is made of chromium. The radioisotope for the measurement is ^{51}Cr with a half-life of 27.7 days.

2. At the end of the measurement a wear depth of only 20 µm is expected.

3. The full circumference of the piston ring shall be measured over the full height of 1.5 mm. The total area to be activated is 377 mm^2.

4. The total oil volume including measurement system is 8 liters.

The linear region for this measurement should be chosen again to be 30 µm. The bombardment of chromium with protons produces ^{51}Cr as the radioisotope to be measured. Unavoidable one produces at the same time a high amount on ^{52}Mn with a half-life of only 5.6 days. After the activation of this ring one has to wait for at least 5 weeks to reduce this ^{52}Mn content compared to the ^{51}Cr activity. Especially if a two-component-measurement with ^{56}Co as the second radioisotope is planned, this waiting time is absolutely necessary.

The number of counts per kBq ^{51}Cr in a 3"x3" NaI-detector is a factor of 20 less than the number of counts per kBq ^{56}Co. The surface of the piston ring is only 1.4 mm compared to the 10 mm band in the TDC of the crankcase. Therefore, the specific activity of ^{51}Cr should be in the range of 200 kBq/mg or more for this measurement, 5 weeks after the day of activation. That corresponds to 538 kBq/µm for the geometry of this example.

The total activities of the piston ring after 5 weeks would be in the range of 25 MBq ^{51}Cr, 0.3 MBq ^{52}Mn and about 10 MBq ^{56}Co from the basic material of the piston ring.

5.3. CASE STUDIES

Wear measurements on thin layer activated wear parts can be performed after two procedures.
In the first case the radioactive wear particles that are removed from the labelled area are measured. In the second case the remaining activity on the labelled part is measured.

Both measurement methods require that the produced wear particles are removed from the area where they were produced.

5.3.1. The Concentration measurement method, CMM

The concentration measurement method always is applied if wear particles from the labelled part are in contact with the lubricating circuit of the system. The principle of this method is shown in Figure 24.

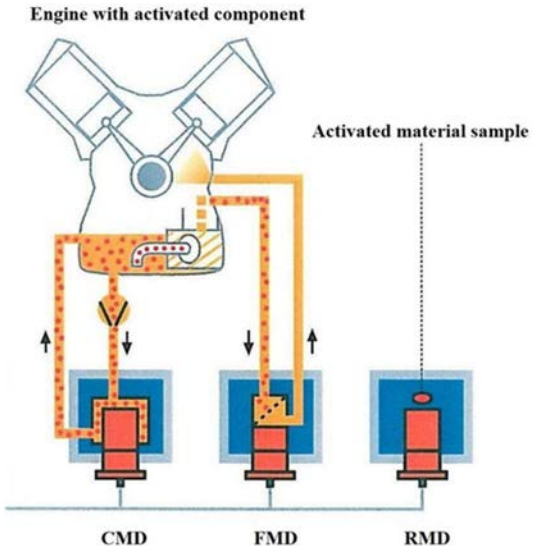

FIG. 24. Principle of a concentration measurement circuit [40].

The engine in this example is equipped e.g. with an activated bearing of the crankshaft. The wear particles enter the oil sump of the engine. This oil is now pumped in a closed loop by an external pump from the oil sump to a measurement chamber. In this chamber a detector records the increasing γ-radiation with increasing wear. This part is called the concentration measurement device (CMD). The activity of the *removed* wear particles is measured.

Any combustion engine has an oil filter to trap wear particles from the oil. The 'normal' oil filter of the engine is located in a second measurement chamber with a second detector that records the trapped radioactive wear particles in the oil filter. This part is called the filter measurement device (FMD).

It is often not possible to produce just one pure radioisotope in the technical material sample. For a possible mixture of radioisotopes it is necessary to know the resulting half-life.

The actual half-life can be easily determined with an identical material sample, activated together with the wear part. The third detector of the reference measurement device RMD records the γ-radiation. From the decrease of counts the half-life can be calculated online.

The total wear is now proportional to the concentration of the particles in the CMD plus the wear particles in the FMD. The calibration of the measurement is done by solid calibration sample of the identical material, activated together with the labelled part. This sample has the identical specific activity (activity per mass unit) as the labelled part. The mass of the sample can be measured and is typically in the range of some milligrams.

Together with geometry factors for each isotope and γ-energy range and the known total oil volume in the system it is possible to calculate the actual wear mass from the number of measured γ-counts. The geometry factors are part of the software of the complete measurement system. Depending on the oil volume in the system and the specific activity of the labelled part wear rates in the range of micrograms per hour [µg/h] can be measured. Because this measurement procedure is based on the measurement of the activity concentration removed from the part under test, CMM is also applicable to neutron activated parts.

5.3.2. Wear test for automotive

Radioactive tracer technology allows extremely high sensivity near real-time in-situ wear measurement of component surfaces in operating engines or other machinery. In the example below, top piston rings with a chrome ring face insert were activated by bulk activation and installed in a 6-cylinder gasoline engine. Bulk activation created the isotope ^{51}Cr ($t_{1/2}$ = 27.7 days) in the ring face, which was used as a radiotracer. Calibration samples of the ring face were activated simultaneously with the rings to the identical activity level and digested to make a calibration solution of known concentration. A gamma spectroscopy system was calibrated using this solution to allow conversion of measured activity to concentration of mass.

The engine's oil sump was modified to allow extraction and return of oil through a gamma spectrometer system during engine operation. As the engine was run, the gamma detection system accumulated and saved a new spectrum every 10 minutes. These spectra were analyzed to determine the number of counts in the ^{51}Cr peak. The collected counts were corrected for time decay, multiplied by the appropriate calibration factor and the total volume of oil in the sump to determine the cumulative mass of ring face wear debris present in the engine oil during each 5-minute increment.

Figure 25 shows cumulative piston ring face wear plotted versus time and operating condition from one test run. The engine was started with fresh oil at time zero and allowed to idle for 1 hour. It is typical to experience higher wear during startup and warmup when parts do not have an established oil film.

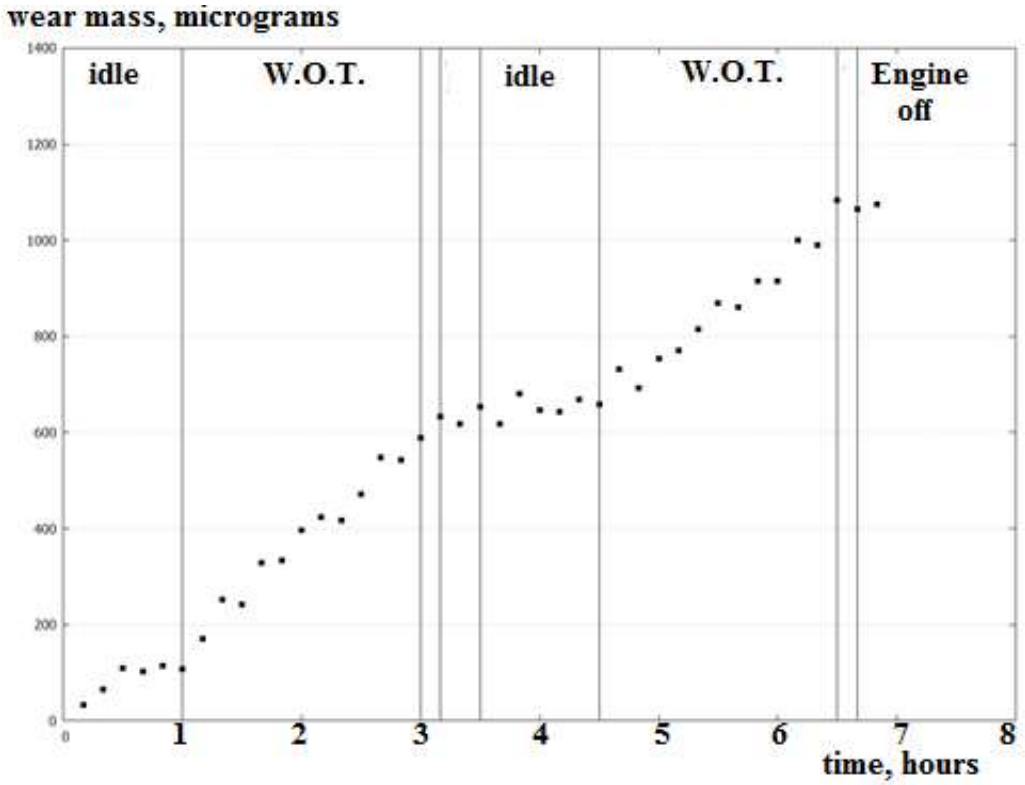

FIG. 25. Cumulative Top Ring Face wear as a function of time and operating condition [42].

After approximately 30 minutes cumulative wear stopped increasing during the engine idle test condition. After 1 hour the engine was taken to Wide Open Throttle (W.O.T.) under load and a higher near constant wear rate was measured. The engine was then allowed to idle for 10 minutes, shut off for 20 minutes and restarted at idle for 1 hour. During this warm start idle condition little additional wear was incurred. The engine was then returned to W.O.T. under the same load and a nearly identical wear rate was measured at this condition.

5.3.3. Wear test of tribometer

Tribometer testing has the big advantage of being focused on the most crucial part of the tribosystem and having a large degree of control over all testing variables, in addition to being less expensive than larger test set-ups. While it is possible to choose testing parameters outside the normal operating conditions of the system under investigation in order to increase wear, producing results as close as possible to application (real world) conditions will always be preferred. Techniques using radioactive isotopes provide unique possibilities of measuring the very small amounts of wear occurring in short tribometer tests in conditions as close as possible to real world conditions. Tribometer testing is usually accomplished using smaller samples and smaller lubricant volumes, which are an advantage for radioactive isotope-based wear measurement.

One tribosystem that has received a lot of attention is the piston ring-cylinder liner system. A case study where piston ring wear was investigated using radioactive isotopes is presented. Figure 26 presents schematic of piston ring and cylinder liner segments; sample holder in testing chamber.

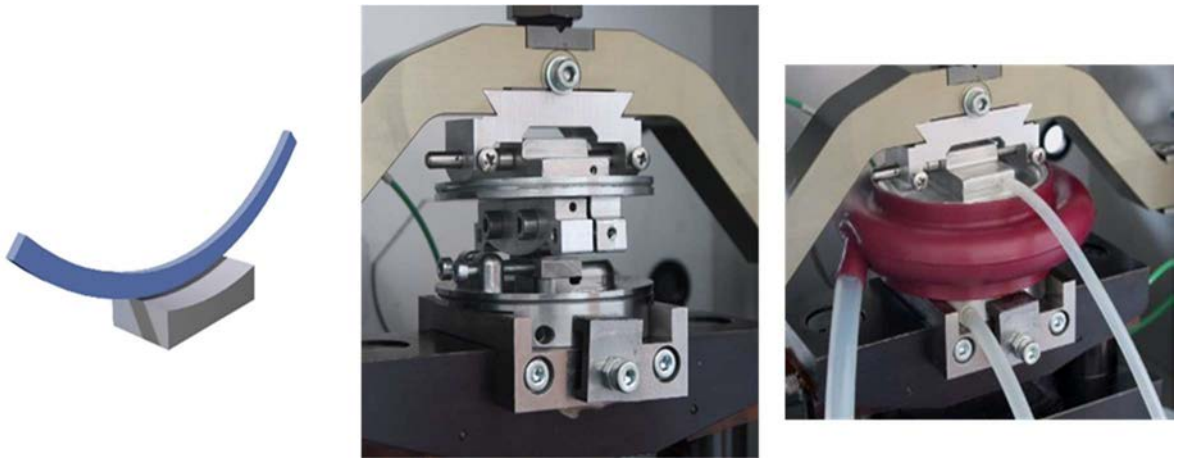

FIG. 26. Schematic of piston ring and cylinder liner segments; sample holder in testing chamber [43] (left: without enclosure; right: with oil circuit enclosure).

For this study, piston ring and cylinder liner segments were used as samples and an area of 2.4x2mm of the piston ring segment was activated for ^{57}Co radioisotope. The activated area is located in the centre of the piston ring segment. During positioning of the samples in the tribometer care has to be taken to position the piston ring and cylinder liner segments so that the activated area is located in the contact area where wear is expected. An enclosure around the sample holder containing piston ring and cylinder liner segments ensures that no wear particles are lost.

5.3.3.1.Correlation of tribological behaviour of engine components in tribometer tests and in real engines

A basic goal in tribological research is the prediction of the friction and wear behaviour of machinery under real operating conditions. Experiments involving the final manufactured product (such as engine bench tests) are usually very expensive and complex. Therefore, fundamental component tests are carried out under simplified conditions in cost-efficient tribometer experiments. For the subsequent prediction of the component lifetime of the final product, it is necessary to establish a quantitative correlation between the measurement results of component test and tribological behaviour under real operating conditions.

The RIC method is uniquely suited for this kind of testing, as the measurement signal – i.e. the measured activity of the wear particles in the oil – is independent from thermal influences or other environmental factors in the engine or tribometer. Therefore, the method can be applied in both environments and the results can be compared. By adapting the loading conditions, it was possible to observe wear behaviour in the component test that is similar to the wear behaviour in the real engine (Fig. 27). Matching the loading conditions provides the basis for studying the influence of different materials and lubricants on wear behaviour in cost-effective tribometer tests.

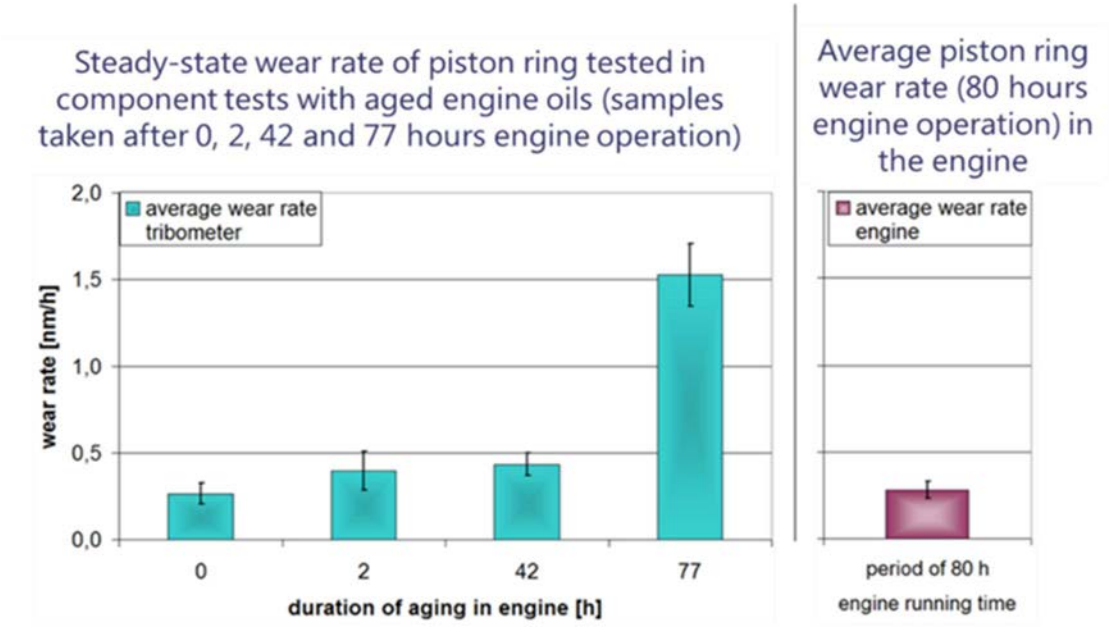

FIG. 27. Comparison of wear rates observed in engine operation (right) and in tribometer experiments with oil samples taken from engine test [41].

Piston ring and cylinder liner tribosystem optimization using state-of-the-art material combinations
Modern combustion engines have to fulfil high requirements with respect to wear resistance and lifetime. Optimized material combinations for the piston rings and cylinder liner contact provide one possibility of achieving these goals. With the help of the RIC method, a ranking of material combinations for the use in internal combustion engines was determined in short term tribometer tests.

Figure 28 shows the wear behaviours of the cylinder liner for different material pairings. This forms the basis for choosing the most promising combinations to be evaluated in engine bench tests.

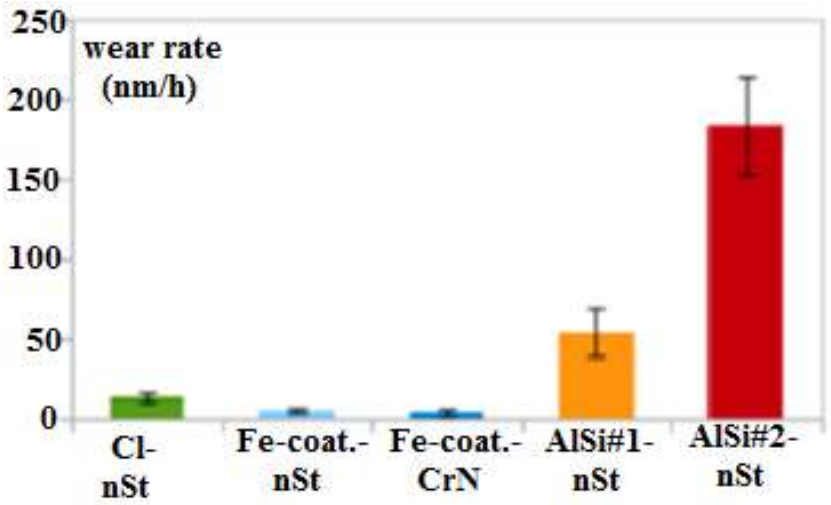

FIG. 28. Wear rate of different cylinder liner materials with nSt and Cr piston rings at the same loading conditions in tribometer set-up [42].

5.3.3.2. Influence of biofuels on wear behaviour

The increasing use of biofuels has the goal of protecting the environment and reducing fossil fuel use. However, biofuel combustion products contaminate the engine oil and subsequently influence the lubricity and the ageing process. Thus, it is important to study the influence of the biofuel and its combustion products in the oil on the wear behaviour of engine components with respect to the oil drain interval. When developing modern combustion engines, the effects of biofuel on the tribological behaviour have to be considered.

Figure 29 depicts the effect of lubricants aged in presence of bioethanol combustion products on the wear behaviour of piston rings. The combustion product-aging of the lubricants lead to reduced wear rates (at least for the short term), which can be attributed to an activation of anti-wear additives [43].

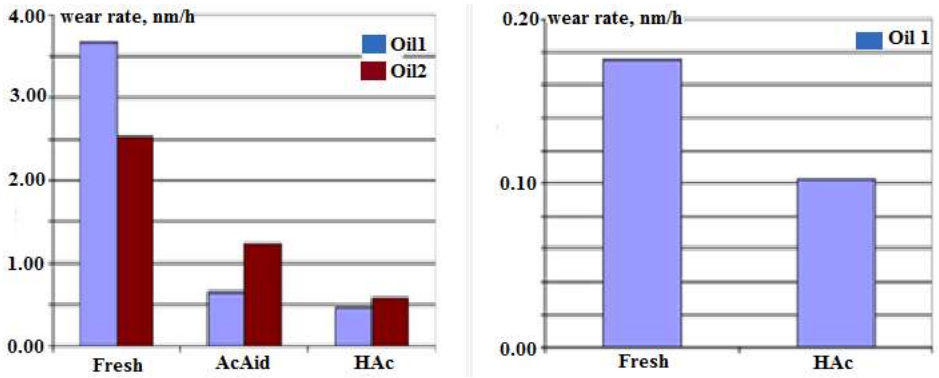

FIG. 29. Influence of oil aged with ethanol combustion products on wear rate of piston rings in tribometer experiment (left) and proof of trend in engine bench test (right) [43].

5.3.4. Direct measurement or Thin Layer Difference Method (TLD)

The principle of the direct measurement maybe elucidated in Figure 30.

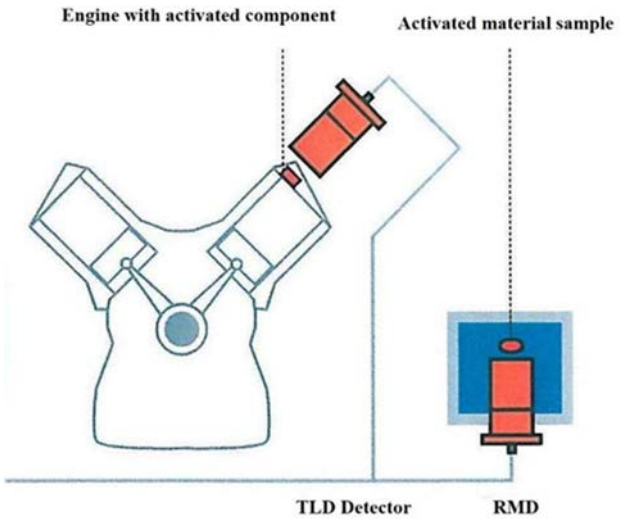

FIG. 30. Principle of a thin layer difference measurement [44].

The engine is equipped with an activated part, in this case now maybe a valve seat of an outlet valve. The wear particles of this valve seat get not into contact with the lubricating oil, they leave the system with the exhaust gas. In this case one takes a detector of the CMM system and records the *remaining* activity of the valve seat.

Again it is often not possible to produce one pure radioisotope in the material. The possible mixture is again measured with an identical material sample in the reference measurement device RMD.

The TLD or direct method must always be used when the wear particles cannot get into the lubricating fluid like oil, water or break fluid. Examples for such parts are sealing surfaces on valves, valve seats in cylinder heads, valve guides in cylinder heads, break parts and so on.

A setup for such a measurement seems to be easy but it is not. The detector cannot be fixed tight to the engine or test bench, it would be destroyed by the vibrations. But if the detector is not mounted at the engine the distance between the activated part and the detector is not fixed. The distance can change by the movement of the running engine, the temperature of the material between activated area and detector changes during the test. All these parameters influence the signal, registered by the detector. To reduce such effects, one has to enlarge the distance between activated part and detector. On the other hand, a longer distance decreases the counting rate and one has to increase the activity of the part. The activity height is limited by the license and by the allowed dose to the engineer. So, it is always necessary to find an ideal setup for such a direct measurement.

Due to these effects, the precision of such measurements is in the range of 0.1 to 1 µm/h.

5.3.5. Rotation detection

Using such detectors of a wear measurement system it is even possible to record the rotation of machine parts. As an instance for such a measurement, Figure 31 shows a tappet in a cylinder head that has one radioactive labelled spot at the side.

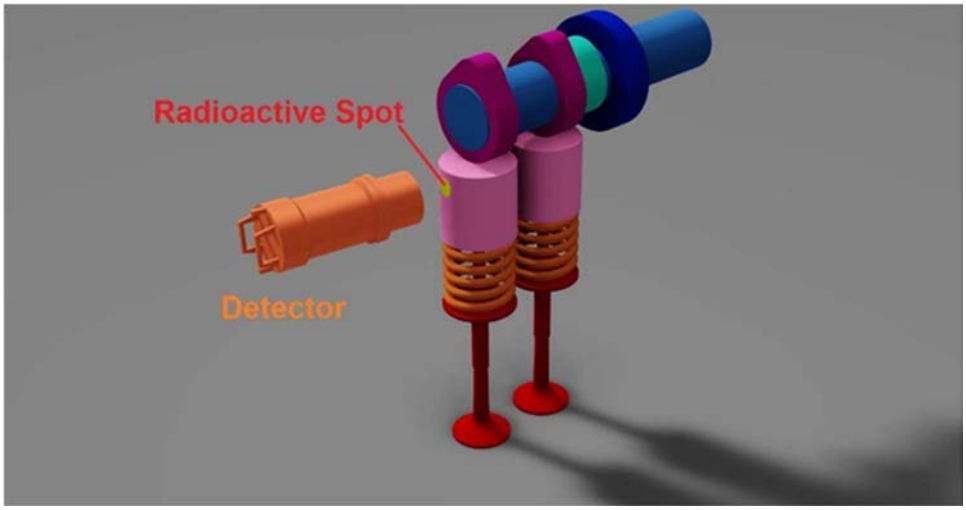

FIG. 31. Cam and tappet system with a radioactive spot on one tappet [45].

If the radioactive spot is nearest to the detector the number of counts in this detector has its maximum. If the tappet rotates the counting rate varies between a maximum and a minimum, if the spot is far away from the detector.

If two detectors can be used and the tappet is labelled with two radioactive spots, 90° displaced from each other, it is even possible to see the rotation direction of the tappet. Such a setup is shown in Figure 32.

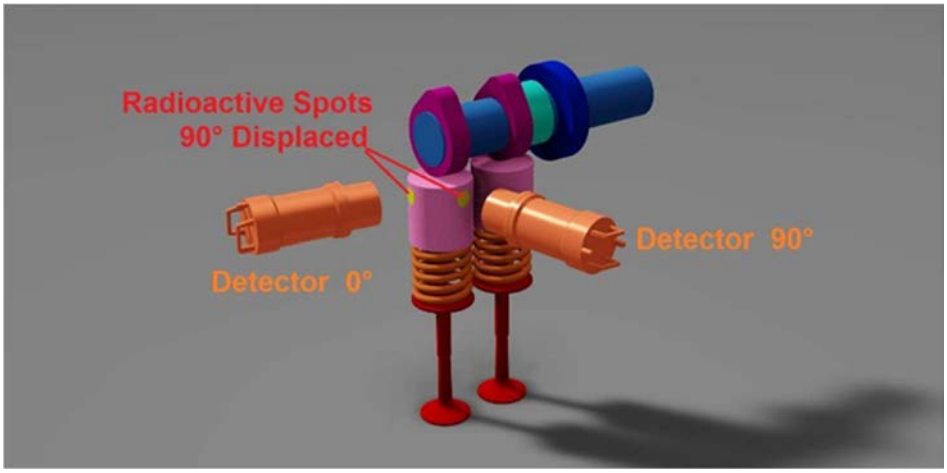

FIG. 32. Cam and tappet system with two radioactive spots on one tappet and two detectors, 90° displaced to each other [45].

In the drawn position both detectors show the highest counting rates. If the tappets rotate to the right the counting rate of the 0° detector decreases whereas the counting rate of the 90° detector nearly stays at the maximum. If the tappet rotates to the left it is vice versa.

The short stroke of the tappet has no influence. The stroke frequency (rotation speed of the engine) is normally much higher than the rotation frequency.

6. CONCLUSIONS

The activation technique or TLA (Thin Layer Activation) is often used for registering online loss material rates with excellent sensitivity. The Thin layer activation technique (TLA) consists of a bombardment of the surface of material by a charged particle beam (generally ^{1}H, ^{2}H, or ^{4}He) delivered by a cyclotron accelerator. The primary beam strikes a precisely defined area of the mechanical piece with energy of a few tens of MeV. Radioactive tracers are created by nuclear reactions in the near surface area of the material at a well-defined depth. The determination of the depth distribution of the inducted radioactivity allows evaluation of wear/abrasion or corrosion rates.

Two modes of radioactivity detection are used:

(i) Measurement of the residual activity (direct measurement technique) of the studied part with a micrometric sensitivity and

(ii) Measurement of the radioactivity increase in the lubricating fluid (indirect or concentration measurement technique) from which the material loss is evaluated with a sensitivity in the order of one nanometer. Multiple wear conditions can typically be measured during a single day with sensitivities in the order of µg/h or nm/h. This allows the end user to correlate operating or lubricating conditions to wear rate and to determine cause and effect.

Measuring wear with radioactive isotopes is a key technology for the investigation of the wear behaviour of machine parts and components, such as piston rings and cylinder liners in combustion engines.

Therefore, TLA for wear and corrosion measurement

- serves as a high-resolution measurement system for fundamental research regarding wear mechanisms
- allows evaluation of new materials, surfaces and lubricants (screening tests, ranking, characteristic factors for the design)
- enables evaluation of functionality and optimization of components or systems (e.g. approval of prototype engines in engine bench tests)
- can also provide online monitoring for hard-to-access surfaces in tribocontacts with respect to other wear phenomena

The technique is highly regarded and is currently applied mostly in the automotive and lubricant industries. However, work has been done in other fields and the technique can certainly be extended to innovative industries that have the need for this type of measurement. TLA wear measurement is the only method capable of detecting wear problems of current machinery and consequently of enhancing efficiency (energy consumption) and prolonging lifetime (resource allocation).

New trends in anti-wear designs of machine parts, such as thin layer coatings, require suitable improvements concerning the wear measurement method. New developments in cyclotron technology enable activation of DLC surface layers as well as implantation of radioactive particles (^{7}Be) into polymers. Nanometer sensitivities using the direct measurement technique have been achieved using an UTLA method based upon recoil implantation of radioactive heavy nuclei into the near surface of materials.

7. REFERENCES

[1] INTERNATIONAL ATOMIC ENERGY AGENCY, The Thin Layer Activation Method and its Applications in Industry, TECDOC-924, January 1997.

[2] TREUHAFT MB, EBERLE DC. The Use of Radioactive Tracer Technology to Measure Real-Time Wear in Engines and Other Mechanical Systems, 2007.

[3] DITRÓI F, TAKÁCS S, WOPELKA T, JECH M, LENAUER C. Investigation of wear process by using radioactive tracers. 20th Int. Conf. Wear Mater., Toronto: 2015, p. 145.

[4] DITRÓI F, TAKÁCS S, TÁRKÁNYI F. Evaluation of reaction cross section data used for thin layer activation technique. Int. Conf. Nucl. Data Sci. Technol. St. Fe, NM, USA, 26 Sept. - 1 Oct., 2004 AIP Conf. Proc. 769 (2005)1654, 2005.

[5] ZAG Zyklotron AG measurement during quality control (internal communications) 2010.

[6] TAKÁCS S. Calculation tool TLA2L. Https://www-Nds.iaea.org/tla/abouttla.html 2010.

[7] LACROIX O, SAUVAGE T, BLONDIAUX G. Methodological aspects of recoil nuclei implantation technique applied in tribology or corrosion studies. Fourteenth Int. Conf. Appl. Accel. Res. Ind., vol. 392, AIP Publishing; 1997, p. 969–72.

[8] HOFFMANN M, ABBAS K, SAUVAGE T, BLONDIAUX G, VINCENT L, STROOSNIJDER M. ^{7}Be recoil implantation for ultra-thin-layer-activation of medical grade polyethylene: Effect on wear resistance. Nucl Instruments Methods Phys Res Sect B Beam Interact with Mater Atoms 2001;183:419–24.

[9] STROOSNIJDER MF, HOFFMANN M, SAUVAGE T, BLONDIAUX G, VINCENT L. Wear evaluation of a cross-linked medical grade polyethylene by ultra thin layer activation compared to gravimetry. Nucl Instruments Methods Phys Res Sect B Beam Interact with Mater Atoms 2005;227:597–602.

[10] LACROIX O, SAUVAGE T, BLONDIAUX G, GUINARD L. Ultra thin layer activation by recoil implantation of radioactive heavy ions: applicability in wear and corrosion studies. Nucl Instruments Methods Phys Res Sect B Beam Interact with Mater Atoms 1997;122:262–8.

[11] WANG Y, NASTASI MA, editors. Handbook of modern ion beam materials analysis. Warrendale, Pennsylvania: Materials Research Society; 2009.

[12] VINCENT L, SAUVAGE T, LACROIX O, SAILLARD M, BLONDIAUX G, GUINARD L. Simplified methodology of the ultra-thin layer activation technique. Nucl Instruments Methods Phys Res Sect B Beam Interact with Mater Atoms 2002;190:831–4.

[13] VINCENT L, SAUVAGE T, LACROIX O, FRADIN J, SAILLARD M. Ultra thin layer activation by implantation of recoil radioactive nuclei: Experiments and simulations. Nucl Instruments Methods Phys Res Sect B Beam Interact with Mater Atoms 2000;161:115–9.

[14] ZIEGLER JF, ZIEGLER MD, BIERSACK JP. SRIM – The stopping and range of ions in matter (2010). Nucl Instruments Methods Phys Res Sect B Beam Interact with Mater Atoms 2010;268:1818–23.

[15] SCHARF W, WAWRZONEK L. Thin layer activity depth distribution for wear measurements of cast iron. Nucl Instruments Methods Phys Res Sect B Beam Interact with Mater Atoms 1985;12:490–5.

[16] BLATCHLEY CC. Radionuclide Methods. ASM Handb., 1999, p. Vol18-7.

[17] BLONDIAUX G, DRAGULESCU E, RACOLTA PM, CRACIUN L, SERBAN AT, STROOSNIJDER MF. Development of Calibration Methods for TLA and UTLA. European Commission Center of Excellence InterDisciplinary Research and Applications Based on Nuclear and Atomic Physics; 2002.

[18] DITRÓI F. Determination of the charged particle beam energy/intensity uncertainties at multi-target irradiations. Nucl Instruments Methods Phys Res Sect B Beam Interact with Mater Atoms 2002;188:115–9.
[19] YOUNG FC, ROSE D V. Radioactivities produced in commonly used materials by proton and deuteron beams up to 10 MeV. At Data Nucl Data Tables 1996;64:223–51.
[20] KIRALY B, TAKACS S, DITRÓI F, TARKANYI F, HERMANNE A., KIRÁLY B, et al. Evaluated activation cross sections of longer-lived radionuclides produced by deuteron induced reactions on natural iron.. Nucl Inst.and Methods Phys Res B 2009;267:15–22.
[21] DITRÓI F. The thin layer activation method and its applications in industry 1997;324.
[22] JECH M, VORLAUFER G, PAUSCHITZ A, WOPELKA T. Verfahren und Messanordnung zur tribometrischen, hochauflösenden Online-Verschleissbestimmung an Probenkörpern, sowie Verfahren und Messsystem zur Ermittlung eines Tiefenprofils der Aktivität von radioaktiven Isotopen an einem Referenzkörper 2008;AT20060002.
[23] Gamma and X-ray detection 6/2006. Canberra Ind Inc 2012.
[24] ANDERSEN HH, ZIEGLER JF. Hydrogen stopping powers and ranges in all elements. The Stopping and ranges of ions in matter, Volume 3. New York: Pergamon Press; 1977.
[25] LANDOLT-BÖRNSTEIN. Numerical date and functional relationships in science and technology. New Series. Group 1: Nuclear and Particles Physics. n.d.
[26] MALUHIN VV, KONSTANTINOV IO. Activation of construction materials on the cyclotron. Isot v SSSR 1975;44.
[27] DMITRIEV PP. The radionuclide yield in the reaction with protons, deuterons, alpha-particles and He-3 ions. Moscow: 1986.
[28] ALBERT P, BLONDIAUX G, DEBRUN JL, GIOVAGNOLI A, VALLADON M. Thick target yields for the production of radioisotopes, Handbook on Nuclear Activation Data. Vienna (Austria): 1987.
[29] KRASNOV NN. Thick target yield. Int J Appl Radiat Isot 1974;25:223–7.
[30] JECH M. Wear Measurement at Nanoscopic Scale by means of Radioactive Isotopes. Vienna University of Technology, 2012.
[31] UNITED STATES NUCLEAR REGULATORY COMMISSION. NRC: 10 CFR 30.18 Exempt quantities. http://www.nrc.gov/reading-rm/doc-collections/cfr/part030/part030-0018.html. 2015.
[32] EUROPEAN UNION. Council Directive 2013/59/Euratom of 5 December 2013 laying down basic safety standards for protection against the dangers arising from exposure to ionising radiation, Annex VII. 2013.
[33] BUNDESREPUBLIK DEUTSCHLAND. Verordnung über den Schutz vor Schäden durch ionisierende Strahlen (Strahlenschutzverordnung -StrlSchV), Anlage III. 2001.
[34] REPUBLIK ÖSTERREICH. Allgemeine Strahlenschutzverordnung, Anlage 1. 2015.
[35] TREUHAFT MB, TIMMONS SA, EBERLE DC, WENDEL GR. Wear Measurement of a Large Hydraulic Fluid Power Pump Using Radioactive Tracer Wear Technology. Fluid Power Syst. Technol., vol. 2003, ASME; 2003, p. 55–64.
[36] EBERLE DCC, WALL CMM, TREUHAFT MBB. Applications of radioactive tracer technology in the real-time measurement of wear and corrosion. Wear 2005;259:1462–71.
[37] Cyclotrons and their Applications, Groningen 2009.
[38] ZAG Zyklotron AG Brochure RTM Wear Diagnostics 2011:11.
[39] KfK Nachrichten 4/86 n.d.:232
[40] ZAG Zyklotron, AG Broschure RTM Wear Measurement Technique 2012:2.
[41] JECH M, LENAUER C, WOPELKA T, NOVOTNY-FARKAS F, FEITZINGER T. Advances in wear measurement – piston rings in component test and engine environment. Int. Colloq. Tribol. - Tech. Akad. Esslingen, 2009.

[42] WOPELKA T, LENAUER C, SEQUARD-BASE J, STEINSCHÜTZ K, SPILLER L, PAUSCHITZ A. Wear of different material pairings for the piston ring – cylinder liner contact. WTC 2013, Turin (I): 2013, p. 75.
[43] LENAUER C, TOMASTIK C, WOPELKA T, JECH M. Piston ring wear and cylinder liner tribofilm in tribotests with lubricants artificially altered with ethanol combustion products. Tribol Int 2015;82:415–22.
[44] JECH M, WOPELKA T, BESSER C, LENAUER C, STEINSCHÜTZ K, NOVOTNY-FARKAS F. Lubricity of engine oils due to aging with ethanol combustion products. 13th EAEC Eur. Automot. Congr., Valencia (ES): 2011.
[45] ZAG, Zyklotron AG measurement during quality control (internal communications) 2015.
[46] INTERNATIONAL ATOMIC ENERGY AGENCY. IAEA Safety Standards for protecting people and the environment. Radiation protection and Safety of Radiation Sources: International Basic Safety Standards; General Safety Requirements Part 3 2014:STi/PUD/1578.
[47] INTERNATIONAL ATOMIC ENERGY AGENCY. Safety Guide No. RS-G-1.7 “Application of the Concepts of Exclusion, Exemption and Clearance.” 2004.
[48] French national plan for the management of radioactive materials and waste 2013-2015 www.french-nuclear-safety.fr/Information/Publications/Others-ASN-reports n.d.
[49] VANDECASTEELE C. Activation analysis with charged particles. Chicester: Ellis Horwood; 1988.
[50] ESSIG G, FEHSENFELD P. Nuclar Physics Methods in Materials Research, K. BETHGE (Ed) 1980;70.

ANNEX I. THEORY OF THE CHARGED PARTICLE ACTIVATION

I-1. INTERACTION OF IONS IN MATTER

When accelerated charged particles penetrate into the matter, the particles gradually lose their energy by inelastic collisions with electrons in the medium and more importantly at low energies by elastic collisions with nuclei of the atoms.

Figure I-1 presents the nuclear and electronic stopping power as a function of energy in pure iron target. The theory of ion-solid interactions has been discussed in detail by Ziegler et al. [14]. The authors also describe the software SRIM (Stopping and Range of Ions in Matter), which can be used for calculating stopping power and range for many ion/target combinations. The stopping power (S) of a medium is defined as the energy loss (−dE/dx) with material thickness (x). It is expressed by a function related to the charge and energy of the incident ion and to the physical characteristics of the medium. This function is well established and is too complex to be presented here. S can be converted to units of MeV/(mg.cm^2) by introducing the volume density of the material in g. cm^{-3}.

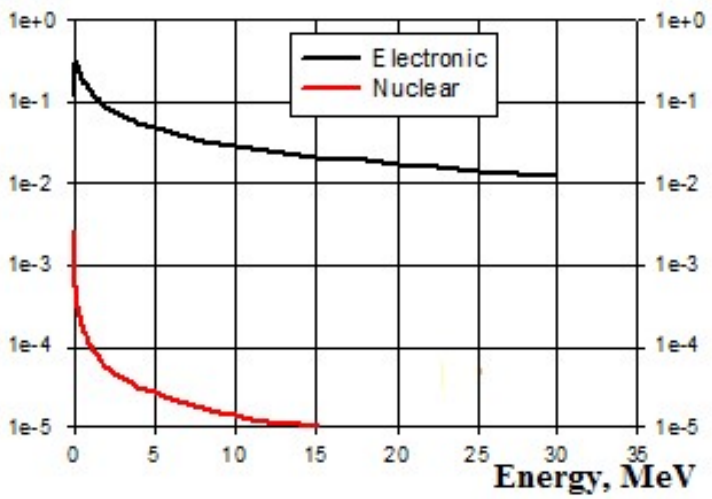

FIG. I-1. Nuclear and electronic stopping power as a function of energy in pure iron target [14].

The range R of an accelerated ion beam with initial energy E_0 can be estimated by the following formula:

$$R = \int_0^{E_0} S^{-1} dE = \int_0^{E_0} \left[-\frac{dE}{dX}\right]^{-1} dE \qquad \text{(I-1)}$$

R is also called the continuous slowing down approximation in charged particles are assumed to lose their energy at a continuous rate given by the stopping power, i.e. without energy-loss fluctuations. The projected range is the average value of the depth, to which an ion will penetrate in the course of slowing down to rest. This depth is measured along the initial direction of the beam. The range R is always greater than R_p, the projected range.

Ranges of charged particles in different elements are well known and information is available (SRIM) to select the appropriate particle energy for a specific problem. Ranges in compounds and alloys can be calculated by applying Bragg's formula:

$$\frac{1}{R_0} = \sum_i \frac{\eta_i}{R_i} \quad \text{(I-2)}$$

where

- R_0, range in compound,
- R_i, range in element i,
- η_i, weight proportion of element i.

In addition to the electronic and nuclear processes of slowing down, a small fraction of charged particles interacts with atomic nuclei of the material, induct a nuclear reaction and produce radioactive nuclides.

I-2. NUCLEAR REACTION

A typical nuclear reaction is written:

$$\boldsymbol{A(a,b)B^*} \quad \text{(I-3)}$$

with two bodies in the final state: **b** and **B***.

- The particle labeled **a** is the projectile. Generally, it is restricted to considering light projectiles with $M_a \leq 4$.
- **A** is the target nucleus.
- The particle **b** is the lighter reaction product, for a group of light products, which usually consists of, protons, neutrons, tritons, ^{3}He and α particles.
- **B***, at its ground or an excited state, is the heavier of the two reaction products, which is usually a radioactive or stable isotope of an element not far from the target element **A**. If it is radioactive and decays through gamma-ray emission, then it can be measured with a suitable counting system.

Iron is one of the most common element found in mechanical components whose wear or corrosion are studied using the marker ^{56}Co produced with the nuclear reaction ^{56}Fe(p,n)^{56}Co. To understand how this reaction is useful, one has to be first familiar with terms like "cross section, Q-values, activity for thick target" which are discussed below.

There is a probability that certain reaction will take place if the particle gets "close enough" to a nucleus and this is expressed by the cross section σ. This quantity σ which has the dimension of area (cm^2) is measured by the experimental ratio:

$$\sigma = \frac{\text{number of emitted particles from reaction}}{(\text{number of beam particles per unit area}) \cdot (\text{number of target nuclei within beam})} \quad \text{(I-4)}$$

The Q value of the reaction is defined in mass energies difference of the products (b and B*) and reactants (a and A). If Q is positive, the reaction is exoergic, while Q is negative for endoergic reaction. The minimum kinetic energy that the projectile must have for the reaction to occur is called the threshold energy E_{th}.

$$Q = [(m_a + m_A) - (m_b + m_B)] \cdot c^i \quad \text{(I-5)}$$

$$E_{th} = -Q \cdot \frac{m_a + m_A}{m_A} \quad \text{(I-6)}$$

As an example, in Figure I-2, the nuclear reaction ^{56}Fe(p,n)^{56}Co with 14 MeV protons in pure iron depicting the variation of nuclear reaction cross section as a function of depth is shown. The angle θ between the beam axis and the normal of the surface is equal to zero.

The cross section unit is in barn, defined as 10^{-24} cm^2. In this example, one can note that the cross section becomes zero at a depth of 370 µm while the incident protons penetrate a depth of 460 µm.

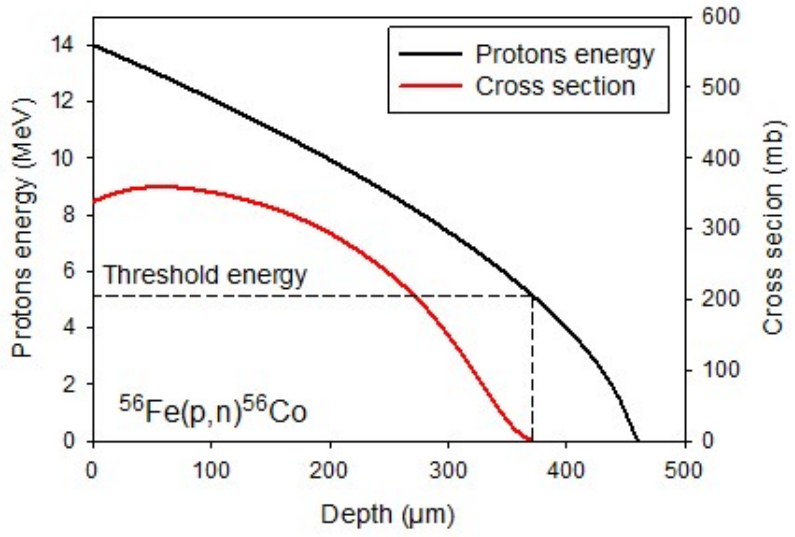

FIG. I-2. Dependence of proton energy and ^{56}Fe(p,n)^{56}Co cross section on depth for 14 MeV protons in pure iron[50].

The depth of the radioactive layer depends on the E_0 particle energy, energy threshold E_{th} of the considered nuclear reaction and beam incidence angle Θ.

$$d = [R(E_0) - R(E_{th})] \cdot \cos\Theta \tag{I-7}$$

The TLA technique allows adjusting the radiolabelled thickness and thereby the sensitivity of the control by varying primary beam energy and Θ angle.

I-3. ACTIVATION FORMULA

The activity for a thick target at the end of irradiation (in Bq) can be expressed by [49]:

$$A_0 = \frac{I}{z \cdot e} \cdot \frac{N_A \cdot C \cdot f}{M} \left(1 - e^{-\lambda t_i}\right) \int_{E_{th}}^{E_0} \frac{\sigma(E)}{S(E)} dE \tag{I-8}$$

Where:
I, the beam intensity which is constant during irradiation (µA);
Ze, charge of the incident particle (µC);
N_A, Avogadro's number;
M, molar mass of the target material (g);
C, mass fraction of the activated element in the target;
f, isotopic abundance of the target isotope A involved in the reaction;
λ, decay constant (s^{-1});
t_i, irradiation time (s);
S(E), stopping power ($MeV.g^{-1}.cm^2$);
σ(E), A(a,b)B nuclear reaction cross section (cm^2);
E_{th}, the threshold energy of the A(a,b)B nuclear reaction.

The data on thick target yields and cross section are largely published in various scientific papers [49, 50]. In general case, the irradiated zone contains a complex mixture of radionuclides produced in various nuclear reactions, which are allowed by interaction energetics. For material loss measurement, the total activity monitoring is inexpedient, since different depth distributions of radionuclides with different decay rates result in diverse and changing in time ratio of radionuclides in every point of material depth. The monitoring should be carried out by measuring the gamma-ray intensity of one selected radionuclide. Such radionuclide must be characterized by long half-life (about several days or more), hard gamma-rays weakly absorbed in the walls of the studied mechanical system and large production yield.

The production of the selected radionuclide is optimized compared to others when the choice of incident particle energy is appropriate in regard to the threshold energies of the occurred nuclear reactions. A decay time to suppress short-lived radionuclides and the selecting of a reduced energy window is always recommended to obtain a pure signal, i.e. without spectral interferences.

A very important characteristic of radio labelling is the depth distribution of the selected radionuclide. It represents the calibration curve used for conversion of the activity change into the thickness of the layer removed.

I-4. ACTIVATION THEORY FOR TLA TECHNIQUE

Two methods are available in order to establish a correlation between the activity variation and the wear/corrosion level. They both comply with the requirements of a metrological method from the accuracy, reproducibility and reliability points of view.

The direct method (DM) is based on the measurement of the remnant activity of the labelled part. To transform an activity loss to material loss, the activity depth profile has to be determined. It is a relative data than can be expressed by the following formula where E_j is the beam energy after passing through the thickness X_j of material to be labelled.

$$\frac{A_j}{A_0} = \frac{\int_{E_j}^{E_0} \frac{\sigma(E)}{S(E)} dE}{\int_{E_{th}}^{E_0} \frac{\sigma(E)}{S(E)} dE} dE \qquad \text{(I-9)}$$

The estimation of the calibration curve $\frac{A_j}{A_0}$ is estimated by varying Ej from E_0 to E_{th} with a constant step width ΔE.

The main error sources are limited to inaccurate incident energy and nuclear reaction cross section. Some cross sections experimentally measured present large discrepancies between authors, especially for exotic nuclear reactions. It is not the case for nuclear reactions commonly used for TLA applications.

The TLA2 in Excel format is a powerful tool for activity depth profile determination and irradiation conditions optimization. (https://www-nds.iaea.org/tla/abouttla.html).

The concentration measurement method (CMM) consists in measuring the activity transferred in lubricant washing the irradiated parts. The estimation of the weight of the worn particles requires the determination of the activity per mass unit. From the above mentioned formula, we reduce the integral to the interval $[E_0 ; E_{SM}]$ for which the cross section is constant. The loss of energy from E_0 to E_{SM} corresponding to a thickness of X_{SM}, it is easy to estimate the activity per unit of mass or volume with the knowledge of the irradiated surface.

Systematic error may occur from inaccurate measurement of the beam intensity on the labelled part. The best way is to determine experimentally the activity per mass unit by irradiating, simultaneously with the part to be studied, a sample with known mass and thickness lower than X_{SM}. This sample has the identical activity per mass unit as the labelled part in the region $[0 ; X_{SM}]$.

ANNEX II. TABLES WITH DIFFERENT ELEMENTS, NUCLEAR REACTIONS AND ACTIVATION PARAMETERS

II-1. ISOTOPES FOR TLA

TABLE II-1. Recommendations on the elements irradiation and activity measurement

Element	Accelerated particle	Measured radionuclide	Energy MeV	Yield kBq/μAh	Radiotracer impurities	Time delay after irradiation	Measured spectrum part, MeV	Possible control duration
Be	^{3}He	^{7}Be(53,3 d)	22.4	407	-	3 d	0.478	5-6 months
C	^{3}He	^{7}Be(53,3 d)	32.1	629	-	3 d	0.478	5-6 months
Mg	d	^{22}Na(2.62 y)	22.8	140.6	^{24}Na	10 d	1.0 - 1.5	years
Al	□	^{22}Na(2.62 y)	42.7	5.92	^{24}Na,^{28}Mg	10 d	1.0 - 1.5	years
	p	^{22}Na(2.62 y)	40	1.2	^{24}Na,^{28}Mg	14 d	1.0 – 1.5	years
Si	d	^{22}Na(2.62 y)	22.3	7.8	-	3 d	1.0 - 1.5	years
Ti	p	^{48}V(16.0 d)	22.5	18870	^{46}Sc,^{47}Sc	20 d	0.9 - 1.5	2 months
V	d	^{51}Cr(27.7 d)	21.6	17020	-	3 d	0.32	3 months
Cr	p	^{52}Mn(5.7 d)	11.0	40737	^{54}Mn	3 d	1.0 - 1.6	3 – 4 weeks
	P	^{51}Cr(27.7 d)	23	16800	^{52}Mn, ^{48}V	40 d	0.32	3 month
	□	^{54}Mn(312.3 d)	45.0	240.5	^{51}Cr,^{52}Mn	40 d	0.84	1 year
Mn	p	^{54}Mn(312.3 d)	22.5	629	^{51}Cr,^{55}Fe	3 d	0.84	1 year
Fe	p	^{56}Co(78.5 d)	13.3	1600	^{57}Co	7 d	0.43 - 2	7-8 months
	d	^{57}Co(271.742 d)	7.2	76	^{55}Co, ^{58}Co, ^{52M}n, ^{54}Mn,	3 d	< 0.15	years
	□	^{58}Co + ^{56}Co	45.0	1110 +59	^{57}Co,^{55}Fe	7 d	0.7 - 0.9	7-8 months
Co	p	^{58}Co(70.8 d)	22.7	4070		7 d	0.81	7-8 months
Ni	d	^{58}Co + ^{56}Co	22.5	196 + 4921	^{57}Co, ^{60}Co	7 d	0.7 - 0.9	7-8 months
	p	^{57}Co(271.742 d)	23.5	1500	^{57}Ni, ^{55}Co	7 d	< 0.15	years
Cu	p	^{65}Zn(244.1 d)	11.0	251.6	-	7 d	< 1.12	1 - 2 years
Zn	d	^{65}Zn(244.1 d)	20.5	469.9	^{67}Ga	3 d	1.12	1 year
Zr	p	^{92m}Nb(10.1 d)	22.4	3885	^{87,88}Y,^{89} Zr	7 d	0.8 - 1.1	1 month
Nb	p	^{92m}Nb(10.1 d)	20.5	469.9	^{89}Zr, ^{93m}Mo	7 d	0.8 - 1.1	1 month
	□	^{95m}Tc(61 d)	45.0	111	^{92m}Nb, ^{96}Tc	1.5 months	0.5 - 1.0	6-7 months
Mo	p	^{95m}Tc(61 d)	22.4	518	^{96}Tc, ^{97}Tc	1 month	0.5 - 1.0	6-7 months
	p	^{96}Tc(4.3 d)	14	10000	^{95m}Tc	1 d	0.7 – 0.9	2 weeks
Sn	d	^{124}Sb(60.2 d)	22.3	333	^{120m}Sb, ^{122}Sb	20 d	1.69	6 months
	p	^{120m}Sb(5.76 d)	12	200	^{122}Sb, ^{124}Sb	1 - 2 d	0.1 – 2	3 weeks
W	p	^{184}Re(38 d)	22.0	2590	^{183}Re	7 d	0.7 - 1.0	4 months

II.2. OTHER TABLES

The following tables are based on (I.O. Konstantinov. Catalogue of Nuclear Data for the Thin Layer Activation Technique).

Content of tables is as follows:

- $Cr + p \rightarrow {}^{52}Mn$ — Tables II-2 to II-4.
- $Al + {}^{3}He \rightarrow {}^{22}Na$ — Table II-5.
- $Ti + p \rightarrow {}^{48}V$ — Tables II-6 to II-8.
- $Ti + d \rightarrow {}^{48}V$ — Tables II-9 to II-10.
- $Ti + \alpha \rightarrow {}^{51}Cr$ — Table II-11.
- $Ti + {}^{3}He \rightarrow {}^{48}V$ — Table II-12.
- $Fe + p \rightarrow {}^{56}Co.$ — Tables II-13, II-14.
- $Fe + d \rightarrow {}^{56,57}Co.$ — Tables II-15 to II-17.
- $Fe + {}^{3}He \rightarrow {}^{56,57,58}Co, {}^{57}Ni$ — Table II-18.
- $Ni + p \rightarrow {}^{57}Co$ — Tables II-19, II-20.
- $Ni + d \rightarrow {}^{56,58}Co$ — Table II-21.
- $Ni + {}^{3}He \rightarrow {}^{56,57,58}Co, {}^{56,57}Ni$ — Table II-22.
- $Cu + p \rightarrow {}^{65}Zn$ — Tables II-23 to II-25.
- $Cu + d \rightarrow {}^{65}Zn$ — Tables II-26, II-27.
- $Cu + {}^{3}He \rightarrow {}^{58,60}Co, {}^{65}Zn, {}^{67}Ga$ — Table II-28.
- $Zn + p \rightarrow {}^{65}Zn, {}^{67}Ga$ — Tables II-29, II-30.
- $Zn + d \rightarrow {}^{65}Zn, {}^{67}Ga$ — Tables II-31, II-32.
- $Zn + {}^{3}He \rightarrow {}^{65}Zn, {}^{67}Ga, {}^{68}Ge$ — Table II-33.
- $Nb + p \rightarrow {}^{89}Zr, {}^{92m}Nb$ — Table II-34.
- $Nb + d \rightarrow {}^{92m}Nb$ — Table II-35.
- $Nb + {}^{3}He \rightarrow {}^{95m}Tc, {}^{88}Y, {}^{92m}Nb$ — Table II-36.
- $Mo + p \rightarrow {}^{95m}Tc, {}^{96}Tc$ — Tables II-37 to II-40.
- $Mo + d \rightarrow {}^{95m}Tc, {}^{96}Tc$ — Table II-41.
- $Mo + {}^{3}He \rightarrow {}^{95m}Tc, {}^{96}Tc, {}^{97}Ru$ — Table II-42.
- $W + p \rightarrow {}^{183}Re, {}^{184g}Re$ — Tables II-43, II-44.
- $W + d \rightarrow {}^{183}Re, {}^{184g}Re$ — Table II-45.
- $W + {}^{3}He \rightarrow {}^{183}Re, {}^{184g}Re, {}^{185}Os$ — Table II-46.

TABLE II-2. Depth distribution of ^{52}Mn in chromium, irradiated by protons:
(Cr+p → ^{52}Mn, Ep=22MeV)

Particle energy E, MeV	Depth x,mg.cm^{-2}	Activity, rel. units A	a
22.0	0	1.000	0
21.5	31.9	0.960	0.040
21.0	63.8	0.920	0.080
20.5	94.5	0.881	0.119
20.0	125.2	0.842	0.158
19.5	154.8	0.800	0.200
19.0	184.4	0.759	0.241
18.5	212.8	0.722	0.278
18.0	241.1	0.685	0.315
17.5	268.4	0.642	0.358
17.0	295.6	0.602	0.398
16.5	321.6	0.562	0.435
16.0	347.6	0.527	0.473
15.5	372.4	0.486	0.514
15.0	397.1	0.446	0.554
14.5	420.7	0.407	0.593
14.0	444.2	0.368	0.632
13.5	471.5	0.328	0.672
13.0	488.8	0.289	0.711
12.5	509.9	0.249	0.751
12.0	530.9	0.211	0.789
11.5	550.6	0.174	0.826
11.0	570.3	0.138	0.862
10.5	588.8	0.100	0.900
10.0	607.2	0.064	0.936
9.5	624.6	0.046	0.954
9.0	641.4	0.029	0.971
8.5	657.4	0.016	0.984
8.0	672.8	0.009	0.991
7.5	687.5	0.006	0.994
7.0	701.4	0.002	0.998

TABLE II-3. Thick target yield of ^{52}Mn in chromium, irradiated by protons:
(Cr + p $\rightarrow$ ^{52}Mn, Ep = 22 MeV)

Particle energy E, MeV	Range, R, mg.cm^{-2}	Yield Y, kBq.μA^{-1}.h^{-1}
22.0	815.0	20350
21.5	783.1	19536
21.0	751.2	18722
20.5	720.5	17945
20.0	689.8	17131
19.5	660.2	16280
19.0	630.6	15429
18.5	602.2	14689
18.0	573.9	13949
17.5	546.6	13061
17.0	519.4	12247
16.5	493.4	11507
16.0	467.4	10730
15.5	442.6	9879
15.0	417.9	9065
14.5	394.3	8288
14.0	370.8	7474
13.5	343.5	6660
13.0	326.2	5883
12.5	305.1	5069
12.0	284.1	4292
11.5	264.4	3626
11.0	244.7	2812
10.5	226.2	2035
10.0	207.8	1295
9.5	190.4	925
9.0	173.6	592
8.5	157.6	325.6
8.0	142.2	192.4
7.5	127.5	125.8
7.0	113.6	59.2

TABLE II-4. Depth distribution of ^{52}Mn in chromium, irradiated by protons
($Cr + p \rightarrow {}^{52}Mn$, Ep = 11 MeV)

Particle energy E, MeV	Depth x, mg.cm^{-2}	Activity, rel. units	
		A	a
11.0	0	1.000	0
10.5	18.5	0.834	0.166
10.0	36.9	0.683	0.317
9.5	54.3	0.533	0.467
9.0	71.1	0.402	0.598
8.5	86.1	0.294	0.706
8.0	102.5	0.201	0.799
7.5	117.2	0.121	0.879
7.0	131.1	0.055	0.945
6.5	144.4	0.019	0.981
6.0	156.9	0.03	0.997

TABLE II-5. Activation of Aluminium by ^{3}He ions (E=30 MeV).
($Al + {}^{3}He \rightarrow {}^{22}Na$)

Particle energy E, MeV	Range R mg/cm^2	Depth x mg/cm^2	Yield Y kBq/μAh	Activity A rel. units
30	127.1	0.0	432.9	1.000
29	119.8	7.3	404.4	0.934
28	112.7	14.4	376.3	0.869
27	105.8	21.3	347.8	0.803
26	99.1	28.0	319.7	0.739
25	92.6	34.5	290.5	0.671
24	86.3	40.8	259.0	0.598
23	80.1	47.0	229.4	0.530
22	74.2	52.9	196.8	0.455
21	68.5	58.6	166.5	0.385
20	63.0	64.1	139.1	0.321
19	57.7	69.4	114.0	0.263
18	52.6	74.5	90.3	0.209
17	47.7	79.4	69.6	0.161
16	43.1	84.1	52.9	0.122
15	38.6	88.5	38.5	0.089
14	34.4	92.8	25.9	0.060
13	30.3	96.8	16.7	0.039
12	26.5	100.6	9.6	0.022
11	23.0	104.1	5.6	0.013
10	19.6	107.5	3.3	0.008
9	16.5	110.6	1.9	0.004
8	13.7	113.4	0.9	0.002
7	11.1	116.0	0.4	0.001

TABLE II-6. Activation of Titanium by protons (E=22 MeV).
($Ti + p \rightarrow {}^{48}V$)

Particle energy E, MeV	Range R mg/cm^2	Depth x mg/cm^2	Yield Y MBq/μAh	Activity A rel. units
22.0	815.0	0.0	2294.0	1.000
21.5	783.1	32.9	2253.3	0.982
21.0	751.2	63.8	2197.8	0.958
20.5	720.5	94.5	2157.1	0.941
20.0	689.8	125.2	2116.4	0.922
19.5	660.2	154.8	2072.0	0.904
19.0	630.6	184.6	2027.6	0.884
18.5	602.3	212.7	1964.7	0.857
18.0	573.9	241.1	1912.9	0.835
17.5	546.6	268.4	1857.4	0.810
17.0	519.4	295.6	1805.6	0.785
16.5	488.4	326.6	1724.2	0.751
16.0	467.4	347.6	1639.1	0.715
15.5	442.6	372.4	1550.3	0.675
15.0	417.9	397.1	1446.7	0.630
14.5	394.3	420.7	1335.7	0.582
14.0	370.8	444.2	1221.0	0.533
13.5	348.5	466.5	1102.6	0.482
13.0	326.2	488.8	984.2	0.429
12.5	305.2	509.8	865.8	0.377
12.0	284.1	530.9	751.1	0.328
11.5	264.4	550.6	643.8	0.281
11.0	244.7	570.3	547.6	0.238
10.5	226.3	588.7	451.4	0.196
10.0	207.8	607.2	362.6	0.158
9.5	190.4	624.6	284.9	0.124
9.0	173.6	641.4	210.9	0.092
8.5	157.6	657.4	136.9	0.060
8.0	142.2	672.8	88.8	0.039
7.5	127.5	687.5	51.8	0.023
7.0	113.6	701.4	24.1	0.011
6.5	100.3	714.2	11.8	0.005
6.0	87.8	727.2	4.8	0.002

TABLE II-7. Activation of Titanium by protons (E=11 MeV).
($Ti + p \rightarrow {}^{48}V$)

Particle energy E, MeV	Range R mg/cm^2	Depth x mg/cm^2	Yield Y MBq/μAh	Activity A rel. units
11.0	244.7	0.0	555.00	1.000
10.5	226.3	18.4	477.30	0.860
10.0	207.8	36.9	399.60	0.720
9.5	190.4	54.3	328.01	0.591
9.0	173.6	71.1	261.96	0.472
8.5	157.6	87.1	202.58	0.365
8.0	142.2	102.5	138.75	0.250
7.5	127.5	117.2	98.79	0.178
7.0	113.6	131.1	63.83	0.115
6.5	100.3	144.4	31.08	0.056
6.0	87.8	156.9	11.10	0.020
5.5	76.0	168.7	2.78	0.005

TABLE II-8. Activation of Titanium by protons (E=7 MeV).
($Ti + p \rightarrow {}^{48}V$)

Particle energy E, MeV	Range R mg/cm^2	Depth x mg/cm^2	Yield Y MBq/μAh	Activity A rel. units
7.0	113.60	0.00	62.90	1.00
6.8	108.30	5.30	47.92	0.76
6.6	103.00	10.60	37.00	0.59
6.4	97.90	15.70	27.57	0.44
6.2	92.80	20.80	19.06	0.30
6.0	87.80	25.80	11.10	0.18
5.8	83.00	30.60	5.37	0.09
5.6	78.30	35.30	1.48	0.02

TABLE II-9. Activation of Titanium by deuterons (E=22 MeV).
($Ti + d \rightarrow {}^{48}V$)

Particle energy E, MeV	Range R mg/cm^2	Depth x mg/cm^2	Yield Y MBq/μAh	Activity A rel. units
22.0	489.50	0.00	1147.00	1.000
21.5	470.40	19.10	1095.20	0.955
21.0	452.00	37.50	1039.70	0.906
20.5	433.60	55.90	980.50	0.855
20.0	415.80	73.30	921.30	0.802
19.5	398.00	91.50	858.40	0.748
19.0	380.90	108.60	795.50	0.695
18.5	363.80	125.70	736.30	0.643
18.0	347.40	142.10	677.10	0.590
17.5	331.00	158.50	614.20	0.537
17.0	315.30	174.20	558.70	0.486
16.5	299.50	190.00	503.20	0.440
16.0	284.50	205.00	455.10	0.396
15.5	269.50	220.00	407.00	0.354
15.0	255.20	234.30	360.01	0.314
14.5	240.80	248.70	316.72	0.276
14.0	227.20	262.30	275.28	0.240
13.5	213.60	275.90	235.32	0.205
13.0	200.70	288.80	194.99	0.170
12.5	187.80	301.70	158.36	0.138
12.0	175.60	313.90	128.39	0.112
11.5	163.40	326.10	98.79	0.086
11.0	152.00	337.50	74.56	0.065
10.5	140.50	349.00	57.35	0.052
10.0	129.90	359.60	45.88	0.040
9.5	119.40	370.10	34.41	0.030
9.0	109.40	380.10	24.09	0.021
8.5	99.65	389.85	16.06	0.014
8.0	90.34	399.16	9.18	0.008
7.5	81.43	408.07	5.18	0.005
7.0	72.92	416.58	1.74	0.002

TABLE II-10. Activation of Titanium by deuterons (E=10 MeV).
(Ti + d → ^{48}V)

Particle energy E, MeV	Range R mg/cm^2	Depth x mg/cm^2	Yield Y MBq/μAh	Activity A rel. units
10.0	129.90	0.0	44.40	1.000
9.8	125.70	4.2	39.89	0.898
9.6	121.60	8.3	35.52	0.800
9.4	117.50	12.4	31.08	0.700
9.2	113.40	16.5	26.79	0.603
9.0	109.40	20.5	23.01	0.518
8.8	105.50	24.4	19.54	0.440
8.6	101.60	28.3	16.65	0.375
8.4	97.86	32.0	13.95	0.314
8.2	94.10	35.8	11.25	0.253
8.0	90.34	39.6	9.07	0.204
7.8	86.76	43.1	7.40	0.167
7.6	83.16	46.7	5.85	0.132
7.4	79.66	50.2	4.44	0.100
7.2	76.24	53.7	3.07	0.069
7.0	72.92	57.0	1.81	0.041
6.8	69.68	60.2	0.67	0.015

TABLE II-11. Activation of Titanium by alpha-particles (E=44 MeV).

			(Ti + α→ ^{51}Cr)		(Ti + α → ^{48}V)	
Particle energy E, MeV	Range R mg/cm^2	Depth *x* mg/cm^2	Yield Y MBq/μAh	Activity A rel. units	Yield Y MBq/μAh	Activity A rel. units
44	245.50	0.0	53.91	1.000	133.20	1.000
43	236.00	9.5	51.43	0.954	132.02	0.991
42	226.80	18.7	48.95	0.908	130.80	0.982
41	217.60	27.9	46.47	0.862	129.61	0.973
40	208.70	36.8	43.99	0.816	128.28	0.963
39	199.70	45.8	41.29	0.766	126.80	0.952
38	191.20	54.3	38.59	0.716	125.21	0.940
37	182.70	62.8	36.11	0.669	123.47	0.927
36	174.50	71.0	33.60	0.623	121.73	0.914
35	166.20	79.3	31.08	0.577	119.95	0.901
34	158.40	87.1	28.60	0.531	118.07	0.886
33	150.40	95.1	26.31	0.488	116.14	0.872
32	143.00	102.5	24.01	0.445	114.15	0.857
31	135.40	110.1	21.83	0.405	112.04	0.841
30	128.30	117.2	19.68	0.365	109.89	0.825
29	121.20	124.3	17.50	0.325	107.74	0.809
28	114.30	131.2	15.21	0.282	105.49	0.792
27	107.50	138.0	13.21	0.245	102.82	0.772
26	101.00	144.5	11.60	0.215	100.05	0.751
25	94.61	150.9	9.99	0.185	96.50	0.728
24	88.41	157.1	8.44	0.157	93.76	0.707
23	82.40	163.1	7.10	0.132	90.17	0.677
22	76.58	168.9	5.77	0.107	86.43	0.649
21	70.94	174.6	4.59	0.085	82.33	0.618
20	65.50	180.0	3.63	0.067	77.26	0.580
19	60.24	185.3	2.86	0.053	71.11	0.534
18	55.18	190.3	2.22	0.041	63.53	0.477
17	50.31	195.2	1.70	0.032	54.46	0.409
16	45.64	199.9	1.26	0.023	46.36	0.348
15	41.17	204.3	0.89	0.017	39.15	0.294
14	36.91	208.6	0.59	0.011	32.23	0.242
13	32.84	212.7	24.49	0.184		
12	28.99	216.5	17.58	0.132		
11	25.34	220.2	11.17	0.084		
10	21.91	223.6	6.14	0.046		
9	18.70	226.8	3.33	0.025		

TABLE II-12. Activation of Titanium by ^{3}He ions.

($Ti + {}^{3}He \rightarrow {}^{48}V$)

Particle energy E, MeV	Range R mg/cm^2	Depth x mg/cm^2	Yield Y MBq/μAh	Activity A rel. units
30	156.20	0.00	194.3	1.000
29	147.40	8.80	164.7	0.848
28	138.90	17.30	138.8	0.714
27	130.50	25.70	112.9	0.581
26	122.50	33.70	92.5	0.476
25	114.60	41.60	74.0	0.381
24	107.00	49.20	58.1	0.299
23	99.57	57.63	45.1	0.232
22	92.40	63.80	35.2	0.181
21	85.47	70.73	27.8	0.143
20	78.78	77.42	21.5	0.111
19	83.87	83.87	17.4	0.090
18	66.12	90.08	13.7	0.071
17	60.16	96.04	10.7	0.055
16	54.45	101.75	7.8	0.040
15	48.98	107.22	5.6	0.029
14	43.78	112.42	3.7	0.019
13	38.83	117.37	2.2	0.011
12	34.14	122.06	0.7	0.004

TABLE II-13. Activation of Iron by protons (E=11 MeV).

($Fe + p \rightarrow {}^{56}Co$)

Particle energy E, MeV	Range R mg/cm^2	Depth x mg/cm^2	Yield Y MBq/μAh	Activity A rel. units
11.0	245.1	0.0	54.39	1.000
10.5	226.7	18.4	45.14	0.830
10.0	208.3	36.8	36.08	0.663
9.5	191.0	54.1	27.64	0.508
9.0	174.3	70.8	20.13	0.370
8.5	158.2	86.9	13.69	0.252
8.0	142.9	102.2	9.51	0.175
7.5	128.2	116.9	5.99	0.110
7.0	114.3	130.8	3.40	0.063
6.5	101.0	144.1	1.74	0.032
6.0	88.5	156.6	0.56	0.010
5.5	65.6	179.5	0.07	0.001

TABLE II-14. Activation of Iron by protons (E=7 MeV).
(Fe + p → ^{56}Co)

Particle Energy E, MeV	Range R mg/cm^2	Depth x mg/cm^2	Yield Y MBq/μAh	Activity A rel. units
7.0	114.3	0.0	5.18	1.000
6.8	108.9	5.3	3.85	0.739
6.6	103.7	10.6	2.48	0.479
6.4	98.5	15.8	1.59	0.305
6.2	93.5	20.8	0.93	0.182
6.0	88.5	25.8	0.48	0.091
5.8	83.8	30.5	0.26	0.044
5.6	79.1	35.2	0.07	0.016

TABLE II-15. Activation of Iron by deuterons (E=22 MeV).

	(Fe + d → ^{56}Co)		(Fe + d → ^{57}Co)			
Particle Energy E, MeV	Range R mg/cm^2	Depth *x* mg/cm^2	Yield Y MBq/μAh	Activity A rel. units	Yield Y MBq/μAh	Activity A rel. units
22.0	490.3	0.0	166.5	1.000	37.00	1.000
21.5	471.6	18.7	159.1	0.958	36.70	0.992
21.0	452.9	34.7	151.0	0.905	36.45	0.985
20.5	434.8	55.5	143.2	0.860	36.08	0.975
20.0	416.8	73.5	135.1	0.810	35.78	0.967
19.5	399.4	90.9	126.9	0.762	35.41	0.957
19.0	382.1	108.2	118.8	0.713	35.00	0.946
18.5	365.4	124.9	111.0	0.667	34.60	0.935
18.0	348.7	141.6	102.5	0.615	34.15	0.923
17.5	332.6	157.7	94.7	0.569	33.74	0.912
17.0	316.6	173.7	86.6	0.516	33.30	0.900
16.5	301.2	189.1	78.4	0.472	32.75	0.885
16.0	285.9	204.4	70.7	0.425	32.12	0.868
15.5	271.2	219.1	62.9	0.377	31.34	0.847
15.0	256.6	233.7	54.8	0.329	30.41	0.822
14.5	242.6	247.7	47.0	0.282	29.34	0.793
14.0	228.7	261.6	38.5	0.232	28.38	0.767
13.5	215.4	274.9	32.6	0.191	27.20	0.735
13.0	202.2	288.1	24.4	0.152	25.97	0.702
12.5	189.6	300.7	19.2	0.115	24.72	0.668
12.0	177.1	313.2	13.7	0.083	23.27	0.629
11.5	165.3	325.0	9.3	0.056	21.83	0.590
11.0	156.6	336.7	5.9	0.036	20.35	0.550
10.5	142.7	347.6	3.7	0.023	18.50	0.500
10.0	131.8	358.5	2.3	0.014	16.65	0.450
9.5	121.2	369.1	1.3	0.008	15.21	0.411
9.0	110.7	379.6	0.5	0.003	13.73	0.371
8.5	101.1	389.2			12.10	0.327
8.0	91.6	398.7			10.43	0.282
7.5	82.9	407.4			8.95	0.242
7.0	74.1	416.2			7.36	0.199
6.5	66.2	424.2			6.11	0.165
6.0	58.2	432.1			4.77	0.129
5.5	51.1	439.2			3.74	0.101
5.0	44.0	446.4			2.78	0.075
4.5	37.7	452.6			1.92	0.052
4.0	31.4	458.9			1.26	0.034
3.5	26.1	464.2			0.81	0.022

Table II-16. Activation of Iron by deuterons (E=10 MeV).
(Fe + d → ^{57}Co)

Particle Energy E, MeV	Range R mg/cm^2	Depth x mg/cm^2	Yield Y MBq/μAh	Activity A rel. units
10.0	131.8	0.0	16.65	1.000
9.5	121.2	10.6	15.21	0.913
9.0	110.7	21.1	13.73	0.824
8.5	101.1	30.7	12.10	0.727
8.0	91.6	40.2	10.43	0.627
7.5	82.9	48.9	8.95	0.538
7.0	74.1	57.7	7.36	0.442
6.5	66.2	65.7	6.11	0.367
6.0	58.2	74.6	4.77	0.287
5.5	51.1	80.7	3.74	0.224
5.0	44.0	87.9	2.78	0.167
4.5	37.7	94.1	1.92	0.116
4.0	31.4	100.4	1.26	0.076
3.5	26.1	105.7	0.81	0.049
3.0	20.7	111.1	0.44	0.027
2.5	15.7	116.1	0.30	0.018
2.0	11.0	120.8	0.07	0.004

TABLE II-17. Activation of Iron by deuterons (E=7 MeV).
(Fe + d → ^{57}Co)

Particle Energy E, MeV	Range R mg/cm^2	Depth x mg/cm^2	Yield Y MBq/μAh	Activity A rel. units
7.0	74.1	0.0	7.40	1.000
6.5	66.2	8.0	6.11	0.825
6.0	58.2	15.9	4.81	0.650
5.5	51.1	23.0	3.70	0.500
5.0	44.0	30.2	2.78	0.375
4.5	37.7	36.4	1.92	0.260
4.0	31.4	42.7	1.26	0.170
3.5	26.1	48.0	0.81	0.110
3.0	20.7	53.4	0.44	0.060
2.5	15.7	58.4	0.30	0.030
2.0	11.0	63.1	0.07	0.010

TABLE II-18. Activation of Iron by ^{3}He ions (E=30 MeV).

			(Fe + 3He → ^{58}Co)		(Fe + 3He → ^{57}Co)	
Particle Energy E, MeV	Range R mg/cm^2	Depth *x* mg/cm^2	Yield Y MBq/μAh	Activity A rel. units	Yield Y MBq/μAh	Activity A rel. units
30	156.60	0.00	5.032	1.000	27.084	1.000
29	147.80	8.80	4.884	0.971	26.085	0.963
28	139.30	17.30	4.718	0.938	25.012	0.924
27	131.00	25.60	4.533	0.901	23.680	0.874
26	122.90	33.70	4.329	0.860	22.311	0.824
25	115.10	41.50	4.107	0.816	20.868	0.771
24	107.50	49.10	3.885	0.772	19.388	0.716
23	100.10	56.50	3.645	0.724	17.686	0.653
22	92.93	63.67	3.404	0.677	16.095	0.594
21	86.01	70.59	3.145	0.625	14.393	0.531
20	79.32	77.28	2.890	0.574	12.691	0.469
19	72.87	83.73	2.646	0.526	10.989	0.406
18	66.66	89.94	2.409	0.479	9.324	0.344
17	60.69	95.91	2.150	0.427	7.659	0.283
16	54.97	101.63	1.902	0.378	5.994	0.221
15	49.50	107.10	1.639	0.326	4.477	0.165
14	44.28	112.32	1.351	0.268	3.160	0.117
13	39.31	117.29	1.058	0.210	2.102	0.078
12	34.61	121.99	0.807	0.160	1.369	0.051
11	30.16	126.44	0.533	0.106	0.851	0.031
10	25.99	130.61	0.322	0.064	0.481	0.018
9	22.09	134.52	0.167	0.033	0.189	0.007
8	18.45	138.15	0.007	0.015	0.037	0.001

TABLE II-18. (cont.) Activation of Iron by 3He ions.

			(Fe + 3He → ^{57}Ni)		(Fe + 3He → ^{56}Co)	
Particle Energy E, MeV	Range R mg/cm^2	Depth x mg/cm^2	Yield Y MBq/μAh	Activity A rel. units	Yield Y MBq/μAh	Activity A rel. units
30	156.60	0.00	257.150	1.000	18.796	1.000
29	147.80	8.80	253.450	0.986	15.799	0.841
28	139.30	17.30	247.530	0.963	12.691	0.675
27	131.00	25.60	239.020	0.930	9.916	0.528
26	122.90	33.70	226.995	0.883	7.215	0.384
25	115.10	41.50	216.820	0.843	5.106	0.272
24	107.50	49.10	204.240	0.794	3.441	0.183
23	100.10	56.50	190.920	0.742	2.120	0.113
22	92.93	63.67	178.007	0.692	1.221	0.065
21	86.01	70.59	162.060	0.630	0.629	0.033
20	79.32	77.28	145.003	0.564	0.274	0.015
19	72.87	83.73	125.985	0.490	0.167	0.009
18	66.66	89.94	106.005	0.412	0.093	0.005
17	60.69	95.91	85.285	0.332		
16	54.97	101.63	66.600	0.259		
15	49.50	107.10	49.617	0.193		
14	44.28	112.32	36.112	0.140		
13	39.31	117.29	25.715	0.100		
12	34.61	121.99	17.797	0.069		
11	30.16	126.44	11.100	0.043		
10	25.99	130.61	5.550	0.022		
9	22.09	134.52	1.924	0.008		
8	18.45	138.15	0.167	0.007		

TABLE II-19. Activation of Nickel by protons (E=22 MeV).
(Ni + p → ^{57}Co)

Particle Energy E, MeV	Range R mg/cm^2	Depth x mg/cm^2	Yield Y MBq/μAh	Activity A rel. units
22.0	806.0	0.0	129.5	1.000
21.5	774.6	31.4	102.5	0.792
21.0	743.3	62.7	75.9	0.585
20.5	713.1	92.9	57.0	0.440
20.0	682.9	123.1	45.9	0.355
19.5	653.8	152.2	37.7	0.290
19.0	624.7	181.3	31.8	0.246
18.5	596.7	209.3	28.1	0.217
18.0	568.8	237.2	25.5	0.196
17.5	542.0	264.0	23.3	0.180
17.0	515.2	290.8	21.1	0.162
16.5	489.6	316.4	19.2	0.148
16.0	464.0	342.0	17.4	0.135
15.5	439.5	366.5	15.5	0.120
15.0	415.1	390.9	13.7	0.106
14.5	391.8	414.2	11.8	0.093
14.0	368.6	437.4	10.4	0.080
13.5	346.6	459.4	8.9	0.068
13.0	324.6	481.4	7.8	0.060
12.5	303.8	502.2	6.7	0.052
12.0	283.1	522.9	5.9	0.046
11.5	263.6	542.4	5.2	0.039
11.0	244.1	561.9	4.4	0.033
10.5	225.8	580.2	3.4	0.026
10.0	207.6	598.4	2.5	0.019
9.5	190.4	615.6	2.1	0.016
9.0	173.8	632.2	1.8	0.014
8.5	157.9	648.1	1.5	0.011
8.0	142.6	663.4	1.2	0.009
7.5	128.0	678.0	0.7	0.005

TABLE II-20. Activation of Nickel by protons (E=10 MeV).
(Ni + p → ^{57}Co)

Particle energy E, MeV	Range R mg/cm^2	Depth x mg/cm^2	Yield Y MBq/μAh	Activity A rel. units
10.0	207.6	0.0	2.405	1.000
9.8	200.7	6.9	2.183	0.908
9.6	193.8	13.8	1.980	0.823
9.4	187.1	20.5	1.776	0.738
9.2	180.4	27.2	1.573	0.654
9.0	173.8	33.8	1.369	0.569
8.8	167.4	40.2	1.184	0.492
8.6	161.1	46.5	0.999	0.415
8.4	154.9	52.7	0.833	0.346
8.2	148.7	58.9	0.685	0.285
8.0	142.6	65.0	0.537	0.223
7.8	136.8	70.8	0.407	0.169
7.6	130.9	76.7	0.296	0.123
7.4	125.3	82.3	0.204	0.085
7.2	119.7	87.9	0.130	0.054
7.0	114.2	93.4	0.056	0.023
6.8	108.9	98.7	0.019	0.008

TABLE II-21. Activation of Nickel by deuterons (E=22 MeV).

			(Ni + d → ^{56}Co)		(Ni + d → ^{58}Co)	
Particle energy E, MeV	Range R mg/cm^2	Depth *x* mg/cm^2	Yield Y MBq/μAh	Activity A rel. units	Yield Y MBq/μAh	Activity A rel. units
22.0	488.3	0.0	19.24	1.000	462.5	1.000
21.5	469.8	18.5	18.69	0.971	432.9	0.937
21.0	451.2	37.1	18.13	0.942	399.6	0.864
20.5	433.3	55.0	17.54	0.912	370.0	0.800
20.0	415.4	72.8	16.65	0.865	340.4	0.735
19.5	398.1	90.2	15.91	0.827	310.1	0.670
19.0	380.9	107.4	14.80	0.769	281.2	0.608
18.5	364.3	124.0	13.69	0.713	253.1	0.547
18.0	347.7	140.6	12.77	0.663	224.2	0.485
17.5	331.8	156.5	11.54	0.600	198.3	0.429
17.0	315.9	172.4	10.18	0.529	172.1	0.372
16.5	300.6	187.7	8.73	0.454	145.8	0.315
16.0	285.3	203.0	7.22	0.375	119.9	0.259
15.5	270.7	217.6	5.55	0.290	95.5	0.206
15.0	256.2	232.1	4.07	0.212	71.8	0.155
14.5	242.3	246.0	2.89	0.150	51.4	0.111
14.0	228.4	259.9	2.04	0.106	37.0	0.080
13.5	215.2	275.1	1.41	0.073	24.4	0.053
13.0	202.1	286.2	1.00	0.052	16.3	0.035
12.5	189.6	298.7	0.70	0.037	8.9	0.019
12.0	177.1	311.2	0.44	0.023	5.2	0.011
11.5	165.3	323.0	0.30	0.015	1.9	0.004
11.0	153.6	334.7	0.15	0.008		
10.5	142.5	345.8	0.04	0.002		

TABLE II-22. Activation of Nickel by 3He ions (E=30 MeV).

			(Ni + ^{3}He → ^{56}Co)		(Ni + ^{3}He → ^{57}Co)	
Particle energy E, MeV	Range R mg/cm^2	Depth *x* mg/cm^2	Yield Y MBq/μAh	Activity A rel. units	Yield Y MBq/μAh	Activity A rel. units
30	156.00	0.00	10.900	1.000	1.339	1.000
29	147.30	8.70	10.323	0.947	1.162	0.867
28	138.90	17.10	9.720	0.892	0.999	0.746
27	130.60	25.40	9.076	0.833	0.855	0.638
26	122.60	33.40	8.399	0.771	0.725	0.541
25	114.80	41.20	7.615	0.699	0.614	0.459
24	107.30	48.70	6.830	0.627	0.518	0.387
23	99.92	56.08	6.031	0.553	0.440	0.329
22	92.80	63.20	5.239	0.481	0.377	0.282
21	85.92	70.08	4.481	0.411	0.329	0.246
20	79.26	76.74	3.770	0.346	0.289	0.216
19	72.85	83.15	3.130	0.287	0.252	0.188
18	66.67	89.33	2.520	0.231	0.222	0.166
17	60.73	95.27	1.980	0.182	0.192	0.144
16	55.03	100.97	1.469	0.135	0.167	0.124
15	49.58	106.42	1.040	0.095	0.141	0.105
14	44.37	111.63	0.703	0.065	0.118	0.088
13	39.42	116.58	0.477	0.044	0.089	0.066
12	34.73	121.27	0.311	0.028	0.059	0.044
11	30.29	125.71	0.170	0.016	0.033	0.025
10	26.12	129.88	0.044	0.004	0.007	0.006

TABLE II-22. (Cont.) Activation of Nickel by ^{3}He ions (E=30 MeV).
($Ni + {}^{3}He \rightarrow {}^{58}Co$)

Particle energy E, MeV	Range R mg/cm^2	Depth *x* mg/cm^2	Yield Y MBq/μAh	Activity A rel. units
30	156.00	0.00	19.299	1.000
29	147.30	8.70	17.101	0.886
28	138.90	17.10	14.900	0.772
27	130.60	25.40	12.698	0.658
26	122.60	33.40	10.501	0.544
25	114.80	41.20	8.628	0.447
24	107.30	48.70	6.849	0.355
23	99.92	56.08	5.298	0.275
22	92.80	63.20	3.952	0.205
21	85.92	70.08	2.871	0.149
20	79.26	76.74	2.079	0.108
19	72.85	83.15	1.521	0.079
18	66.67	89.33	1.121	0.058
17	60.73	95.27	0.858	0.045
16	55.03	100.97	0.636	0.032
15	49.58	106.42	0.474	0.025
14	44.37	111.63	0.311	0.016
13	39.42	116.58	0.141	0.007
12	34.73	121.27	0.081	0.004
11	30.29	125.71	0.044	0.002
10	26.12	129.88	0.022	0.001

TABLE II-22. (cont.) Activation of Nickel by ^{3}He ions.

			($Ni + {}^{3}He \rightarrow {}^{56}Ni$)		($Ni + {}^{3}He \rightarrow {}^{57}Ni$)	
Particle energy E, MeV	Range R mg/cm^2	Depth x mg/cm^2	Yield Y MBq/μAh	Activity A rel. units	Yield Y MBq/μAh	Activity A rel. units
30	156.00	0.00	2.146	1.000	106.01	1.000
29	147.30	8.70	2.054	0.957	97.68	0.922
28	138.90	17.10	1.939	0.903	89.32	0.843
27	130.60	25.40	1.798	0.838	81.03	0.764
26	122.60	33.40	1.654	0.771	72.52	0.686
25	114.80	41.20	1.510	0.703	65.56	0.619
24	107.30	48.70	1.362	0.635	59.02	0.557
23	99.92	56.08	1.199	0.559	53.35	0.503
22	92.80	63.20	1.051	0.490	48.29	0.456
21	85.92	70.08	0.899	0.419	43.40	0.409
20	79.26	76.74	0.747	0.345	38.52	0.363
19	72.85	83.15	0.607	0.283	34.30	0.324
18	66.67	89.33	0.485	0.226	30.30	0.286
17	60.73	95.27	0.381	0.178	26.01	0.245
16	55.03	100.97	0.289	0.135	22.50	0.212
15	49.58	106.42	0.215	0.100	19.20	0.181
14	44.37	111.63	0.159	0.074	15.98	0.151
13	39.42	116.58	0.104	0.048	13.28	0.125
12	34.73	121.27	0.059	0.028	10.80	0.102
11	30.29	125.71	0.019	0.009	8.44	0.080
10	26.12	129.88	0.007	0.003	5.92	0.056
9	22.22	133.78	4.070	0.038		
8	18.59	137.41	2.590	0.024		
7	15.24	140.76	1.480	0.014		

TABLE II-23. Activation of Copper by protons (E=22 MeV).
($Cu + p \rightarrow {}^{65}Zn$)

Particle energy E, MeV	Range R mg/cm^2	Depth x mg/cm^2	Yield Y MBq/μAh	Activity A rel. units
22.0	849.0	0.0	61.1	1.000
21.5	816.0	33.0	60.3	0.990
21.0	783.0	66.0	59.9	0.981
20.5	751.2	97.8	59.2	0.970
20.0	719.4	129.6	58.8	0.961
19.5	688.8	160.2	57.7	0.948
19.0	658.2	190.8	57.0	0.935
18.5	628.8	220.2	56.2	0.922
18.0	599.4	249.6	55.5	0.910
17.5	571.2	277.8	54.4	0.893
17.0	543.0	306.0	53.7	0.876
16.5	516.0	333.0	52.2	0.855
16.0	489.1	359.9	51.1	0.834
15.5	463.3	385.7	49.2	0.807
15.0	437.6	411.4	47.7	0.781
14.5	413.1	435.9	45.5	0.748
14.0	388.7	460.3	43.7	0.716
13.5	365.5	483.5	41.4	0.676
13.0	342.4	506.6	38.9	0.636
12.5	320.5	528.5	36.3	0.593
12.0	298.6	550.4	33.7	0.551
11.5	278.0	571.0	30.7	0.503
11.0	257.5	591.5	27.8	0.455
10.5	238.3	610.7	24.4	0.388
10.0	219.1	629.9	21.1	0.345
9.5	201.0	648.0	17.0	0.279
9.0	183.5	665.5	14.1	0.230
8.5	166.7	682.3	11.5	0.187
8.0	150.6	698.4	9.3	0.149
7.5	135.3	713.7	7.0	0.116
7.0	120.6	728.4	5.6	0.089
6.5	106.7	742.3	4.4	0.070
6.0	93.6	755.4	3.0	0.050
5.5	81.2	767.8	2.1	0.034
5.0	69.6	779.4	1.3	0.022
4.5	58.7	790.3	0.9	0.014
4.0	48.7	800.3	0.4	0.008

TABLE II-24. Activation of Copper by protons (E=11 MeV).
(Cu + p → ^{65}Zn)

Particle energy E, MeV	Range R mg/cm^2	Depth x mg/cm^2	Yield Y MBq/μAh	Activity A rel. units
11.0	257.5	0.0	27.01	1.000
10.5	238.3	19.2	23.68	0.876
10.0	219.1	38.4	20.13	0.745
9.5	201.0	56.5	16.76	0.620
9.0	183.5	74.0	13.47	0.498
8.5	166.7	90.8	10.73	0.397
8.0	150.6	106.9	7.99	0.296
7.5	135.3	122.2	6.14	0.228
7.0	120.6	136.9	4.70	0.174
6.5	106.7	150.8	3.44	0.127
6.0	93.6	163.9	2.33	0.086
5.5	81.2	176.3	1.44	0.053
5.0	69.6	187.9	0.74	0.028
4.5	58.7	198.8	0.30	0.011
4.0	48.7	208.3	0.15	0.007
3.5	39.5	218.0	0.07	0.005
3.0	31.0	226.5	0.04	0.002

TABLE II-25. Activation of Copper by protons (E=7 MeV).
($Cu + p \rightarrow {}^{65}Zn$)

Particle energy E, MeV	Range R mg/cm^2	Depth x mg/cm^2	Yield Y MBq/μAh	Activity A rel. units
7.0	120.6	0.0	4.440	1.000
6.8	114.0	6.6	3.848	0.863
6.6	109.7	10.9	3.293	0.738
6.4	104.6	16.0	2.886	0.647
6.2	99.2	21.4	2.479	0.561
6.0	93.6	27.0	2.072	0.468
5.8	88.6	32.0	1.739	0.390
5.6	83.8	36.8	1.369	0.311
5.4	78.9	41.7	1.073	0.245
5.2	74.0	46.6	0.851	0.189
5.0	69.6	51.0	0.666	0.148
4.8	65.1	55.0	0.518	0.117
4.6	60.8	59.8	0.407	0.088
4.4	56.6	65.0	0.285	0.064
4.2	52.6	68.0	0.204	0.046
4.0	48.7	71.9	0.130	0.029
3.8	44.9	75.7	0.078	0.018
3.6	41.3	79.3	0.063	0.014
3.4	37.7	82.9	0.044	0.010
3.2	34.3	86.3	0.026	0.006
3.0	31.1	89.6	0.015	0.003

TABLE II-26. Activation of Copper by deuterons (E=22 MeV).
($Cu + d \rightarrow {}^{65}Zn$)

Particle energy E, MeV	Range R mg/cm^2	Depth x mg/cm^2	Yield Y MBq/μAh	Activity A rel. units
22.0	512.2	0.0	70.30	1.000
21.5	495.6	19.6	67.71	0.962
21.0	476.1	39.1	65.12	0.924
20.5	457.2	58.0	62.16	0.882
20.0	438.4	76.8	59.20	0.841
19.5	420.2	95.0	55.87	0.796
19.0	402.1	113.1	52.91	0.752
18.5	384.6	130.6	49.58	0.704
18.0	367.1	148.1	46.25	0.656
17.5	350.3	164.9	42.92	0.609
17.0	333.5	181.7	39.59	0.562
16.5	317.4	197.8	36.26	0.515
16.0	301.4	213.8	32.93	0.468
15.5	286	229.2	29.82	0.424
15.0	270.6	244.6	26.71	0.380
14.5	256	259.2	23.68	0.337
14.0	241.4	273.8	20.72	0.294
13.5	227.5	287.7	17.95	0.255
13.0	213.6	301.6	15.17	0.216
12.5	200.4	314.8	13.32	0.189
12.0	187.2	328.0	10.84	0.154
11.5	174.8	340.4	8.81	0.125
11.0	162.5	352.8	6.88	0.098
10.5	150.8	364.4	5.33	0.076
10.0	139.2	376.0	4.07	0.058
9.5	128.1	387.1	2.89	0.041
9.0	117.3	397.9	1.96	0.028
8.5	107.7	407.5	1.41	0.020
8.0	97.4	417.8	0.85	0.012
7.5	87.9	427.3	0.56	0.008
7.0	78.9	436.3	0.30	0.004

TABLE II-27. Activation of Copper by deuterons (E=10 MeV).
($Cu + d \rightarrow {}^{65}Zn$)

Particle energy E, MeV	Range R mg/cm^2	Depth x mg/cm^2	Yield Y MBq/μAh	Activity A rel. units
10.0	139.2	0	4.070	1.000
9.8	134.8	4.4	3.515	0.864
9.6	130.3	8.9	3.053	0.750
9.4	125.9	13.3	2.646	0.650
9.2	121.6	17.6	2.257	0.555
9.0	117.3	21.9	1.961	0.482
8.8	113.5	25.7	1.635	0.402
8.6	109.6	29.6	1.395	0.343
8.4	105.5	33.7	1.195	0.294
8.2	101.4	37.8	1.006	0.247
8.0	97.4	41.8	0.851	0.209
7.8	93.6	45.6	0.725	0.178
7.6	89.8	49.4	0.592	0.145
7.4	86.1	53.1	0.488	0.120
7.2	82.5	56.7	0.389	0.095
7.0	78.9	60.3	0.296	0.073
6.8	75.3	63.9	0.204	0.050
6.6	71.8	67.4	0.148	0.036
6.4	68.4	70.8	0.096	0.024

TABLE II-28. Activation of Copper by ^{3}He ions (E=30 MeV).

			(Cu + $^{3}He \rightarrow ^{58}Co$)		(Cu + $^{3}He \rightarrow ^{60}Co$)	
Particle energy E, MeV	Range R mg/cm^2	Depth *x* mg/cm^2	Yield Y MBq/μAh	Activity A rel. units	Yield Y MBq/μAh	Activity A rel. units
30	164.60	0.0	518.00	1.000	7.400	1.0000
29	155.50	9.1	481.00	0.929	5.994	0.8100
28	146.60	18.0	444.00	0.856	4.884	0.6600
27	137.90	26.7	404.04	0.780	3.848	0.5200
26	129.50	35.1	360.38	0.696	3.071	0.4160
25	121.30	43.3	314.87	0.608	2.368	0.3170
24	113.30	51.3	272.69	0.526	1.850	0.2510
23	105.50	59.1	232.36	0.448	1.406	0.1880
22	98.04	66.6	192.77	0.372	1.036	0.1390
21	90.78	73.8	156.51	0.302	0.777	0.1030
20	83.76	80.8	123.21	0.238	0.555	0.0770
19	77.00	87.6	90.28	0.174	0.407	0.0520
18	70.48	94.1	67.71	0.131	0.248	0.0330
17	64.21	100.4	49.21	0.095	0.152	0.0200
16	58.20	106.4	35.85	0.069	0.081	0.0110
15	52.45	112.2	25.01	0.048	0.044	0.0060
14	46.96	117.6	16.80	0.032	0.011	0.0016
13	41.73	122.9	11.17	0.022		
12	36.78	127.8	7.10	0.014		
11	32.09	132.5	3.52	0.007		
10	27.68	136.9	1.15	0.002		

TABLE II-28. (cont.) Activation of Copper by ^{3}He ions (E=30 MeV).

			(Cu + $^{3}He \rightarrow {}^{65}Zn$)		(Cu + $^{3}He \rightarrow {}^{67}Ga$)	
Particle energy E, MeV	Range R mg/cm^2	Depth *x* mg/cm^2	Yield Y MBq/μAh	Activity A rel. units	Yield Y MBq/μAh	Activity A rel. units
30	164.60	0.0	7.400	1.000	8.732	1.000
29	155.50	9.1	6.623	0.896	8.399	0.962
28	146.60	18.0	5.883	0.793	8.103	0.926
27	137.90	26.7	5.143	0.694	7.733	0.886
26	129.50	35.1	4.403	0.595	7.363	0.843
25	121.30	43.3	3.959	0.504	6.993	0.801
24	113.30	51.3	3.108	0.418	6.623	0.759
23	105.50	59.1	2.516	0.338	6.253	0.716
22	98.04	66.6	1.998	0.270	5.883	0.674
21	90.78	73.8	1.591	0.216	5.513	0.631
20	83.76	80.8	1.258	0.168	5.143	0.589
19	77.00	87.6	0.962	0.129	4.773	0.547
18	70.48	94.1	0.740	0.098	4.366	0.500
17	64.21	100.4	0.555	0.074	3.922	0.449
16	58.20	106.4	0.444	0.058	3.471	0.398
15	52.45	112.2	0.340	0.046	3.012	0.345
14	46.96	117.6	0.266	0.036	2.549	0.292
13	41.73	122.9	0.204	0.028	2.120	0.243
12	36.78	127.8	0.148	0.020	1.687	0.194
11	32.09	132.5	0.096	0.013	1.280	0.147
10	27.68	136.9	0.059	0.008	0.925	0.106
9	23.56	141.0	0.026	0.003	0.566	0.065
8	19.72	144.9	0.007	0.001	0.348	0.040
7	16.18	148.4	0.159	0.018		
6	12.94	151.7	0.030	0.003		

TABLE II-29. Activation of Zinc by protons (E=22 MeV).

			($Zn + p \rightarrow {}^{65}Zn$)		($Zn + p \rightarrow {}^{67}Ga$)	
Particle energy E, MeV	Range R mg/cm^2	Depth *x* mg/cm^2	Yield Y MBq/μAh	Activity A rel. units	Yield Y MBq/μAh	Activity A rel. units
22	849.0	0	44.40	1.000	2516	1.000
21	783.0	66.0	35.52	0.800	2123.8	0.844
20	719.4	129.6	26.27	0.592	1757.5	0.699
19	658.2	190.8	18.50	0.417	1406	0.559
18	599.4	249.6	12.21	0.275	1110	0.441
17	543.0	306.0	7.03	0.158	832.5	0.331
16	489.1	359.9	3.145	0.071	640.1	0.254
15	437.6	411.4	1.295	0.029	510.6	0.203
14	388.7	460.3	0.444	0.010	425.5	0.169
13	342.4	506.6			370	0.147
12	298.6	550.4			296	0.118
11	257.5	591.5			196.1	0.078
10	219.1	629.9			111	0.044
9	183.5	665.5			66.6	0.026
8	150.6	698.4			37	0.015
7	120.6	728.4			18.5	0.007
6	93.6	755.4			7.4	0.003

TABLE II-30. Activation of Zinc by protons (E=11 MeV).

			($Zn + p \rightarrow {}^{67}Ga$)	
Particle energy E, MeV	Range R mg/cm^2	Depth X mg/cm^2	Yield Y MBq/μAh	Activity A rel. units
11.0	257.5	0	185.0	1.000
10.5	237.7	19.8	148.0	0.800
10.0	219.1	38.4	111.0	0.600
9.5	201.0	56.5	87.0	0.470
9.0	183.5	74.0	66.6	0.360
8.5	166.7	90.8	48.1	0.260
8.0	150.6	106.9	37.0	0.200
7.5	135.3	122.2	26.6	0.144
7.0	120.6	136.9	18.5	0.100
6.5	106.7	150.8	12.2	0.066
6.0	93.6	163.9	7.4	0.040

TABLE II-31. Activation of Zinc by deuterons (E=22 MeV)

			(Zn + d → ^{65}Zn)		(Zn + d → ^{67}Ga)	
Particle energy E, MeV	Range R mg/cm^2	Depth *x* mg/cm^2	Yield Y MBq/μAh	Activity A rel. units	Yield Y MBq/μAh	Activity A rel. units
22	515.2	0.0	48.10	1.000	2146	1.000
21	476.1	39.1	44.03	0.915	1949.9	0.909
20	438.4	76.8	40.33	0.838	1776	0.828
19	402.1	113.1	37.37	0.777	1613.2	0.752
18	362.1	153.1	34.78	0.723	1480	0.690
17	333.5	181.7	32.41	0.674	1339.4	0.624
16	301.4	213.8	30.41	0.632	1209.9	0.564
15	270.6	244.6	28.12	0.585	1110	0.517
14	241.4	273.8	25.90	0.538	980.5	0.457
13	213.6	301.6	22.76	0.473	862.1	0.402
12	187.2	328.0	19.72	0.410	762.2	0.355
11	162.4	352.8	16.28	0.338	636.4	0.297
10	139.2	376.0	12.95	0.269	510.6	0.238
9	117.3	397.9	9.25	0.192	344.1	0.160
8	97.4	417.8	6.11	0.127	203.5	0.095
7	78.9	436.3	3.33	0.069	92.5	0.043
6	62.1	453.1	2.04	0.042	44.4	0.021
5	47.1	468.1	0.93	0.019	7.4	0.003
4	33.8	481.4	0.48	0.010		

TABLE II-32. Activation of Zinc by deuterons (E=10 MeV).

			(Zn + d → ^{65}Zn)		(Zn + d → ^{67}Ga)	
Particle energy E, MeV	Range R mg/cm^2	Depth *X* mg/cm^2	Yield Y MBq/μAh	Activity A rel. units	Yield Y MBq/μAh	Activity A rel. units
10.0	139.2	0.0	12.95	1.000	518	1.000
9.5	128.1	11.1	11.10	0.857	425.5	0.821
9.0	117.3	21.9	9.25	0.714	351.5	0.679
8.5	107.7	31.5	7.70	0.594	270.1	0.521
8.0	97.4	41.8	6.11	0.471	203.5	0.393
7.5	87.9	51.3	4.63	0.357	118.4	0.229
7.0	78.9	60.3	3.52	0.271	92.5	0.179
6.5	70.3	68.9	2.59	0.200	66.6	0.129
6.0	62.1	77.1	2.04	0.157	44.4	0.086
5.5	54.4	84.8	1.41	0.109	22.2	0.043
5.0	47.1	92.1	0.93	0.071	7.4	0.014
4.5	40.2	99.0	0.59	0.046		
4.0	33.8	105.4	0.41	0.031		

TABLE II-33. Activation of Zinc by 3He ions (E=30 MeV).
($Zn + {}^{3}He \rightarrow {}^{65}Zn$)

Particle energy E, MeV	Range R mg/cm^2	Depth *X* mg/cm^2	Yield Y MBq/μAh	Activity A rel. units
30	164.6	0.0	15.17	1.000
29	155.5	9.1	14.25	0.945
28	146.6	18.0	13.47	0.883
27	137.9	26.7	12.58	0.829
26	129.5	35.1	11.80	0.771
25	121.3	43.3	10.99	0.655
24	113.3	51.3	9.32	0.597
23	105.5	59.1	8.51	0.532
22	98.0	66.6	7.59	0.468
21	90.8	73.8	6.66	0.405
20	83.8	80.8	5.77	0.343
19	77.0	87.6	4.88	0.286
18	70.4	94.2	4.07	0.226
17	64.2	100.4	3.22	0.174
16	58.2	106.4	2.48	0.130
15	52.5	112.1	1.85	0.091
14	46.9	117.7	1.30	0.060
13	41.7	122.9	0.85	0.034
12	36.8	127.8	0.48	0.018
11	32.1	132.5	0.26	0.000

TABLE II-33.(Cont.) Activation of Zinc by ^{3}He ions (E=30 MeV).

			($Zn + {}^{3}He \rightarrow {}^{67}Ga$)		($Zn + {}^{3}He \rightarrow {}^{68}Ge$)	
Particle energy E, MeV	Range R mg/cm^2	Depth *X* mg/cm^2	Yield Y MBq/μAh	Activity A rel. units	Yield Y MBq/μAh	Activity A rel. units
30	164.6	0.0	499.5	1.000	2.78	1.000
29	155.5	9.1	477.3	0.956	2.44	0.880
28	146.6	18.0	455.1	0.911	2.15	0.773
27	137.9	26.7	429.2	0.859	1.85	0.667
26	129.5	35.1	403.3	0.807	1.59	0.573
25	121.3	43.3	377.4	0.756	1.37	0.493
24	113.3	51.3	347.1	0.695	1.15	0.413
23	105.5	59.1	316.7	0.634	0.93	0.333
22	98.0	66.6	284.9	0.570	0.74	0.267
21	90.8	73.8	252.0	0.504	0.59	0.213
20	83.8	80.8	219.8	0.440	0.48	0.173
19	77.0	87.6	187.6	0.376	0.37	0.133
18	70.4	94.2	156.5	0.313	0.30	0.107
17	64.2	100.4	130.6	0.261	0.22	0.080
16	58.2	106.4	100.6	0.201	0.15	0.053
15	52.5	112.1	79.6	0.159	0.07	0.027
14	46.9	117.7	59.2	0.119		
13	41.7	122.9	40.7	0.081		
12	36.8	127.8	25.9	0.052		
11	32.1	132.5	14.8	0.030		
10	27.7	136.9	8.5	0.017		

TABLE II-34. Activation of Niobium by protons (E=22 MeV).

			(Nb + p → ^{89}Zr)		(Nb + p → ^{92m}Nb)	
Particle energy E, MeV	Range R mg/cm^2	Depth *X* mg/cm^2	Yield Y MBq/μAh	Activity A rel. units	Yield Y MBq/μAh	Activity A rel. units
22.0	954.4	0.0	22.20	1.000	370.0	1.000
21.5	917.7	36.7	17.32	0.780	318.2	0.860
21.0	881.1	73.3	12.65	0.570	273.8	0.740
20.5	845.7	108.7	8.88	0.400	233.1	0.630
20.0	810.3	144.1	5.85	0.263	199.8	0.540
19.5	776.2	178.2	3.81	0.172	166.5	0.450
19.0	742.2	212.2	2.74	0.123	133.2	0.360
18.5	709.4	245.0	1.41	0.063	107.3	0.290
18.0	776.6	177.8	0.33	0.015	85.1	0.230
17.5	645.1	309.3			62.9	0.170
17.0	613.7	340.7			48.1	0.130
16.5	583.6	370.8			37.0	0.100
16.0	553.6	400.8			29.6	0.080
15.5	524.8	429.6			24.1	0.065
15.0	496.1	458.3			18.5	0.050
14.5	468.7	485.7			14.8	0.040
14.0	441.4	513.0			11.1	0.030
13.5	416.4	538.0			7.4	0.020
13.0	389.5	564.9			3.7	0.010

TABLE II-35. Activation of Niobium by deuterons (E=22 MeV).
(Nb + d → ^{92m}Nb)

Particle energy E, MeV	Range R mg/cm^2	Depth X mg/cm^2	Yield Y MBq/μAh	Activity A rel. units
22	588.8	0.0	76.96	1.000
21	544.9	43.9	59.015	0.767
20	502.4	86.4	42.291	0.550
19	461.5	127.3	29.008	0.377
18	422.0	166.8	21.312	0.277
17	384.1	204.7	16.502	0.214
16	347.8	241.0	12.987	0.169
15	318.0	270.8	9.99	0.130
14	279.8	309.0	7.696	0.100
13	248.2	340.6	5.698	0.074
12	218.3	370.5	3.996	0.052
11	190.0	398.8	2.812	0.037
10	163.4	425.4	1.813	0.024
9	138.5	450.3	0.814	0.011
8	115.4	473.4	0.296	0.004

TABLE II-36. Activation of Niobium by ^{3}He ions (E=30 MeV).
($Nb + {}^{3}He \rightarrow {}^{95m}Tc$)

Particle energy E, MeV	Range R mg/cm^2	Depth *X* mg/cm^2	Yield Y kBq/μAh	Activity A rel. units
30	188.6	0.0	44.40	1.000
29	178.3	10.3	42.18	0.950
28	168.3	20.3	40.33	0.908
27	158.5	30.1	38.67	0.871
26	149.0	39.6	37.07	0.835
25	139.7	48.9	35.52	0.800
24	130.7	57.9	34.04	0.767
23	121.9	66.7	32.26	0.727
22	113.4	75.2	30.53	0.688
21	105.2	83.4	28.86	0.650
20	97.2	91.4	27.31	0.615
19	89.5	99.1	25.64	0.578
18	82.1	106.5	23.75	0.535
17	75.0	113.7	21.76	0.490
16	68.1	120.5	19.80	0.446
15	61.5	127.1	21.31	0.480
14	55.2	133.4	15.43	0.348
13	49.2	139.4	13.14	0.296
12	43.5	145.1	10.58	0.238
11	38.1	150.5	7.77	0.175
10	33.0	155.6	6.29	0.142
9	28.2	160.4	4.59	0.103
8	23.7	164.9	2.96	0.067
7	19.6	169.0	1.48	0.033
6	15.7	172.9	0.37	0.008

TABLE II-36. (Cont.) Activation of Niobium by ^{3}He ions (E=30 MeV).

			(Nb + $^{3}He \rightarrow {}^{88}Y$)		(Nb+ $^{3}He \rightarrow {}^{92m}Nb$)	
Particle energy E, MeV	Range R mg/cm^2	Depth *x* mg/cm^2	Yield Y kBq/μAh	Activity A rel. units	Yield Y MBq/μAh	Activity A rel. units
30	188.6	0.0	72.15	1.000	4.81	1.000
29	178.3	10.3	51.06	0.708	3.89	0.808
28	168.3	20.3	38.11	0.528	3.15	0.654
27	158.5	30.1	28.12	0.390	2.70	0.562
26	149.0	39.6	19.61	0.272	2.29	0.477
25	139.7	48.9	13.69	0.190	1.96	0.408
24	130.7	57.9	8.88	0.123	1.67	0.346
23	121.9	66.7	5.55	0.077	1.41	0.292
22	113.4	75.2	2.96	0.041	1.11	0.231
21	105.2	83.4	1.11	0.015	0.85	0.177
20	97.2	91.4			0.67	0.138
19	89.5	99.1			0.4995	0.104
18	82.1	106.5			0.3404	0.071
17	75.0	113.7			0.2294	0.048
16	68.1	120.5			0.1332	0.028
15	61.5	127.1			0.0629	0.013
14	55.2	133.4			0.0222	0.005

TABLE II-37. Activation of Molybdenum by protons (E=22 MeV).

			(Mo + p → ^{95m}Tc)		(Mo + p → ^{96}Tc)	
Particle Energy E, MeV	Range R mg/cm^2	Depth *x* mg/cm^2	Yield Y MBq/μAh	Activity A rel. units	Yield Y MBq/μAh	Activity A rel. units
22	967.8	0.0	53.28	1.000	2072	1.000
21	893.6	74.2	48.10	0.903	1850	0.893
20	822.0	145.8	42.85	0.804	1646.5	0.795
19	753.0	214.8	37.93	0.712	1457.8	0.704
18	686.6	281.2	33.52	0.629	1269.1	0.613
17	622.9	344.9	28.97	0.544	1110	0.536
16	562.0	405.8	24.61	0.462	950.9	0.459
15	503.8	464.0	19.50	0.366	839.9	0.405
14	448.3	519.5	15.43	0.290	703	0.339
13	395.8	572.0	11.43	0.215	555	0.268
12	346.1	621.7	7.81	0.147	407	0.196
11	299.3	668.5	4.70	0.088	277.5	0.134
10	255.5	712.3	3.03	0.057	192.4	0.093
9	214.7	753.1	2.22	0.042	122.1	0.059
8	177.0	790.8	1.11	0.021	62.9	0.030
7	142.5	825.3	0.74	0.014	29.6	0.014
6	111.3	856.5			11.1	0.005

TABLE II-38. Activation of Molybdenum by protons (E=11 MeV).

			(Mo + p → ^{95m}Tc)		(Mo + p → ^{96}Tc)	
Particle energy E, MeV	Range R mg/cm^2	Depth *x* mg/cm^2	Yield Y MBq/μAh	Activity A rel. units	Yield Y MBq/μAh	Activity A rel. units
11.0	299.30	0.00	4.699	1.000	277.5	1.000
10.5	277.30	22.00	3.885	0.827	230.1	0.829
10.0	255.50	43.80	3.219	0.685	194.3	0.700
9.5	234.70	64.60	2.609	0.555	154.3	0.556
9.0	214.70	84.60	2.054	0.437	121.7	0.439
8.5	195.50	103.80	1.591	0.339	91.0	0.328
8.0	177.00	122.30	1.210	0.257	65.1	0.235
7.5	159.40	139.90	0.907	0.193	45.5	0.164
7.0	142.50	156.80	0.666	0.142	30.3	0.109
6.5	126.50	172.80	0.481	0.102	17.4	0.063
6.0	111.30	188.00	0.303	0.065	9.4	0.034
5.5	96.93	202.37	0.185	0.039	4.8	0.017
5.0	83.41	215.89	0.107	0.023	2.6	0.009
4.5	70.77	228.53	0.048	0.010	1.5	0.005
4.0	59.00	240.30	0.022	0.005		

TABLE II-39. Activation of Molybdenum by protons (E=7 MeV).

			(Mo + p → ^{95m}Tc)		(Mo + p → ^{96}Tc)	
Particle energy E, MeV	Range R mg/cm^2	Depth *x* mg/cm^2	Yield Y MBq/μAh	Activity A rel. units	Yield Y MBq/μAh	Activity A rel. units
7.0	142.5	0.00	0.640	1.000	29.60	1.000
6.8	135.9	6.60	0.559	0.873	24.94	0.843
6.6	129.5	13.00	0.481	0.751	19.02	0.643
6.4	123.2	19.30	0.411	0.642	15.61	0.528
6.2	117.2	25.30	0.352	0.549	11.84	0.400
6.0	111.3	31.20	0.300	0.468	9.51	0.321
5.8	105.5	37.00	0.252	0.393	7.18	0.243
5.6	99.79	42.71	0.211	0.329	5.55	0.188
5.4	94.23	48.27	0.174	0.272	4.07	0.138
5.2	88.81	53.69	0.137	0.214	2.96	0.100
5.0	83.41	59.09	0.104	0.162	2.22	0.075
4.8	78.24	64.26	0.074	0.116	1.63	0.055
4.6	73.22	69.28	0.048	0.075	1.11	0.038
4.4	68.33	74.17	0.026	0.040	0.74	0.025

TABLE II-40. Activation of Molibdenum by deuterons (E=22 MeV).

			(Mo + d → ^{95m}Tc)		(Mo + d → ^{96}Tc)	
Particle energy E, MeV	Range R mg/cm^2	Depth *x* mg/cm^2	Yield Y MBq/μAh	Activity A rel. units	Yield Y MBq/μAh	Activity A rel. units
22	598.7	0.0	27.75	1.000	2146	1.000
21	554.2	44.5	26.34	0.949	1953.6	0.910
20	511.1	87.6	24.72	0.891	1724.2	0.803
19	469.6	129.1	22.94	0.827	1509.6	0.703
18	429.6	169.1	21.20	0.764	1298.7	0.605
17	391.1	207.6	19.31	0.696	1091.5	0.509
16	354.2	244.5	17.39	0.627	917.6	0.428
15	318.9	279.8	15.47	0.557	765.9	0.357
14	285.2	313.5	13.43	0.484	651.2	0.303
13	253.1	345.6	11.32	0.408	547.6	0.255
12	222.7	376.0	9.18	0.331	429.2	0.200
11	193.9	404.8	6.99	0.252	333	0.155
10	166.9	431.8	4.66	0.168	247.9	0.116
9	141.6	457.1	2.66	0.096	166.5	0.078
8	118.0	480.7	1.30	0.047	81.4	0.038
7	96.3	502.4	0.59	0.021	44.4	0.021

TABLE II-41. Activation of Molibdenum by ^{3}He ions (E=30 MeV).
(Mo + $^{3}He \rightarrow {}^{95m}Tc$)

Particle energy E, MeV	Range R mg/cm^2	Depth *X* mg/cm^2	Yield Y MBq/μAh	Activity A rel. units
30	191.8	0.0	0.925	1.000
29	181.4	10.4	0.8251	0.892
28	172.2	19.6	0.7326	0.792
27	161.3	30.5	0.6512	0.704
26	151.6	40.2	0.5809	0.628
25	142.2	49.6	0.5106	0.552
24	133.0	58.8	0.4403	0.476
23	124.2	67.6	0.3737	0.404
22	115.5	76.3	0.3108	0.336
21	107.2	84.6	0.2516	0.272
20	99.08	92.7	0.1998	0.216
19	91.27	100.5	0.1554	0.168
18	83.73	108.1	0.1147	0.124
17	76.47	115.3	0.0814	0.088
16	69.49	122.3	0.0518	0.056
15	62.80	129.0	0.0296	0.032
14	56.40	135.4	0.0148	0.016
13	50.30	141.5	0.0074	0.008

TABLE II-41. (Cont.) Activation of Molibdenum by ^{3}He ions (E=30 MeV).

			($Mo + {}^{3}He \rightarrow {}^{96}Tc$)		($Mo + {}^{3}He \rightarrow {}^{97}Ru$)	
Particle energy E, MeV	Range R mg/cm^2	Depth *x* mg/cm^2	Yield Y MBq/μAh	Activity A rel. units	Yield Y MBq/μAh	Activity A rel. units
30	191.8	0.0	138.8	1.000	547.6	1.000
29	181.4	10.4	123.2	0.888	511.3	0.934
28	172.2	19.6	109.2	0.787	475.1	0.868
27	161.3	30.5	96.2	0.693	438.5	0.801
26	151.6	40.2	84.4	0.608	401.8	0.734
25	142.2	49.6	72.9	0.525	365.2	0.667
24	133.0	58.8	61.4	0.443	328.9	0.601
23	124.2	67.6	51.1	0.368	296.0	0.541
22	115.5	76.3	42.6	0.307	264.92	0.484
21	107.2	84.6	34.8	0.251	233.84	0.427
20	99.08	92.7	28.1	0.203	202.76	0.370
19	91.27	100.5	22.2	0.160	172.05	0.314
18	83.73	108.1	17.4	0.125	141.71	0.259
17	76.47	115.3	13.0	0.093	112.85	0.206
16	69.49	122.3	9.3	0.067	88.8	0.162
15	62.80	129.0	5.9	0.043	64.75	0.118
14	56.40	135.4	3.3	0.024	45.51	0.083
13	50.30	141.5			30.34	0.055
12	44.48	147.3			15.91	0.029
11	38.98	152.8			0.74	0.001

TABLE II-42. Activation of Tungsten by protons (E=22 MeV).

			(W + p → ^{183}Re)		(W + p → ^{184g}Re)	
Particle energy E, MeV	Range R mg/cm^2	Depth *x* mg/cm^2	Yield Y MBq/μAh	Activity A rel. units	Yield Y MBq/μAh	Activity A rel. units
22	1222.0	0.0	125.8	1.000	296.00	1.000
21	1131.0	91.0	117.7	0.935	214.60	0.725
20	1042.0	180.0	108.0	0.859	145.04	0.490
19	957.1	264.9	96.2	0.765	96.20	0.325
18	875.0	347.0	79.2	0.629	66.01	0.223
17	796.0	426.0	61.8	0.491	46.77	0.158
16	720.0	502.0	42.6	0.338	34.63	0.117
15	647.4	574.6	31.5	0.250	28.71	0.097
14	578.6	643.4	22.9	0.182	22.20	0.075
13	512.7	709.3	15.5	0.124	16.87	0.057
12	450.3	771.7	8.9	0.071	13.85	0.047
11	391.4	830.6	4.8	0.038	8.88	0.030
10	336.0	886.0	1.9	0.015	5.92	0.020
9	284.2	937.8	0.7	0.006	0.30	0.001
8	236.1	985.9			0.09	0.000

TABLE II-43. Activation of Tungsten by protons (E=11 MeV).

			(W + p → ^{183}Re)		(W + p → ^{184g}Re)	
Particle energy E, MeV	Range R mg/cm^2	Depth *x* mg/cm^2	Yield Y MBq/μAh	Activity A rel. units	Yield Y MBq/μAh	Activity A rel. units
11.0	391.4	0.0	4.81	1.000	8.99	1.000
10.5	363.5	27.9	3.03	0.631	7.40	0.823
10.0	336.0	55.4	1.78	0.369	5.81	0.646
9.5	309.7	81.7	1.04	0.215	4.29	0.477
9.0	284.2	107.2	0.63	0.131	2.78	0.309
8.5	259.7	131.7	0.352	0.073	1.63	0.181
8.0	236.1	155.3	0.204	0.042	0.93	0.103
7.5	213.5	177.9	0.107	0.022	0.463	0.051
7.0	191.8	199.6	0.059	0.012	0.196	0.022
6.5	171.1	220.3	0.022	0.005	0.056	0.006

TABLE II-44. Activation of Tungsten by deuterons (E=22 MeV).

			(W + d → ^{183}Re)		(W + d →^{184g}Re)	
Particle energy E, MeV	Range R mg/cm^2	Depth *x* mg/cm^2	Yield Y MBq/μAh	Activity A rel. units	Yield Y MBq/μAh	Activity A rel. units
22	782.9	0.0	148.00	1.000	111.0	1.000
21	726.7	56.2	127.28	0.860	101.75	0.917
20	672.2	110.7	106.56	0.720	93.24	0.840
19	619.5	163.4	87.32	0.590	89.91	0.810
18	568.6	214.3	71.19	0.481	82.88	0.747
17	519.6	263.3	57.13	0.386	76.22	0.687
16	472.4	310.5	43.66	0.295	69.19	0.623
15	427.1	355.8	32.56	0.220	57.35	0.517
14	383.7	399.2	23.09	0.156	48.47	0.437
13	342.2	440.7	16.13	0.109	37.37	0.337
12	302.7	480.2	10.95	0.074	27.38	0.247
11	265.2	517.7	6.81	0.046	17.76	0.160
10	229.7	553.2	3.40	0.023	9.99	0.090
9	196.2	586.7	1.78	0.012	4.07	0.037
8	164.9	618.0	0.59	0.004	1.85	0.017

TABLE II-45. Activation of Tungsten by ^{3}He ions (E=30 MeV).

Particle energy E, MeV	Range R mg/cm^2	Depth *x* mg/cm^2	(W + ^{3}He → ^{183}Re) Yield Y MBq/μAh	(W + ^{3}He → ^{183}Re) Activity A rel. units	(W + ^{3}He → ^{184g}Re) Yield Y MBq/μAh	(W + ^{3}He → ^{184g}Re) Activity A rel. units
30	251.8	0.0	9.62	1.000	6.51	1.000
29	238.6	13.2	8.251	0.858	5.51	0.847
28	225.7	26.1	6.882	0.715	4.51	0.693
27	213.1	38.7	5.513	0.573	3.70	0.568
26	200.7	51.1	4.144	0.431	2.85	0.438
25	188.7	63.1	2.923	0.304	2.04	0.313
24	177.0	74.8	2.035	0.212	1.41	0.216
23	165.6	86.2	1.443	0.150	0.96	0.148
22	154.5	97.3	1.036	0.108	0.59	0.091
21	143.8	108.0	0.629	0.065	0.37	0.057
20	133.3	118.5	0.333	0.035	0.19	0.028
19	123.2	128.6	0.111	0.012		0.000

TABLE II-45. (Cont.) Activation of Tungsten by ^{3}He ions (E=30 MeV).

Particle energy E, MeV	Range R mg/cm^2	Depth *x* mg/cm^2	*(W + ^{3}He → ^{185}Os)* Yield Y MBq/μAh	*(W + ^{3}He → ^{185}Os)* Activity A rel. units
30	251.8	0.0	3.33	1.000
29	238.6	13.2	2.775	0.833
28	225.7	26.1	2.257	0.678
27	213.1	38.7	1.776	0.533
26	200.7	51.1	1.332	0.400
25	188.7	63.1	0.925	0.278
24	177.0	74.8	0.592	0.178
23	165.6	86.2	0.333	0.100
22	154.5	97.3	0.185	0.056
21	143.8	108.0	0.074	0.022

II-3. USEFUL ISOTOPES FOR BULK ACTIVATION

TABLE II-46. Useful isotopes for bulk activation

Parent Element	Base Element	Abundance [52]	Nuclide made	$t_{½}$ days [53]	Gammas keV	Cross-section barns [51]
Fe	^{58}Fe	0.282	^{59}Fe	44.6	1099, 1291	1.28
Cr	^{50}Cr	4.345	^{51}Cr	27.7	320	15.9
Sn	^{112}Sn	0.973	^{113}Sn	115	255	1.01
Ni	^{58}Ni	68.077	^{58}Co	70.8	811	4.6
Zn	^{64}Zn	48.63	^{65}Zn	244	1115	0.76
In	^{113}In	4.288	^{114}mIn	49.5	190	12.0
Co	^{59}Co	100	^{60}Co	1925	1173, 1332	37.18
Sb	^{123}Sb	42.787	^{124}Sb	60.3	602.7, 1691	4.1

Acronyms

ACRONYMS

Acronyms for activation:

- TLA Thin Layer Activation;
- SLA Surface Layer Activation;
- UTLA Ultra Thin Layer Activation;

Acronyms for measurements:

- RNT Radionuclide Technology;
- RTM Radionuclide Technology in Mechanical engineering;
- RATT Radioactive Tracer Technology;
- n-RAI Radionuclide measurement technology in model testing;
- RIC (nVCT) Radioisotope Concentration Method;
- CMM Concentration Measurement Method;
- TLD Thin Layer Difference measurement method;
- DM Direct Method.

Acronyms for devices, instrumentation:

- CMD Concentration Measurement Device;
- FMD Filter Measurement Device;
- RMD Reference Measurement Device;
- NaI(Tl) Sodium Iodide detector, doped with Thallium (Scintillation detector);
- HpGe High Purity Germanium detector (Semi-conductor detector);
- GeLi Lithium drifted Germanium detector (Semi-conductor detector);
- PMT Photo Multiplier Tube.

.

CONTRIBUTORS TO DRAFTING AND REVIEW

BRISSET, Patrick	International Atomic Energy Agency, Austria
DITROI, Ferenc	Academy of Science, Debrecen, Hungary
EBERLE, Douglas	Southwest Research Institute ,Texas, USA
JECH, Martin	AC2T research GmbH, Austria
KLEINRAHM, Achim	ZAG Zyklotron AG, Germany
LENAUER, Claudia	AC2T research GmbH, Austria
SAUVAGE, Thierry	CEMHTI – CNRS, France
THERESKA, Jovan	Consultant, Albania

IAEA
International Atomic Energy Agency

No. 26

ORDERING LOCALLY

IAEA priced publications may be purchased from the sources listed below or from major local booksellers.

Orders for unpriced publications should be made directly to the IAEA. The contact details are given at the end of this list.

NORTH AMERICA

Bernan / Rowman & Littlefield
15250 NBN Way, Blue Ridge Summit, PA 17214, USA
Telephone: +1 800 462 6420 • Fax: +1 800 338 4550
Email: orders@rowman.com • Web site: www.rowman.com/bernan

Renouf Publishing Co. Ltd
22-1010 Polytek Street, Ottawa, ON K1J 9J1, CANADA
Telephone: +1 613 745 2665 • Fax: +1 613 745 7660
Email: orders@renoufbooks.com • Web site: www.renoufbooks.com

REST OF WORLD

Please contact your preferred local supplier, or our lead distributor:

Eurospan Group
Gray's Inn House
127 Clerkenwell Road
London EC1R 5DB
United Kingdom

Trade orders and enquiries:
Telephone: +44 (0)176 760 4972 • Fax: +44 (0)176 760 1640
Email: eurospan@turpin-distribution.com

Individual orders:
www.eurospanbookstore.com/iaea

For further information:
Telephone: +44 (0)207 240 0856 • Fax: +44 (0)207 379 0609
Email: info@eurospangroup.com • Web site: www.eurospangroup.com

Orders for both priced and unpriced publications may be addressed directly to:

Marketing and Sales Unit
International Atomic Energy Agency
Vienna International Centre, PO Box 100, 1400 Vienna, Austria
Telephone: +43 1 2600 22529 or 22530 • Fax: +43 1 26007 22529
Email: sales.publications@iaea.org • Web site: www.iaea.org/publications

International Atomic Energy Agency
Vienna
ISBN 978–92–0–101520–4
ISSN 1011–4289